Svoluji k zapůjčení své diplomové práce ke studijním účelům a prosím, aby byla vedena přesná evidence vypůjčovatelů. Převzaté údaje je vypůjčovatel povinen řádně ocitovat.

Charles University

Faculty of Science

Study program: Biology

Study branch: Genetics, Molecular Biology and Virology

Bc. Anna Hustedová

Targeting of Viral Nanoparticles to CD44 via Hyaluronic Acid

Cílení virových nanočástic na CD44 receptor pomocí kyseliny hyaluronové

Diploma Thesis

Supervisor: RNDr. Hana Španielová Ph.D.

Prague, 2020

Prohlášení:

Prohlašuji, že jsem závěrečnou práci zpracovala samostatně a že jsem uvedla všechny použité informační zdroje a literaturu. Tato práce ani její podstatná část nebyla předložena k získání jiného nebo stejného akademického titulu.

V Praze, 7.8.2020

Podpis

Acknowledgements

Abstract

Hyaluronic acid (HA) is widely studied as a targeting moiety to CD44 overexpressing cancer cells. Various types of nanoparticles (NPs) were modified by HA. Virus-like particles (VLPs) derived from mouse polyomavirus are an interesting class of NPs that can be modified by various targeting agents to increase their potential as gene or drug delivery vehicles for e.g. theragnostic purposes. HA has not been tested as a targeting moiety on VLPs, hence this was the focus of the current study. HA (~14 kDa) was attached to the VLPs via a bispecific Bodipy-derived fluorescent probe. To test the targeting potential of HA on comparable non-viral NPs, nanodiamonds were prepared in a similar manner. NPs functionalized with HA, together with Bodipy-labeled control variants, were tested on interactions with MDA-MB-231 cells overexpressing CD44.

The NP-cell interaction via CD44 was assessed by a competitive cell-binding assay, where non-labeled HA competed for HA-binding sites at CD44 with the NPs. CD44 specific cell interactions were detected in studies with HA functionalized nanodiamonds, whereas VLP-HA* associated with cells in a less specific manner. Control VLPs with polyethylene glycol (PEG) did not interact with the cells. Results indicate that the HA targeting strategy for the VLPs requires optimization to achieve suitable coverage of the VLP surface by HA molecules that could shield virus-specific interactions (as seen in VLP-PEG*) and provide re-targeting to CD44.

Keywords

Abstrakt

Kyselina hyaluronová (HA) je testována jako agens cílící na rakovinné buňky nadměrně exprimující CD44. Mnohé typy nanopartikulí (NPs) byly využity k povrchové modifikaci pomocí HA. Viru podobné partikule myšího polyomaviru (VLPs) jsou zajímavou skupinou NPs. Kvůli zvýšení jejich potenciálu v rámci theragnostiky, mohou být VLPs modifikovány různými cílícími agens. HA však nebyla dosud testována jako cílící agens na VLPs, proto se tato práce zaměřuje právě na toto téma. HA (~14 kDa) byla připojena na VLPs skrze bispecifickou fluorescenční sondu odvozenou od Bodipy. Aby bylo možné otestovat cílící potenciál HA na srovnatelných nevirových NPs, byly podobným způsobem modifikovány nanodiamanty.

NPs modifikované HA spolu s kontrolními variantami označenými Bodipy byly testovány na interakce s MDA-MB-231 buňkami nadměrně exprimujícími CD44. Interakce NPs s buňkami skrze CD44 byla zhodnocena pomocí kompetitivní vazebné eseje, kdy neznačená HA kompetovala s NPs o HA vazebná místa na CD44. CD44 specifické interakce byly detekovány v experimentech u HA modifikovaných nanodiamantů, zatímco VLP-HA* interagovaly s buňkami méně specificky. Kontrolní VLPs s polyethylenglykolem (PEG) s buňkami téměř neinteragovaly. Výsledky naznačují, že strategie cílení pomocí HA vyžaduje optimalizaci, aby bylo možné dosáhnout dostatečného povrchového pokrytí VLPs HA molekulami, které by dokázalo zakrýt virus-specifické interakce (jako u VLP-PEG*) a poskytlo tak specifické cílení na CD44.

Klíčová slova

Kyselina hyaluronová, CD44, klik chemie, myší polyomavirus, nanopartikule, viru-podobné partikule, cílení

Table of contents

List of Abbreviations

Af488	Alexa Fluor™ 488 azide
Alkyne linker	Propargyl-N-hydroxysuccinimidyl ester linker
Bp	Heterobifunctional bodipy – containing azide and aminooxy functionality, produced by Jan Bartoň
BSA	Bovine serum albumin
CD44s	Standard isoform of CD44
CD44v	CD44 splicing variants
Click chemistry	Cu^I-catalyzed alkyne-azide cycloaddition
Click reaction	Cu^I-catalyzed alkyne-azide cycloaddition
dH$_2$O	Destilled water
ddH$_2$O	Double destilled water
EPR effect	Enhanced permeability and retention effect
FBS	Fetal bovine serum
FC experiments	Flow cytometry NP-cell interaction studies
FC1	Flow cytometry experiment 1
FC2	Flow cytometry experiment 2
FC3	Flow cytometry experiment 3
FL experiments	Fluorescence microscopy NP-cell interaction studies
FL1	Fluorescence experiment 1
FL2	Fluorescence experiment 2
FDA	Food and Drug Administration
Free controls	HA*, PEG*, Bp
Free HA	Non-labeled HA (8-15 kDa)
HA	Hyaluronic acid
HA*	Fluorescently labeled HA; Bp-HA produced by Jitka Nebůrková (IOCB)
IgG	Immunoglobulin G
IMDM medium	Iscove's modified Dulbecco's medium
LYVE1	Lymphatic vessel endothelial hyaluronan receptor 1
MDA cells	MDA-MB-231 cells
MPyV	Mouse polyomavirus
MPyV VLPs	MpyV VP1 virus-like particles
NC	Negative control
ND-Bp	Nanodiamonds with Bp attached
ND-HA* + HA	Nanodiamonds with HA* attached incubated with free HA
ND-HA*	Nanodiamonds with HA* attached
NDs	Nanodiamonds
NHS ester	N-hydroxysuccinimidyl ester

NPs	Nanoparticles
NP-Bp	VLP-Bp and ND-Bp
NP-HA	Nanoparticles modified with HA
NP-HA*	VLP-HA* and ND-HA*
PEG	Polyethylene glycol
PEG*	Fluorescently labeled PEG; Bp-PEG produced by Jitka Nebůrková (IOCB)
pfu	Plaque-forming unit
Rec Bac VP1	Recombinant baculovirus containing gene encoding MPyV VP1
RT	Room temperature
SDS	Sodium dodecyl sulfate
SDS-PAGE	SDS polyacrylamide gel electrophoresis
TEM	Transmission electron microscopy
VLP-alkyne	MPyV VLPs with alkyne linker attached
VLP-Bp	MPyV VLP-alkyne with Bodipy attached
VLP-HA* + HA	MPyV VLP-alkyne with HA* attached incubated with free HA
VLP-HA*	MPyV VLP-alkyne with HA* attached
VLP-PEG*	MPyV VLP-alkyne with PEG* attached
VLPs	MPyV VP1 VLPs
VP1	Main structural mouse polyomaviral protein

1. Introduction

Cancer is one of the leading causes of death worldwide. In 2018, 65 456 cancer cases were detected in the Czech Republic and 26 980 deaths were attributable to cancer (WHO, 2020). Chemotherapeutics used in cancer treatment often come with a variety of side effects, among which non-target healthy cells are often affected and therefore more specific targeting approaches are needed (Höfling and Bolte, 1981). Extensive research regarding this issue focuses on the use of nanocarriers, which can provide many advantages in cancer diagnosis and treatment.

Nanocarriers can protect the often hydrophobic chemotherapeutic drugs, or another payload (e.g. siRNA) and release them at target site (Byeon et al., 2018). This can be achieved via the enhanced permeability and retention effect (EPR effect) at the tumor site. Newly formed vessels at the tumor site are often abnormal as wide fenestrations are present between the endothelial cells, therefore nanocarriers are preferentially accumulated there due to their size (Fang et al., 2020). Furthermore, the surface of the nanocarriers can be modified with targeting moieties to increase the targeting specificity. Various types of targeting moieties were used; among the most common types, antibodies specific against receptors overexpressed in cancer cells or their ligands were utilized (Xiao et al., 2015; Su et al., 2019). Thus, using nanocarriers with a surface targeting moiety can achieve a combination of targeting to tumor site via the EPR effect and of active targeting, using targeting moieties for enhancing the targeting specificity (Fang et al., 2020; Sanfilippo et al., 2020).

Hyaluronic acid (HA) is extensively studied and used in many areas of medical research. In addition, HA has been conjugated onto nanocarriers and used as a targeting moiety to CD44 overexpressing cancer cells (Eliaz and Szoka, 2001; Ganesh et al., 2013b; Byeon et al., 2018). The CD44 receptor is the primary receptor for hyaluronic acid with a function in many cellular processes and is frequently overexpressed on solid tumors. It has also been determined as a biomarker in the so-called cancerous stem cells, that possess the cancer initiating ability (Prince et al., 2007; Du et al., 2008; Takaishi et al., 2009).

Mouse polyomavirus virus-like particles (VLPs) are particles self-assembled from the main structural viral protein (VP1). They possess many advantages, such as stability, natural origin, the possibility of surface modification by targeting moieties and encapsulation of payloads. However, VP1 receptors are ubiquitous and therefore, VLPs interact with a wide range of cells. Nonetheless, because the surface can be modified by targeting moieties, the MPyV VLPs VP1-mediated interactions can be shielded (when a large targeting moiety is used) and simultaneously, VLPs can be re-targeted to a different receptor (Zackova Suchanova et al., 2017). Nevertheless, HA has not yet been tested as a targeting and shielding moiety on VLPs. This will therefore be the focus of this thesis.

2. Literature Review

2.1 Nanoparticles and Tumor Targeting

Classical methods used in cancer therapy and diagnosis are often insufficiently specific and often also provide undesirable side-effects that research is still trying to address (Sarafraz et al., 2018; Streckmann et al., 2018; Georgakopoulos et al., 2019; Mallepally et al., 2019). Hence, research focuses on testing new approaches of cancer therapy and diagnosis, which could eliminate these drawbacks. The current study will focus on one of the new approaches, the use of nanoparticles (NPs).

Research regarding NPs has been evolving since the 1990s, but especially in the last 20 years, there has been a sharp increase in both, studies of nanoparticles used in cancer research and reviews mapping the issue (Fig. 1). The topic is therefore very extensive.
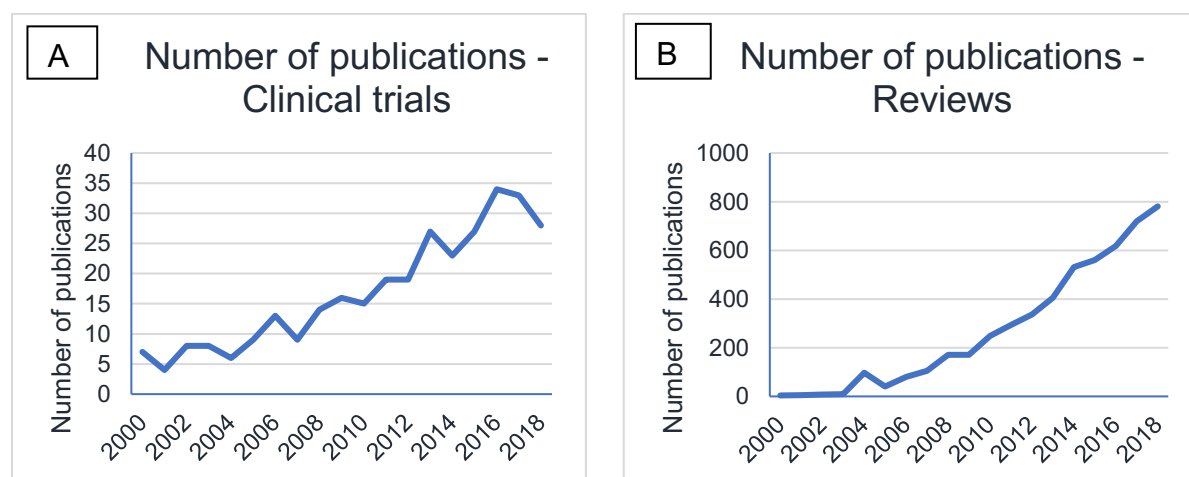
Figure 1 Graphs representing data from PubMed, search: Cancer; nanoparticle summarizing A) the number of publications regarding clinical trials in years 2000-2018 and B) the number of reviews published on the topic in years 2000-2018. Data show an increasing trend in published reviews on the topic.

In general, two types of NPs are produced, organic (e.g. liposomes, polymeric, protein-based NPs) and inorganic (e.g. nanocrystals, gold, iron oxide NPs), hybrid NPs can also be produced (Cho et al., 2011; Nair et al., 2011; Lee et al., 2013; Li et al., 2014; Byeon et al., 2018; Karakocak et al., 2018; Sanfilippo et al., 2020). Organic nanoparticles provide many advantages over free chemotherapeutics, including increased circulation time, drug protection, controlled release of the drug, and targeting the tumor site (Zhao et al., 2015; Li et al., 2016).

Inorganic NPs offer additional advantages. Namely stimuli-responsive functions, like magnetic responses (used e.g. in magnetic resonance imaging) (Lee et al., 2013; Li et al., 2014). The main advantage of NPs is their versatility of use as delivery system platforms. The encapsulated substance can vary and the targeting moieties on the surface of the particles can be adapted too.

The first NP approved by the Food and Drug Administration (FDA) was Doxil in 1995: Polyethylene glycol (PEG; often used as a shielding agent in nanomedicine) - functionalized liposomes encapsulating the chemotherapeutic drug Doxorubicin. Doxorubicin, like many different chemotherapeutic agents, is not readily soluble. Negative side effects are also associated with the application of free doxorubicin. By encapsulating doxorubicin in liposomes and subsequently coating the liposomes with PEG, many improvements have been achieved at the same time, such as increased circulation time, reduction of side effects (cardiotoxicity) and transport of NPs to the tumor site via the EPR effect. Nonetheless, in some aspects additional research was needed (Safra et al., 2000; Barenholz, 2012).

To further increase the specificity of tumor site targeting, surface modifications of NPs by targeting moieties have also been studied. As of 2016, however, most FDA approved NPs were based only on accumulation at the tumor site by the EPR effect (Bobo et al., 2016). Nevertheless, methods of active cancer cell biomarkers targeting are being extensively studied. Usually, the targets are receptors overexpressed on cancer cells. In active cancer cell targeting, antibodies, antibody fragments against cancer cell biomarkers, or ligands of the overexpressed receptors are most often used for surface modification of NPs. Many studies using actively targeted nanoparticles have already achieved clinical trials. The most common targets are often the epidermal growth factor receptor, human epidermal growth factor receptor 2, the transferrin receptor, or the prostate-specific membrane antigen (Davis et al., 2010; Lee et al., 2017; van Zandwijk et al., 2017; Autio et al., 2018). In recent years, the CD44 receptor has also been significantly studied as a target for active cancer cell targeting (Yang et al., 2015; Xiong et al., 2016).

2.2 Hyaluronic Acid and the CD44 Specific Targeting

2.2.1 Hyaluronic Acid

Hyaluronic acid was first found in cattle vitreous humor in 1934 by Karl Meyer and John W. Palmer. The name originated from hyaloid (vitreous) and uronic acid (Meyer and Palmer, 1934). HA is a naturally occurring linear glycosaminoglycan, that consists of a repeating disaccharide composed of D-glucuronic acid and N-acetylglucosamine connected by alternating β-1,3 and β-1,4 glycosidic bonds (Fig. 2) (Liu et al., 2011; Fallacara et al., 2018). In the human body, HA is synthesized by hyaluronan synthases and degraded either nonspecifically by the damage caused by reactive oxygen species or specifically by the hyaluronidase enzymes (Csóka et al., 1999; Usui, 2003).
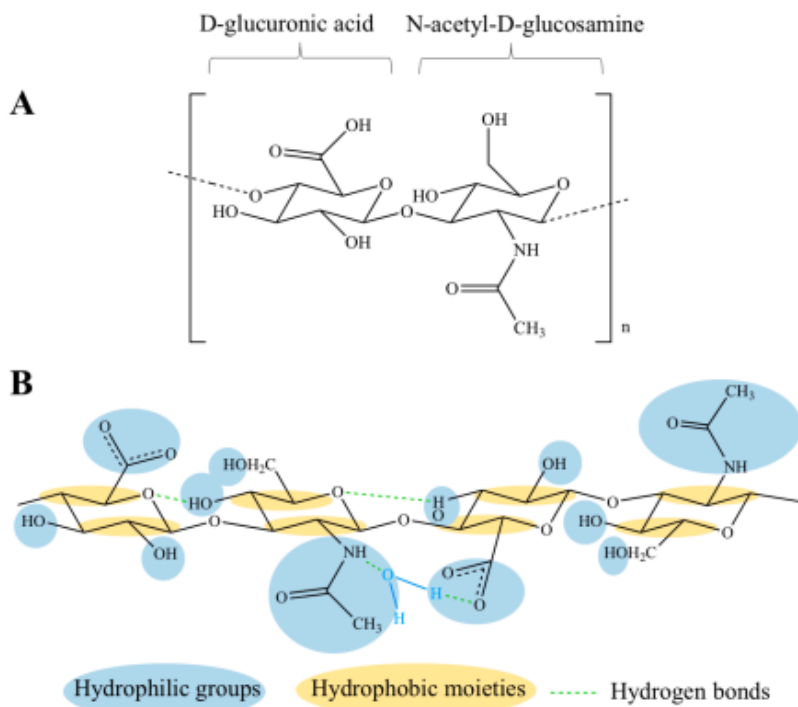
Figure 2 HA is composed of a repeating disaccharide of D-glucuronic acid and N-acetyl-D-glucosamine, structure shown in A). Hyaluronic acid is highly hydrophilic, the hydrophilic and hydrophobic moieties present in its structure are shown in B). Adapted from (Fallacara et al., 2018).

In the human body, hyaluronic acid is most abundant in the extracellular matrix of soft tissues, in umbilical cords, in synovial fluid and in vitreous humor. The physiological functions of HA are derived from its interaction with proteins (hyaladherins), and its unique hydrodynamic functions (linear structure; in tissue, HA immobilizes water molecules) (Fallacara et al., 2018).

Several HA-binding receptors have been determined, the primary receptor being CD44, the other being the receptor for HA-mediated motility, the hyaluronan receptor for endocytosis, or the lymphatic vessel endothelial hyaluronan receptor 1 (LYVE1) (Harris and Weigel, 2008; ; Misra et al., 2015; Lawrance et al., 2016).

The biological functions of HA include roles in cell motility, embryogenesis, signal transduction. Hyaluronic acid also hydrates tissues, lubricates joints, supports the structure of the extracellular matrix and regulates innate immunity. Naturally occurring HA usually has molecular weight (Mw) of 1000 to 8000 kDa (Cowman et al., 2015). The specific biological functions of HA are often derived from the HA Mw, and are frequently opposite in high and low Mw HA, e.g. changes in the phenotype of macrophages induced by HA are completely different in high and low Mw HA (Rayahin et al., 2015).

High Mw HA has often space-filling, anti-inflammatory and anti-angiogenic functions. In synovial fluid it is responsible for the lubricating function (Gupta et al., 2019); also high Mw HA has shown to inhibit cell cycle progression in smooth muscle cells (Kothapalli et al., 2007). Low Mw HA contains pro-inflammatory (supports the production of pro-inflammatory cytokines in macrophages), immunostimulatory and antioxidant function. It promotes angiogenesis and promotes cell cycle progression in smooth muscle cells (Ke et al., 2011; Rayahin et al., 2015; Gupta et al., 2019). Given the importance of HA Mw in its functions in the human body, it is clear that the distribution and HA Mw can be an indicator of various diseases, such as liver fibrosis (Jeffers et al., 2007; Orasan et al., 2016). Therefore, it is important that new methods for HA size analysis are being developed (Rivas et al., 2018).

Thanks to its unique properties, HA has gained wide use. Among other things, it is used in cosmetics, in soft tissue reconstruction, in some ophthalmological surgeries, and for improvements of function in arthritic patients (Holmberg and Philipson, 1984; Sun et al., 2006; Nobile et al., 2014; Cheng et al., 2017).

Another use relates to the main HA receptor, CD44. CD44 is a transmembrane glycoprotein made of 4 domains: extracellular HA binding and stalk domains, transmembrane domain and the cytosolic domain. It is overexpressed on many cancer cells and has been detected as a biomarker of cancer stem cells, which possess the cancer-initiating ability (Prince et al., 2007; Du et al., 2008; Takaishi et al., 2009).

There are various isoforms of CD44 produced by alternative splicing, the standard isoform (CD44s) is ubiquitous and the variants (CD44v) are present mostly in cancer cells. CD44v are associated with progression in various types of cancer. E.g. high levels of CD44v6 are connected to poor prognosis in colon cancer (Garouniatis et al., 2013; Todaro et al., 2014).

The N-terminus of CD44 binds HA and the binding affinity is affected by the HA Mw. The higher HA Mw, the higher the binding affinity - the saturation point has been investigated and proposed to be 262 kDa (Wolny et al., 2010). High Mw HA also promotes CD44 aggregation, as multivalent binding can occur in longer HA chains and CD44 molecules can move along the HA chains. The aggregation is however not present in CD44-HA oligosaccharide binding. Low HA Mw also showed reversible CD44 binding, while HA with Mw higher than 10 kDa showed irreversible CD44 binding (Wolny et al., 2010). Three modes how CD44 binds HA been proposed (Fig. 3) (Vuorio et al., 2017).
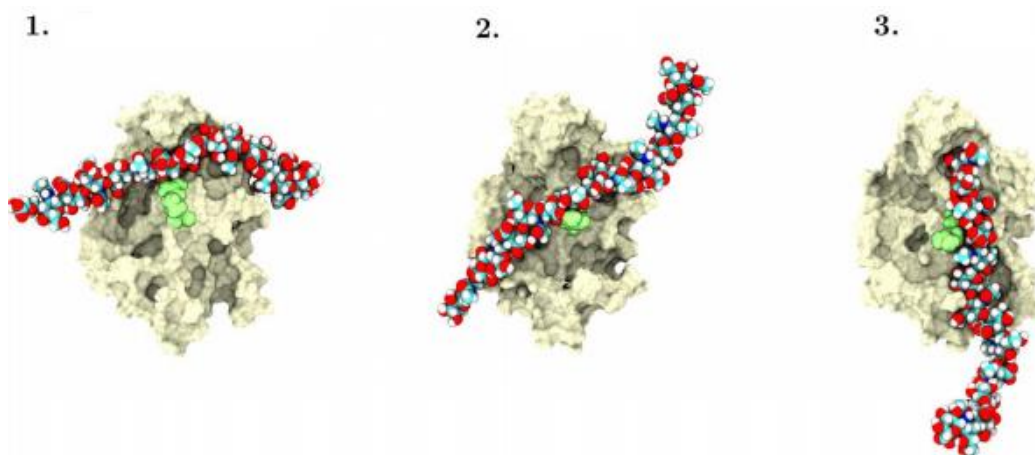
Figure 3 Three different modes how CD44 binds HA, figure shows HA-binding domains (grey) and HA$_{16}$ oligomer (multicolor rod) and the R41 residue (light green) important for HA binding in all CD44 modes. Edited from Vuorio et al., 2017

Hyaluronic acid was utilized as a molecule targeting the CD44 overexpressing cancer cells. The targeting was achieved e.g. by a direct conjugation of chemotherapeutics to HA, or by conjugation of nanocarriers with HA (Gibbs et al., 2008; Nair et al., 2011).

2.2.2 HA-NPs in Active Tumor Targeting

In the last twenty years, active targeting utilizing hyaluronic acid as a targeting moiety has been extensively studied. In 2014, for example, the chemotherapeutic Irinotecan, conjugated to HA for patients with metastatic colorectal cancer, entered clinical trials (Gibbs et al., 2008). A wide range of types of nanocarriers conjugated with HA was developed, most often liposomes, polymeric, or inorganic NPs were investigated (examples shown in Figure 4).

Xiao et al., 2015 – Polymeric NPs	Li et al., 2016 – Liposome encapsulated NPs
Li et al., 2014 - Iron Oxide NPs	Zhao et al., 2015 – Mesosporous silica NPs
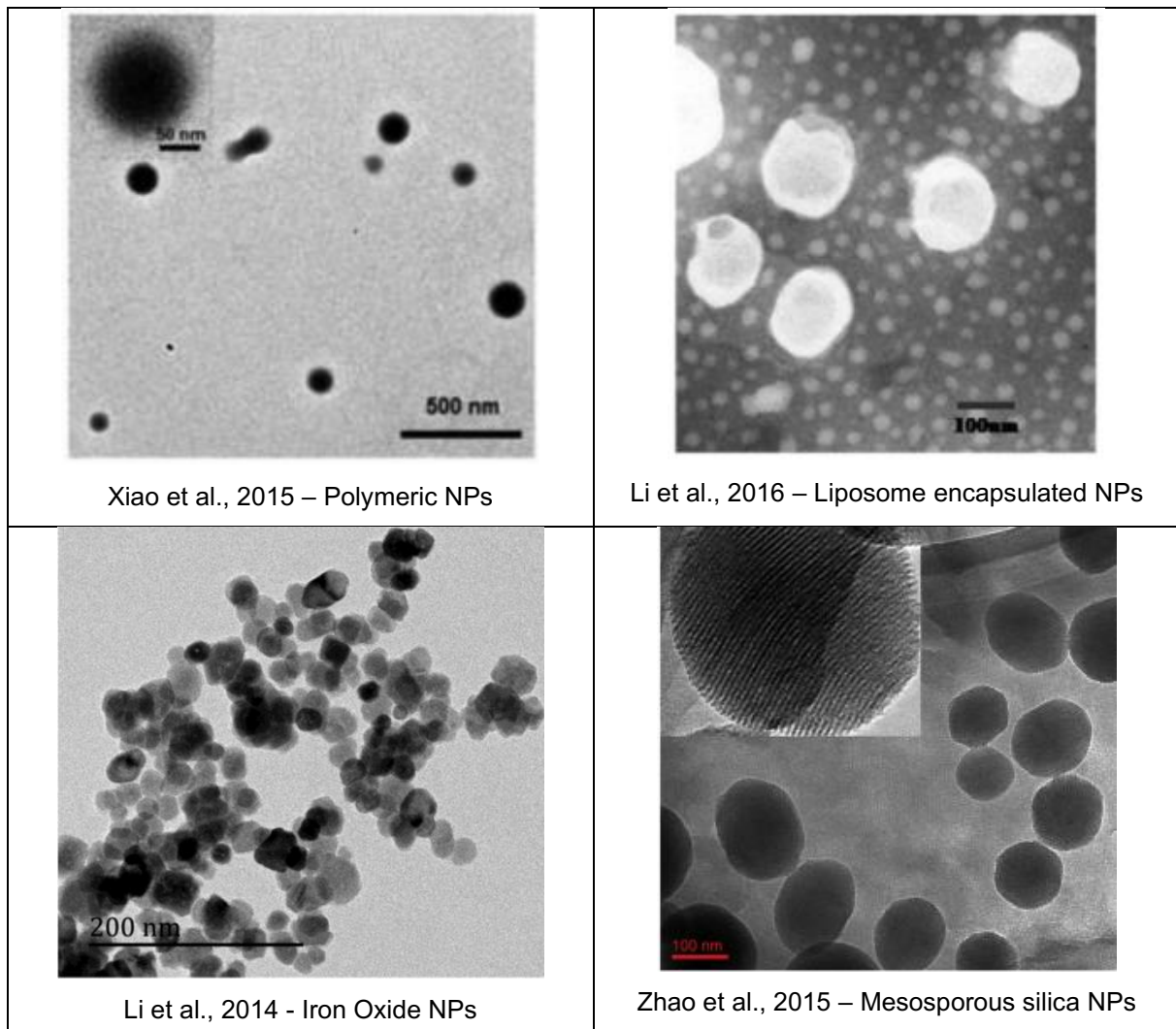
Figure 4 TEM micrographs of examples of various HA-NP types studied and the corresponding reference.

Nanoparticles usually mediated drug delivery. Most commonly poorly water-soluble chemotherapeutics (doxorubicin, letrozole, campothecin, paclitaxel, docetaxel) (Eliaz and Szoka, 2001; Cho et al., 2011; Xiao et al., 2015; Zhao et al., 2015; Zhong et al., 2015; Byeon et al., 2018) , or siRNA were encapsulated in NPs and targeted to cancer cells (Ganesh et al., 2013b, 2013a; Yang et al., 2015).

Moreover, delivery of the detection signal (e.g. fluorescent substance) into cancer cells with overexpressed CD44 was facilitated by NPs modified with HA (Surace et al., 2009; Choi et al., 2010). The size of the NPs was usually between 100-500 nm, because there is an increased accumulation of particles of that size at the tumor site due to the enhanced EPR effect (Fang et al., 2020).

Alternatively, inorganic CD44 targeted NPs have also been produced for specific diagnosis by MRI. The NPs were usually made of gold or iron oxide (Lee et al., 2013; Li et al., 2014; Karakocak et al., 2018; Sanfilippo et al., 2020). These particles were often significantly smaller in size (~ 16 nm), however a selective NP-cell interaction with cancer cells overexpressing the CD44 receptor was detected (Li et al., 2014). Su et alia (2019) also developed superparamagnetic iron oxide NPs targeted to the CD44 receptor via an anti-CD44 antibody. Nanoparticles selectively killed tumor cells overexpressing the CD44 receptor in alternating magnetic field (Su et al., 2019). HA--modified NPs were extensively tested both *in vitro* on targeting the CD44 overexpressing cancer cells and *in vivo,* usually in xenograft models (Choi et al., 2010; Zhong et al., 2015). Factors affecting *in vitro* and *in vivo* cancer cell targeting by HA will be summarized and discussed in the following text.

In vitro, NPs targeting CD44 are usually tested on NP-cell interaction via fluorescence microscopy, flow cytometry, or are tested on intracellular localization by confocal scanning light microscopy. Usually cancer cells overexpressing the CD44 receptor are incubated with the NPs for a selected time and then the fluorescent signal is detected. Also, to confirm that NPs enter the cells via the CD44 receptor a competitive cell-binding assay is usually performed. Hereby either an anti-CD44 antibody blocks the HA binding site or excess of free HA is delivered and competes with HA-NPs CD44 binding (Surace et al., 2009; Choi et al., 2010). In these experiments, various factors that can affect the NP-cell binding rate have been studied.

Among these factors are HA Mw, cell surface coverage by HA, NP size, the length of incubation time of NPs with cells, NP concentration used for incubation with cells, the free HA concentration used for receptor competitive cell-binding assay, pre/co-incubation of NPs and free HA with cells and the cell type. Examples of the CD44 targeting studies including some of the mentioned factors affecting the studies are summarized in Table 1.

It has been proven that high Mw HA has higher affinity for the CD44 receptor than low Mw HA. This was shown in various studies testing more different HA Mw on NPs. Three different HA Mw (7, 63, 102 kDa) used as targeting moiety on NPs were compared for cancer cell targeting. It would be expected that due to the highest Mw, 102 kDa HA-NPs would provide the highest signal in NP-cell interaction. Even though 102 kDa Mw provides the highest CD44 binding affinity, the highest NP-cell interaction was detected for 63 kDa HA (Zhong et al., 2019). In the study, it was explained that both HA-CD44 binding affinity and HA-NPs-induced clustering of CD44 receptors depended on HA Mw. However, although HA with the highest Mw has the highest binding affinity for the CD44 receptor, due to multivalent binding to the receptors it triggers their clustering. As a result, there are fewer receptors available to interact with other HA modified NPs.

Also, Li et alia in 2014 attached HA onto magnetic iron oxide NPs. Two HA Mw were tested: ~6 kDa and ~31 kDa; higher Mw HA caused lower surface coverage by HA. It was suggested that due to a large size of HA some areas were inaccessible for conjugation (Li et al., 2014). It was also shown that multiple CD44 bind to a single HA chain (in high Mw HA) and that HA binding shows an increasing trend with higher HA Mw and with a saturation point at HA Mw ≥ 262 kDa (Wolny et al., 2010).

HA oligomers were also tested in CD44 targeting. In 2001 Eliaz et alia showed that a high copy number of low affinity oligomers on liposomes provided enhanced targeting to murine melanoma B16F10 cells compared to control normal African green monkey CV-1 kidney cells. Oligo HA possess low affinity for the CD44 receptor and *in vitro*, hyaluronan-grafted liposomes showed higher NP-cell interaction with higher HA Mw (Qhattal et al., 2014). Therefore, an appropriate HA Mw should be utilized in similar studies.

Qiu et alia also showed that an increasing degree of substitution in HA-octadecylamine micelles showed decreasing size and higher NP-cell interaction. They propose that the HA carboxyl groups and the size of the NPs matter, with lower size of NPs and higher number of HA available for CD44 interaction showing the highest HA-micelle-cell interaction (Qiu et al., 2016).

Table 1 Summarized factors plausibly affecting the NP-cell interaction and results of competitive cell-binding assay in previously published studies. Free HA indicates non-labeled HA delivered to cells and NPs during competitive cell-binding assay, free HA competes with HA-modified NPs for binding sites at CD44; ↑ indicates overexpressed CD44 ↓ indicates low or no CD44 expression.

Reference	NP type	Cargo	NP size (nm)	HA Mw	Cell types used in NP-cell interaction studies	Incubation with NPs	Pre- or co-incubation with free HA	Free HA concentration (mg/ml)	Results of competitive cell-binding assay
Eliaz and Szoka, 2001	Liposomes	Doxorubicin	110-140 ± 40	oligo HA	↑B16F10 ↓CV-1	3 h, 4 or 37° C	Co-incubation	Increasing HA concentration HA Mw 50 kDa	Maximal free HA concentration: NP-cell interaction comparable to liposomes not containing HA
Surace et al., 2009	Lipoplexes	Plasmid pCMV-luc	250-300	1500 kDa	↑MDA-MB-231 ↓MCF-7	-	-	αCD44 mAb	Decrease of NP-cell interaction on control cell level
Choi et al., 2010	Self-assembled hydrophobically modified HA	Cy5.5	237-424	234.4 kDa	↑SSC-7 ↓CV-1	1.5 h	Co-incubation	10 mg/ml	Decrease of NP-cell interaction on control cell level
Ganesh et al., 2013b	Polymeric	siRNA	~100-300	20 kDa	↑MDA-MB468	12 h	Preincubation	10 mg/ml	NP-cell interaction reduced by 85 % (flow cytometry), by 90 % (fluorescence microscopy)
Zhong et al., 2015	HA-(Lysine methylester)-(Lipoic acid) reduction sensitive	Doxorubicin	152-219	35 kDa	↑MCF-7/ADR	10 h	Preincubation	5 mg/ml	Reduction of anti-tumor activity of NPs when cells pre-treated with free HA

Reference	NP type	Cargo	NP size (nm)	HA Mw	Cell types used in NP-cell interaction studies	Incubation with NPs	Pre- or co-incubation with free HA	Free HA c (mg/ml)	Results of competitive cell-binding assay
Zhao et al., 2015	Mesosporous silica NPs reduction responsive	Doxorubicin	~256	200 kDa	↑ HCT-116 ↓ NIH-3T3	2 h, 4 or 37° C	Preincubation	2 mg/ml	Decrease by half when cells pre-treated with free HA NPs: concentration dependent cellular uptake
Xiao et al., 2015	Polymeric	Campothecin, curcumin	221-269	-	↑ Colon-26	1.5 or 3 h	Co-incubation	5 mg/ml	Reduction by 1/2 after 1.5 h, reduction by 1/6 after 3 h of coincubation with free HA HA-concentration dependent cellular uptake
Li et al., 2016	Liposomes (LPs) x NPs	Doxorubicin	HA-NPs ~ 180; HA-LPs ~ 131	-	↑ B16F10 ↑ A549 ↑ H22 ↓ HK2	2 or 4 h	Co-incubation	10 mg/ml	Differences in reduction due to co-incubation in cell types, usualy by 1/3 max by 1/2 Highest NP-cell interaction after 4 h of NP-cell incubation
Wang et al., 2018	Nanomicelles	Curcumin analogue	129.4	13 kDa	↑ MDA-MB-231 ↑ MDA-MB-468	3 h (fluorescence microscopy)	-	5 mg/ml	Improvement of cell viability after blocking CD44
Zhong et al., 2019	HA grafted - HPCD self-assembled	Doxorubicin	137-140	7; 63; 102 kDa	↑ Hela ↑ H460 ↓ A549 ↓ MCF-7	1 or 3 h	Preincubation	5 mg/ml	Decrease of NP-cell interaction by 1/2, by 1/3 in highest HA Mw NPs

The incubation time can also affect the resulting NP-cell interaction signal. In 2001, Eliaz and Szoka investigated the influence of incubation time on CD44-targeted doxorubicin encapsulating liposome – cell (B16F10) interaction. They have shown that liposome-CD44 interaction shows saturation kinetics and that the interaction first reaches its maximum after two hours of incubation of cells with liposomes (Fig. 5A). This was measured *in vitro*. Nevertheless, the situation can be different with different types of particles (as the size of NPs and HA Mw might differ from liposomes used in Eliaz and Szoka) and in the *in vivo* experiments. Regarding NP concentration in NP-cell incubation assays, various HA-NP studies showed increasing NP-cell interactions with higher concentrations of NPs used for incubation with cells (Xiao et al., 2015; Zhao et al., 2015).
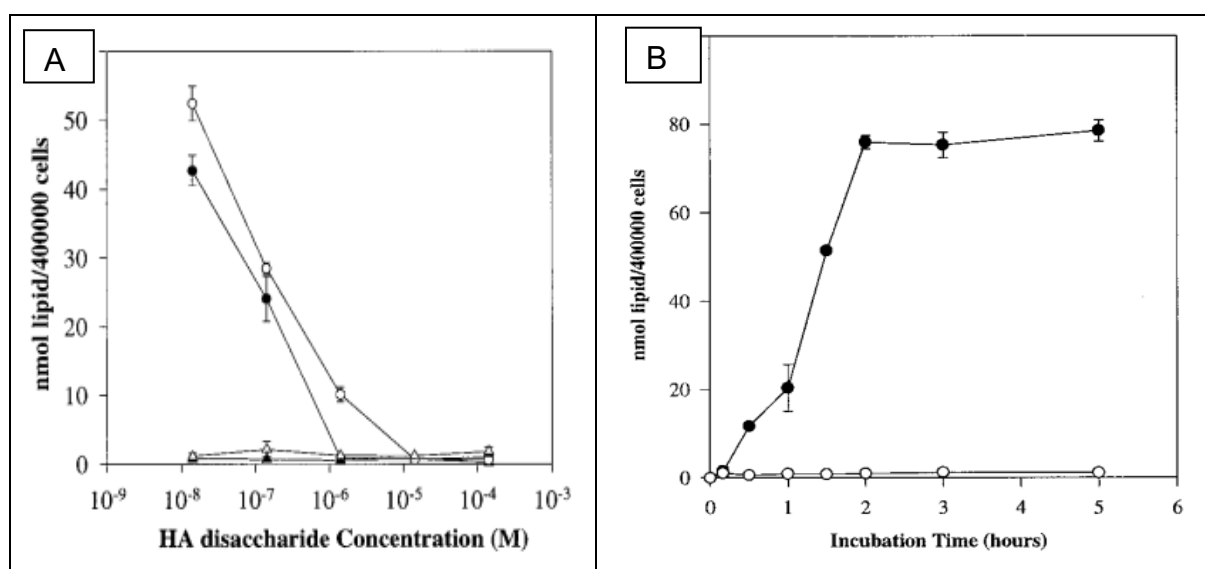

Figure 5 In this figure, results from Eliaz and Szoka, 2001 are shown. A) Reduced liposome NP-cell interaction in the presence of increasing free HA concentration during the competitive cell-binding assay. Dots show HA-containing liposomes, triangles show HA-free liposomes. Full dots and triangles show preincubation with free HA (1 hour prior to incubation of cells with liposomes) and empty dots and triangles show co-incubation of increasing concentration of free HA, with liposomes and cells (3 h, 37° C). As the study worked with HA oligomers attached to liposomes, the HA concentration is shown as concentration of HA-disaccharide equivalent in the polymer. B) the interaction of liposomes with B16F10 cells dependent on incubation time, liposomes containing HA (full dots) compared to liposomes not containing HA (empty dots), the maximum is reached after 2 h of incubation.

Furthermore, in 2001 Eliaz and Szoka also tested increasing concentration of free HA used in the competitive cell-binding assay and they showed a reducing trend of liposome-cell interactions with higher concentration of free HA being present in the incubation of free HA and NPs with the cells. The highest reduction of liposome-cell interactions was comparable to the non-HA-containing liposomes-cell interactions (Fig. 5B).

The interaction of HA-CD44 is strong. Thus, it is necessary to provide a high excess of free HA in the competitive cell-binding assay (Eliaz and Szoka, 2001).

It has also been shown, that different cell types might possess different affinity of the CD44 receptor towards hyaluronan (Lesley et al., 1995). These differences were proposed to be the result of N-glycosylation of the CD44 receptor. Conformational changes might affect the affinity too (English et al., 1998; Skelton et al., 1998). It is expected, that CD44 possesses two conformational states; A and B, and conformation B is stabilized by HA binding (Vuorio et al., 2017). It has also been shown that the NP binding ability of the cancer cells might be affected by the aggregation of the CD44 receptors. Hence high Mw HA can trigger aggregation of the CD44, while oligo HA cannot (Sleeman et al., 1996; Wolny et al., 2010; Yang et al., 2012). This has already been shown for another HA-binding receptor, LYVE-1 (Lawrance et al., 2016).

The drug delivery of HA-modified NPs was also tested *in vivo* on tumor xenograft models (Nair et al., 2011; Zhong et al., 2015) and compared to *in vitro* experiments. Additional factors have been shown to be important. *In vivo*, it is of great importance that NPs are non-toxic, stable, can reach specifically the target cells (the circulation time is essential) and that the encapsulated drug is released at the target site. Some drawbacks of this issue were also presented in HA-CD44 targeting research. In hyaluronan-modified liposomes *in vivo* tumor targeting experiments, it was shown that attachment of HA negatively affects the circulation time of the liposomes, with higher Mw HA liposomes (175-350 kDa) cleared faster from the circulation than lower Mw liposomes (5-8 kDa; 50-60 kDa). Therefore, PEG was also co-attached on the surface of liposomes to enhance the circulation time (Qhattal et al., 2014). Regarding the issue of drug release at target site, various types of NPs were prepared to release the content in cell. Among the most interesting is the reduction-sensitive release, where release is triggered by the reducing environment in the cytoplasm, causing the reduction of the SS bonds in NPs (tested *in vitro* in Zhao et al., 2015; Rezaei et al., 2020; Zhang et al., 2020) (and also *in vivo* in mice in Zhong et al., 2015; Hu et al., 2016)

2.3 Mouse Polyomavirus Virus-Like Particles

Virus-like particles are structures reminiscent of the native viruses, which are usually formed only by viral structural proteins. Mouse polyomavirus (MPyV) is a small tumorigenic non-enveloped dsDNA virus. Its genome encodes early non-structural and late structural proteins. The main structural protein of MPyV, VP1, can be produced via various expression systems (mammalian, yeast, insect and prokaryotic) (Pattenden et al., 2005). In this study, the VP1 protein was produced via the baculovirus expression system. Hereby the produced VP1 protein alone is capable of self-assembly into virus-like particles, hence VLPs (Fig. 6) (Montross et al., 1991). The VLPs have a diameter of around ~45-50 nm and are capable of disassembly and re-assembly (Polidarová, 2016). Due to their origin, VLPs are non-toxic and biodegradable, and so they have the potential to be used as nanoplatforms for drug delivery, diagnostic or both (as theragnostic agents). VLPs have already been studied as gene delivery nanocarriers and as vaccine platforms (Forstová et al., 1995; Fraiberk et al., 2017).
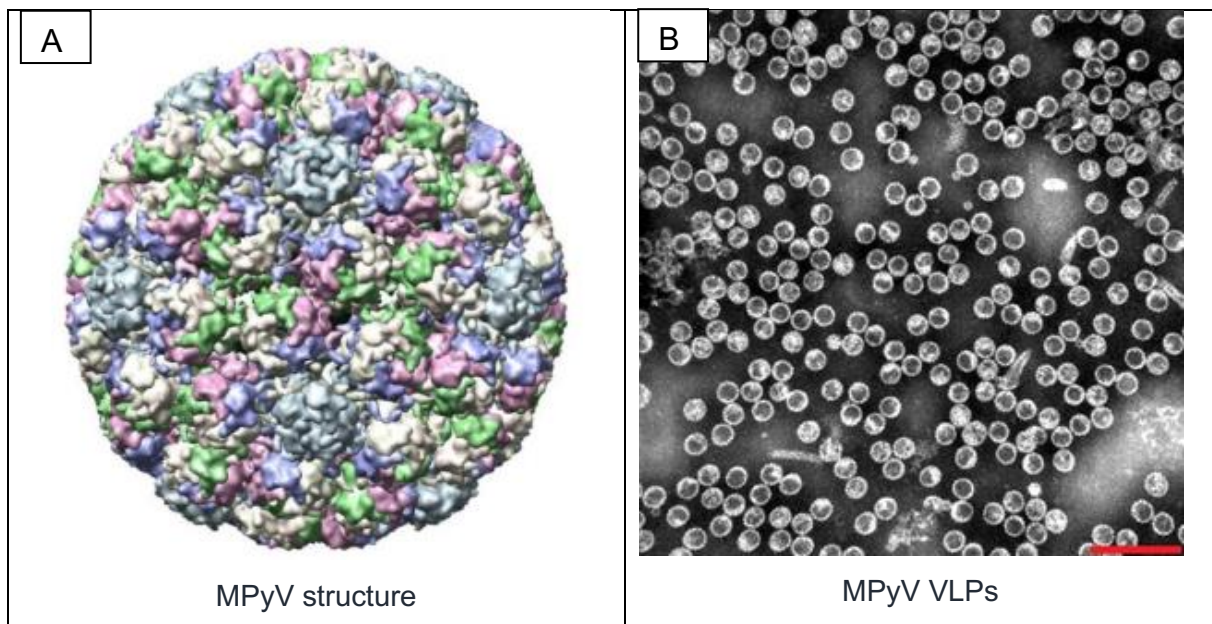

A	B
MPyV structure	MPyV VLPs

Figure 6 Figure shows A) Protein data bank ´1sie´ X -ray crystallography structure of MPyV viral capsid; 3,6 Å (Stehle and Harrison, 1996). And B) shows MPyV VLPs micrograph with negative staining acquired by transmission electron microscopy – fraction 4 from MPyV VLP isolation 4. Scalebar represents 200 nm.

Gangliosides (glycosphingolipids containing sialic acid) are the natural receptors for MPyV VP1. However, they are omnipresent on the surface of most cell types, mainly the cells of the nervous system (Smith et al., 2003; You et al., 2015). This is a major drawback in the use of VLPs as nanocarriers, as the interaction of VLPs with cells is very broad.

Nonetheless, surface lysines of VLPs can be chemically modified and a targeting moiety can be conjugated onto the surface of the VLPs. Hereby, the moiety might provide both, shielding the broad VP1-mediated cell interactions and active targeting to a specific receptor. On VLPs, this was already tested in 2017 by Zackova Suchanova et alia, as transferrin was conjugated onto the surface of VLPs (Zackova Suchanova et al., 2017). The transferrin receptor is overexpressed on many cancer cell types. Thus, transferrin is broadly studied as a cancer cell targeting moiety (Calzolari et al., 2007; Chan et al., 2014). Nevertheless, despite that HA is extensively studied as a cancer cell targeting moiety, it has not yet been tested on VLPs and therefore, it will be the focus of this study.

3. Aims and Objectives

MPyV VLPs could be potentially used as a theragnostic tool. However, their interaction with cells is mainly determined by the VP1-mediated interaction with sialic acid containing receptors. The long-term goal of the research in the laboratory of virology is to develop VLPs with the binding specificity to cancer-specific receptors. This could be achieved by using a targeting agent.

HA has been used in many studies as a targeting agent for NPs to cancer cells overexpressing the CD44 receptor. An interesting strategy for HA conjugation to NPs has been developed by the collaborating Laboratory of Synthetic Nanochemistry from the IOCB that produced another type of biocompatible NPs, nanodiamonds (NDs), that were also conjugated with HA (ND-HA*). To our knowledge, HA has not yet been conjugated as a targeting moiety onto the surface of MPyV VLPs, nor was such conjugate tested on interactions with CD44 overexpressing cancer cells.

By using the same strategy as was used for ND-HA*, we intended to modify MPyV VLPs with HA. Hence the main specific aims of the diploma project were:

    i.   ***To determine whether the VLPs modified by HA (VLP-HA*) can be re-targeted from the natural receptor to CD44 on cancer cells;***

    ii.   ***To compare VLP-HA* with ND-HA* nanoparticles in their targeting potential to CD44***

These specific aims were addressed in two main sub-goals:

    I.   To produce fluorescently labeled MPyV VLPs with attached HA and concurrently also control VLPs

    II.   To test the interaction of VLP and ND variants with cancer cells overexpressing the CD44 receptor, specifically with the MDA-MB-231 cells

4. Study Design

The procedure of the current thesis is summarized in figure 7 and was briefly as follows: MPyV VP1 VLPs were produced, the surface of the VLPs was chemically modified by Propargyl-N-hydroxysuccinimidyl ester linker (alkyne linker), resulting in "VLPs-alkyne" that contain alkyne functionality. To assess the number of alkyne linkers attached per VLP, VLPs-alkyne were characterized by conjugation with a fluorescent probe, Alexa Fluor™ 488 azide (Af488). Conjugation was performed via Cu^I-catalyzed Alkyne-Azide cycloaddition ("click chemistry"). The number of Af488 molecules bound per VLP-alkyne was estimated and thus the number of alkyne-linker molecules bound per VLP was calculated.

VLP-alkyne was further used for conjugation of the Bodipy fluorescent dye (containing azide functionality) (Bp) prepared by Jan Bartoň (IOCB), or Bp-conjugated HA (HA*) or Bp-conjugated PEG (PEG*) (both molecules: HA* and PEG* were prepared by Jitka Nebůrková, IOCB). Hereby three types of VLP constructs were produced; VLP-alkyne with conjugated Bp (VLP-Bp), VLP-alkyne with conjugated HA* (VLP-HA*) and VLP-alkyne with conjugated PEG* (VLP-PEG*).

HA should provide the VLPs with a shielding capacity from the VP1-mediated interactions and moreover, provide a re-targeting capacity from VP1 specific receptors to the CD44 receptor, that is often overexpressed on cancer cells. Therefore, the three types of VLP constructs were tested on interactions with the human breast cancer MDA-MB231 cells (MDA cells), which overexpress CD44. The NP-cell interactions were tested via incubation of the MDA cells with the three types of VLP constructs or with their counterparts, another type of NPs, nanodiamonds with Bp (ND-Bp) or HA* (ND-HA*) conjugated, that were produced by Jitka Nebůrková (IOCB).

To determine whether the NPs interact with the cells via the CD44 receptor, the competitive cell-binding assay was performed; the MDA cells were incubated with a mixture of non-labeled (free HA) and NPs. Free HA would compete for the HA-binding sites at CD44 receptors with NPs and reduce NP-cell interactions, if NPs enter the cells mainly via the CD44 receptors.
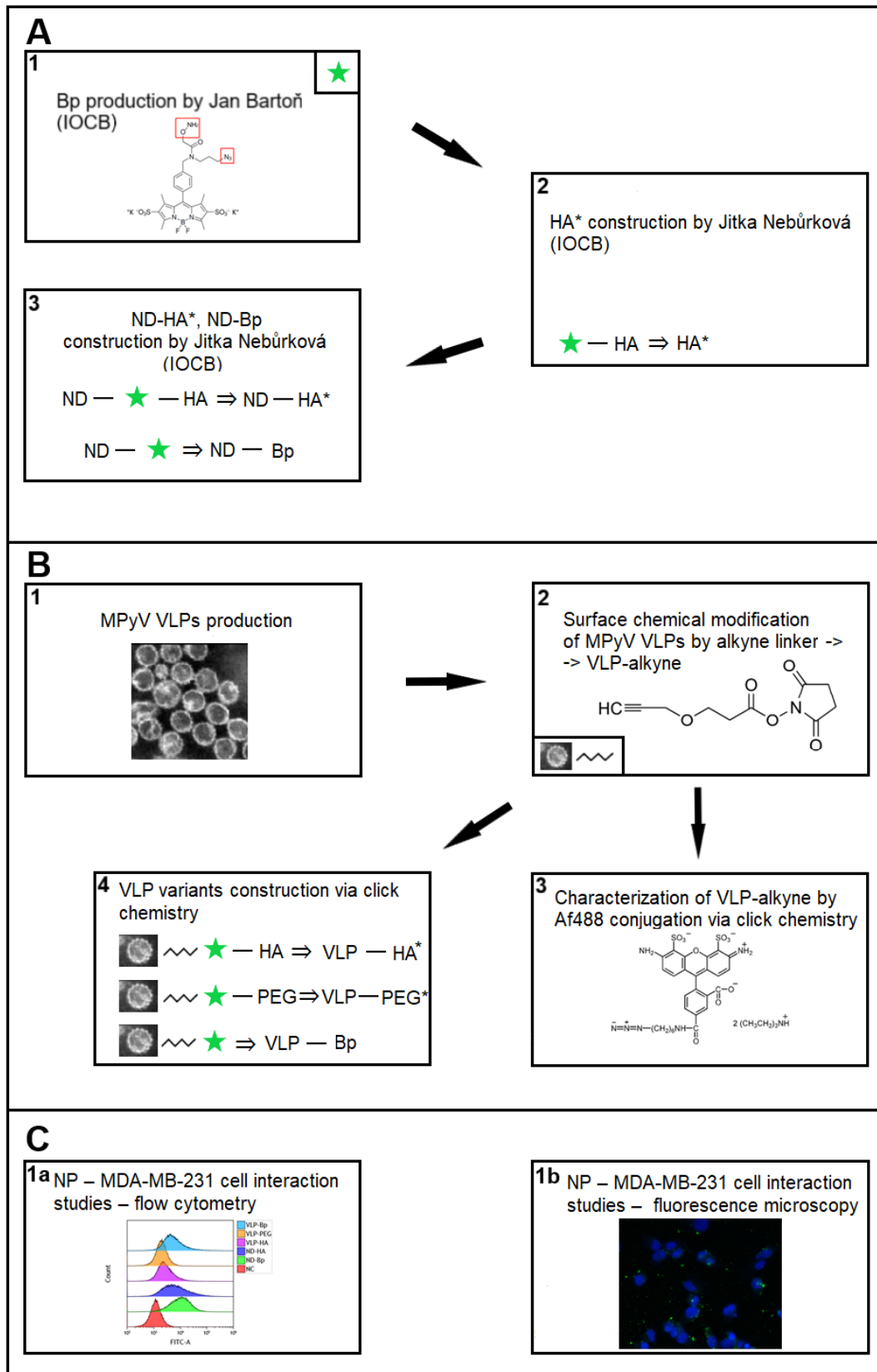
Figure 7 Summary of the study design in the current thesis: A) shows steps prepared by 1 – Jan Bartoň (IOCB), 2+3 – Jitka Nebůrková (IOCB), B) shows VLP variants production and C) shows NP-cell interaction experiments, where both ND and VLP variants were tested on interaction with MDA cells. B+C were performed in this thesis. Green stars indicate heterobifunctional fluorescent dye Bodipy (Bp) and ∿ indicates alkyne linker.

5. Materials and Methods

5.1 Materials

5.1.1 Laboratory Equipment

Centrifuge GS-15R (Beckman Coulter®, USA)

Centrifuge (MSE, UK)

Centrifuge Universal 320R (Hettich, Germany)

Centrifuge Microfuge® 16 (Beckman Coulter®, USA)

Ultracentrifuge optima TM L-90K (Beckman Coulter®, USA)

Rocker Duomax 1030 (Heidolph, Germany)

Sonicator Q500 (Qsonica, USA)

Sonicator UP50H (Dr. Hielscher GmbH, Germany)

Fraction recovery system (Beckman Coulter®, USA)

Refractometer ABBE (Carl Zeiss Jena, DDR)

Shaker (Bio-Rad, USA)

Shaker 30 (Labnet, USA)

Fusion-FX6.EDGE V.070 (Vilber, France)

Qubit® fluorometer (Invitrogen, USA)

Transmission electron microscope JEOL JEM 1200EX (JEOL, Japan)

Molecular imager Fx (Bio-Rad, USA)

Fluorescent microscope BX60F-3 (Olympus, Japan)

Rotator YC-80 (Miulab, China)

Epoch™ Microplate Spectrophotometer (BioTek Instruments, USA)

Spectrophotometer Specord 250 (Analytik Jena, Germany) – measurement performed by Jitka Nebůrková (IOCB)

SDS-PAGE Mini-PROTEAN® Tetra System (Bio-Rad, USA)

Western Blot Apparatus (Bio-Rad, USA)

Bürker Chamber Assistant (BLAUBRAND®, Germany)

Thermobox LBT 165 (Zanussi, Italy) - for Sf-9 cells incubation

Thermobox Sartorius Stedim (BioTech, Germany) - for MDA-MB-231 cells incubation

Dry Block Heating Thermostat BioTDB-100 (Biosan, Latvia)

Scales Pioneer™ (OHAUS®, China)

Scales Kern 440-33 (Kern&Sohn, Germany)

Magnetic Stirrer MST (VELP®Scientifica, Italy)

Vortex Genie-2 (Scientific Industries, USA)

Laminar Box 1201 (Forma Scientific, USA)

5.1.2 Software

Microplate data collection and analysis software: Gen5 1.10 (BioTek, USA)

Imaging software itTEM 5.1 (Olympus soft imaging solutions, Germany)

Fluorescence analysis software Quantity One 4.6.9 (Basic) (Bio-Rad, USA)

Flow cytometry data analysis software: Kaluza Analysis 2.1 (Beckman, USA)

Imaging software: NIS-Elements AR 2.30 (Nicon®, USA)

GraphPad Prism 8 (GraphPad software, USA)

5.1.3 Frequently Used Solutions and Chemicals

TNM - FH Insect medium (Sigma-Aldrich, USA)

TNM - FH Insect medium with serum:

TNM - FH Insect medium (Sigma-Aldrich, USA)

10 % Fetal bovine serum (Gibco™ Thermo Fisher Scientific, USA)

1/100 (v/v) Antibiotic mixture

Antibiotic mixture (Gibco™ Thermo Fisher Scientific, USA)

100x concentrated solution in 1 ml:

10 000 units of penicillin

10 mg streptomycin

25 mg amphotericin B (Gibco™ Thermo Fisher Scientific, USA)

Phosphate buffered saline (PBS):

10 mM Na_2HPO_4 (Penta, Czech Republic)

137 mM NaCl (Lach-ner, Czech Republic)

2.7 mM KCl (Lachema, Czech Republic)

1.8 mM Kh_2PO_4 (Lach-ner, Czech Republic)

pH 7.4

Buffer B:

150 mM NaCl (Lach-ner, Czech Republic)

10 mM Tris-HCl, pH 7.4 (Serva Electrophoresis, Germany)

0.01 mM $CaCl_2$ (Sigma-Aldrich, USA)

Cesium chloride (Carl Roth GmbH, Germany)

Paraffin oil (Carl Roth GmbH, Germany)

Dried milk (Aditiva, Czech Republic)

Developing solution (1:1 A:B)

    A:

        2 ml Tris-HCl 0.1 M, pH 8.5: Tris-(hydroxymethyl)-aminomethane in ddH_2O (Penta, Czech Republic), pH adjusted with HCl (Lachner, Czech Republic)

        200 µl 250 mM Luminol/DMSO (Sigma Aldrich, USA)

        80 µl 90 mM p-coumaric Acid/DMSO (Sigma Aldrich, USA)

    B:

        2 ml Tris-HCl 0.1 M, pH 8.5 (Penta, Czech Republic)

        18 ml dH_2O

        12 µl 30 % H_2O_2 (Sigma Aldrich, USA)

Sucrose (Lach-Ner, Czech Republic)

Phospowolframic acid 2 % (Sigma-Aldrich, USA)

HEPES (Sigma-Aldrich, USA)

Propargyl-N-hydroxysuccinimidyl ester linker (Sigma-Aldrich, USA)

DMSO (Penta, Czech Republic)

Alexa Fluor™ 488 azide 10 mM (Life Sciences™ Thermo Fisher Scientific, USA)

BTTP - Mw 430.56 (from Petr Cígler Nanochemistry group, IOCB)

$CuSO_4·5H_2O$ (Sigma-Aldrich, USA)

Sodium Ascorbate (Sigma-Aldrich, USA)

Amoninoguanidin.HCl (Sigma-Aldrich, USA)

Versen 0.02 % in PBS (Sevac, Czech Republic)

Trypsin 0.25 % in PBS (Sigma-Aldrich, USA)

Iscove's Modified Dulbecco's Medium (Sigma Aldrich, USA) (IMDM medium)

IMDM medium with serum:

    IMDM medium (Sigma Aldrich, USA)

    10 % Fetal bovine serum (Gibco™ Thermo Fisher Scientific, USA)

    GlutaMAX™ Supplement (Gibco™ Thermo Fisher Scientific, USA)

Soybean trypsin inhibitor (Gibco™ Thermo Fisher Scientific, USA)

BSA 0.5 % (Sigma-Aldrich, USA)

DAPI (Sigma-Aldrich, USA)

Paraformaldehyde 3.7 % (Sigma-Aldrich, USA)

Triton X-100 0.5 % (Serva Electrophoresis, Germany)

Glycerol (Lach-Ner, Czech Republic)

5.1.4 Nanoparticles

ND-HA* (10 mg/ml) - Nanodiamonds with Bodipy and HA (Mw 8-15 kDa) attached by click chemistry, produced by Jitka Nebůrková, IOCB

ND-Bp (5 mg/ml) - Nanodiamonds with heterobifunctional Bodipy attached, produced by Jitka Nebůrková, IOCB

5.1.5 Cell Lines and Viruses

SF9 Cell line: *Spodoptera frugiperda* ovarian cells

MDA-MB-231 cell line (ATCC® HTB-26™): human breast adenocarcinoma cells

MPyV VP1 expressing recombinant baculovirus (Rec Bac VP1): VP1 gene was derived from MPyV - BG strain (GenBank accession number: AF442959), prepared with the use of the Bac-to-Bac system (Thermo Fisher Scientific, USA; cat.nr.10359016) by M. Marek (Marek, 2007).

5.1.6 Commercial Kits

Qubit® Protein Assay Kit (Invitrogen, USA)

5.1.7 Molecular Markers

Spectra ™ Multicolor Broad Range Protein Ladder (Thermo Fisher Scientific, USA) (shown in figure 8)
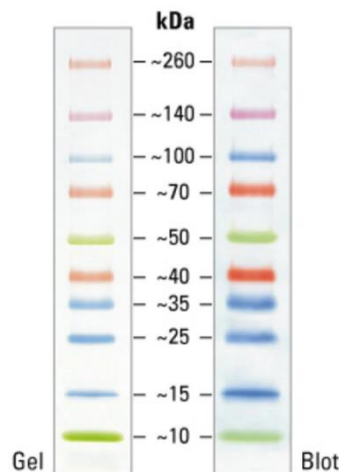

Figure 8 Spectra ™ Multicolor Broad Range Protein Ladder (Thermo Fisher Scientific, USA)

5.1.8 Antibodies

Primary antibody: Mouse monoclonal IgG antibody anti-MPyV VP1, dilution 1:100 (Forstova et al., 1993)

Secondary antibody: Horse radish peroxidase conjugated goat antibody anti-mouse IgG, FC fragment specific, dilution 1:1000 (Bio-Rad, USA)

5.1.9 Other Laboratory Material

Petri Dish (d = 60 mm) (BioFil, Hungary)

Petri Dish (d = 150 mm) (BioFil, Hungary)

Conical Centrifuge Tubes (BioFil, Hungary)

Polypropylene Centrifuge Tubes (Beckman Coulter®, USA)

Nitrocellulose Membrane Amersham™ Protran™ 0.45 µm NC (GE Healthcare Life Sciences, Germany)

Dialysis Tubing MWCO (d = 16 mm) 12000-14000 Servapor® (Serva Electrophoresis, Germany)

Dialysis Tubing MWCO (d = 6 mm) 12000-14000 Servapor® (Serva Electrophoresis, Germany)

Copper Grids FCF200-CU (Electro Microscopy Sciences, USA)

Centrifuge Tubes ART.00279-00 (Kartell Spa, Italy)

Amicon® Ultra, 15 ml, 100K (Merck Millipore, Ireland)

Amicon® Ultra, 0.5 ml, 30K, (Merck Millipore, Ireland)

Parafilm PN-996 (Bemis, USA)

12-Well plate (TPP, Switzerland)

24-Well plate (BioFil, Hungary)

Microtitration plate (Gama, Czech Republic)

FACS Centrifugation tubes (Sarstedt, Germany)

Microscope Slides (Knittel Glass, Germany)

Microscope Cover Glasses 12 mm (VWR, Germany)

5.2 Methods

5.2.1 MPyV VLP-HA* and Control Production

5.2.1.1 MPyV VP1 VLPs Production

For each VLP preparation, approx. $9.6*10^7$ Sf9 cells were used. Before infection, the cells were freshly seeded: the Sf9 cells from the Petri dishes (d = 60 mm) with cells grown to confluency were scraped and transferred onto a new Petri dish (d = 150 mm) in serum-free TNM-FH insect medium. The cells were left to attach to the dish in a thermostat (1.5 h, 27° C). The medium was aspirated, and the cells were infected with RecBac VP1 inoculum (3 ml) with multiplicity of infection approx. 10 pfu/cell. The cells were placed on a rocker (1 h, RT). After adding the virus, medium containing fetal bovine serum and antibiotics was added (22 ml) to the Petri dish and the cells were cultivated in a thermostat in 27° C. The cells were harvested seventy-two hours post infection. Briefly, the cells were scraped into conical centrifuge tubes (50 ml) and centrifuged (1500x g, 5 min, RT). The supernatant was discarded, and the pellet was washed with PBS, centrifuged (1500x g, 5 min, RT) and stored (-20° C).

The pelleted Sf9 cells were lysed by sonication on ice (2 mm probe, 4 x 45 s, 30 s break, 40 % amplitude) and centrifuged (4300 rpm, 10 min, 4° C). The supernatant was transferred to a clean ultracentrifugation tube and the samples were further purified by isopycnic ultracentrifugation in cesium chloride gradient (SW41, 35000 rpm, 20 h, 18° C) (Ultracentrifuge Optima TM L-90K, Beckman) (see 5.2.1.2).

The samples were subsequently divided into subfractions and analyzed. Refractive indices of the subfractions were measured and Immunodot blot was performed (see 5.2.1.3). The subfractions were merged based on the refractive indices and the Immunodot blot signal (as indicated in the Results 6.1.1), dialyzed against buffer B (72 h, 4° C, 1.5 l; buffer changed once after 1 h) and concentrated through a sucrose cushion (See 5.2.1.4). After centrifugation, the supernatant was carefully discarded and the pelleted material was resuspended in an appropriate buffer (usually buffer B, 200 µl). Due to aggregates persisting, the samples were shortly sonicated on ice and the protein concentration was measured by Qubit (Qubit® Fluorometer, Invitrogen) (See 5.2.1.5). The samples were analyzed by transmission electron microscopy (TEM) (See 5.2.1.6) and stored at -20° C.

5.2.1.2 Purification by Cesium Chloride Gradient

The cell lysates were centrifuged (SW41, 4300 rpm, 10 min, 4° C) and the supernatant was transferred to a clean ultracentrifugation tube. Buffer B was added to the supernatant, to reach 8 g and 3.7 g of cesium chloride were added. The refractive index was measured to be 1.364-1.365. Paraffin oil was layered on top of the samples, and the samples were centrifuged in the ultracentrifuge Optima TM L-90K (SW41, 35000 rpm, 20 h, 18° C).

5.2.1.3 Immunodot Blot and Chemiluminescence Detection

2 µl of vortexed sample were loaded on a nitrocellulose membrane. After drying, the membrane was blocked in 5 % low fat dry milk in PBS (1 h, RT). The primary antibody was added, and the membrane was incubated on a shaker (1 h, RT). The membrane was washed three times by PBS (10 min, RT, shaker). The secondary antibody was added, and the membrane was incubated on a shaker (30 min, RT). Next, the membrane was washed three times by PBS (10 min, RT, shaker), PBS was discarded, the membrane was developed using the developing solution and the chemiluminescent signal was detected by Fusion-FX6.EDGE V.070.

5.2.1.4 Concentration of Samples by Ultracentrifugation through Sucrose Cushion

The samples in an appropriate buffer (e.g. buffer B) were collected into clean ultracentrifugation tubes. The appropriate buffer (e.g. buffer B) was added to the ultracentrifugation tubes and 10 % (alternatively 20 %) sucrose was layered under the sample. The samples were concentrated by ultracentrifugation (SW41, 35000 rpm, 18° C, 3 h) in ultracentrifuge Optima TM L-90K.

5.2.1.5 Protein Concentration Measurement by Qubit®

Qubit® working solution was prepared by diluting the Qubit® Protein Reagent 1:200 in Qubit® Protein Buffer. 190 µl of Qubit® working solution was added to each of the tubes used for standards, 10 µl of each Qubit® standard was added to the appropriate tube and tubes were mixed by vortexing. Qubit® working solution was added to individual assay tubes with the samples (usually separately 2 µl non-diluted and 2 µl of 10x diluted samples) so that the final volume in each tube after adding the sample was 200 µl. The samples were mixed by vortexing, incubated (15 min, RT) and the protein concentration was read by Qubit®.

5.2.1.6 Transmission Electron Microscopy - Negative Staining

The samples were shortly vortexed and 5 µl of the samples were transferred onto parafilm. Electron microscope grids were laid on top of the samples and incubated with the samples (10 min, RT). The grids were transferred onto filtered ddH$_2$O (two times 100 µl) (two times 1 min, RT) and then onto 2 % phosphotungstic acid (two times 50 µl) (two times 30 s, RT). Afterwards, samples were observed via transmission electron microscopy by the JEOL JEM-1011 microscope with CDD camera and electron micrographs were acquired using the itTEM 5.1 imaging software.

5.2.1.7 VLP-alkyne Construction

Fractions of VLPs from multiple isolation experiments with the best preserved integrity were thawed on ice, merged for further experiments (Results – Table 6), dialyzed against HEPES buffer (0.1 mM, pH 7.9, 48 h, 4° C, buffer changed 3 times: 0.5 l, 0.5 l, 1.5 l) and transferred to a clean Eppendorf tube (5 ml). VLPs were further used for the conjugation of a Propargyl-N-hydroxysuccinimidyl ester linker. As it was proposed in earlier studies, 35-molar excess of MPyV VP1 VLP surface lysines of alkyne linker (Sigma Aldrich) was added to the sample (10 % DMSO) (Zackova Suchanova et al., 2020).

35-times molar excess of MPyV VP1 VLP surface lysines was determined as follows: Briefly, the number of particles in the sample was calculated by dividing total protein content weight by the weight of 1 VLP ($2.69*10^{-14}$ mg). To obtain the total number of exposed lysines, the number of particles in the sample was multiplied by 720 (number of surface lysines/VLP). Next, the amount of substance of the total surface lysines was calculated by dividing the total number of exposed lysines by the Avogardo constant. The amount of substance of the total surface lysines in the sample was multiplied by 35. After adding the appropriate amount of alkyne linker, the sample was incubated at a rotator (24 h, RT) (Rotar, Miulab).

The sample was dialyzed against HEPES buffer (0.1 mM, pH 7.4, 48 h; first 2 changes 10 % DMSO, 0.5 l, 0.5 l 1.5 l) and concentrated (Amicon®Ultra, 15 ml, 100K, Merck Millipore) (3*10 min, 5000x g, RT), Amicon tubes were washed to prevent sample losses. Protein concentration was measured by Qubit® (See 5.2.1.5) and samples were stored (-20° C).

5.2.1.8 Characterization of VLP-alkyne Constructs – Af488 Conjugation via Click Chemistry

To determine the number of available alkyne groups on VLPs, a control reaction was performed using conjugation of Af488 fluorescent dye onto a small amount (60 µg) of VLP-alkyne via click chemistry. The reaction was run in total volume of 100 µl and the molar ratio of reagents was kept the same as in Besanecey-Webler et alia from 2011 as follows: Molar ratio - Alkyne : BTTP : CuSO4 : sodium ascorbate; 1:5:2.5:25. Moreover, the molar ratio of protein to Af488 was 1:100 as determined in (Hustedová, 2019).

The reaction was performed as follows: 60 µg of protein were added to a clean centrifuge tube, ddH_2O, 10 mM Af488 were added and the sample was gently mixed by a pipette, 5 mM $CuSO_4 \cdot 5H_2O$ with 50 mM BTTP ligand were added and the samples were gently resuspended. Furthermore, 10 mM Aminoguanidin·HCl was added. Lastly, 100 mM sodium ascorbate was added, the samples were resuspended, sealed with parafilm, covered by aluminium foil and left in dark for incubation (2 h, RT).

The sample was dialyzed against buffer B (4° C, 24 h; 0.5 l, 0.5 l, 1.5 l), washed by buffer B (5 times) (Amicon®Ultra, 0.5 ml, 30K, Merck Millipore) (14000x g, RT, five times 4 min). The protein concentration was determined by Qubit® (See 5.2.1.5) and the samples were analyzed by TEM (See 5.2.1.6). The number of Af488 molecules bound per VLP was determined from absorbance measurement of labeled VLPs (See 5.2.1.9 and 5.2.1.10).

5.2.1.9 Absorbance Measurement

The samples were vortexed and 60 µl per well were applied per well in a microtitration plate. Absorption spectra were measured (300 – 900 nm, alternatively 300-700 nm) by Epoch™ microplate spectrophotometer. Data were collected and analyzed by microplate data collection and analysis software: Gen5 1.10.

5.2.1.10   Determination of the Number of Dye Molecules per VLPs from Absorption Spectrum

The number of dye molecules per one VLP was calculated from a linear equation after subtracting the VLP scattering from the VLP-dye absorption spectrum as follows:

First, dye dilution and determination of factor were performed. A 50x dilution series of dye was prepared, and the absorbance spectra of the individual dilutions were measured by Epoch™ Microplate spectrophotometer (60 µl; 300-700 nm). The OD values at dye absorbance maximum (488 nm for Af488; 498 nm for Bp) were plotted against the concentrations of the dilutions and a linear regression curve was added. The factor was acquired from the equation for further calculations of number of dye (Bp, Af488) molecules bound per VLP.

Next, the absorption spectra of the fluorescently labeled samples were measured by Epoch™ Microplate spectrophotometer (60 µl; 300-900 nm) (see 5.2.1.9). The calculations of the number of dye molecules bound per VLP are summarized in table 2. The peak at dye maximum (488 nm for Af488; 498 nm for Bp) of the absorption spectrum curve of VLP labeled samples was measured (A $_{Dye\,max}$), and the difference at the dye maximum wavelength compared to non-fluorescent control (A $_{NC}$) was calculated (assigned as A $_{Peak\,size}$). Furthermore, the peak size absorbance was divided by the factor from the dye dilution standard curve (0.0902 for Af488, 0.0948 for Bp) to calculate the x unknown of the regression curve equation. Subsequently, the weight of dye in sample was calculated by multiplying the x unknown by the volume of the measured sample.

$y = factor*x$ A $_{Dye\,max}$ − A $_{NC}$ = A $_{Peak\,size}$ A $_{Peak\,size}$/ factor = x m $_{dye\,in\,sample}$ (µg) = x * V $_{sample}$ n $_{dye\,in\,sample}$ = m $_{dye\,in\,sample}$ * 10^{-6}/Mw $_{dye}$ N $_{dye\,molecules\,in\,sample}$ = n $_{dye\,in\,sample}$ * N$_A$ N $_{VLPs\,in\,sample}$ = V $_{sample}$ * c (µg/ml) * N $_{number\,VLPs\,in\,1\,µg}$ N $_{dye\,molecules/\,1\,VLP}$ = N $_{dye\,molecules\,in\,sample}$ / N $_{VLPs\,in\,sample}$	<u>Af488 (A max at 488 nm):</u> y = 0.0902x Mw = 825.46 <u>Bp (A max at 498 nm):</u> y = 0.0948x Mw = 668 V $_{sample}$ = 0.06 ml N $_{number\,VLPs\,in\,1\,µg}$ = $3.71*10^{10}$

Table 2 Summary of the calculation of the dye molecules number bound per 1 MPyV VP1 VLP in the left. And equations obtained from the regression curves in the first step – dye dilution, standard curve preparation, providing the factor for each dye type.

Next, the amount of substance of the dye was calculated by dividing the weight of the dye in sample by the molecular weight of the dye (Af488 825.46; Bp 668). The number of dye molecules in sample was calculated by multiplying the amount of substance of the dye by the Avogadro constant. The number of VLPs in the sample was calculated by multiplying the volume of the sample by the concentration of the protein in the sample and by the number of VLPs in 1 µg ($3.71*10^{10}$). And finally, the number of the molecules of the dye per VLP was calculated by dividing the number of the dye molecules in the sample by the number of VLPs in the sample. The number of alkyne linkers conjugated per VLP was estimated to be equal to the number of Af488 molecules bound per VLP.

5.2.1.11   Click Reaction – VLP-HA*, VLP-PEG*, VLP-Bp Construction

<u>Materials</u>

HA (Mw 8-15 kDa) (Contipro, Czech Republic)

Heterobifunctional Bodipy (produced by Jan Bartoň, IOCB)

HA* (produced by Jitka Nebůrková, IOCB from Contipro HA)

PEG* (produced by Jitka Nebůrková, IOCB from PEG Mw 20 kDa – Jenkem, USA)

The stock of VLP-alkyne sample was used for conjugation of HA* or PEG* or Bp. All three compounds contain the azide functionality. In VLP-HA* and VLP-PEG* production, 1.5 mg of VLP-alkyne was used for conjugation of HA* (Mw 8-15 kDa) or PEG* (Mw 20 kDa) via click reaction using a final molar ratio in reaction 1:1.125 (azide:alkyne). Ratios of the other reagents and the procedure were the same as in click reaction in VLP-alkyne characterization (See 5.2.1.8).

Since the low molecular weight Bp reacts with different efficiency during click reaction, three various molar ratios of VLP-alkyne to Bp were tested first, to obtain approximately the same labeling as subsequently determined in VLP-HA* a VLP-PEG* samples. For testing, 50 µg of VLP-alkyne were used with VLP-alkyne to Bp ratios: 1:1, 1:0.5, 1:0.125. The other reagents ratio remained as described earlier (5.2.1.8). Protein concentration was measured in all samples by Qubit (5.2.1.5) and the absorption spectra were measured (300-900 nm) (5.2.1.9).

The number of Bp molecules bound per VLP-alkyne was counted based on the Bp standard curve (See 5.2.1.10). Because the number of Bp molecules bound per VLP-alkyne was the most similar to VLP-HA* in VLP-alkyne to Bp ratio 1:0.5, that ratio was used for the final preparation of VLP-Bp sample (where 1 mg of VLP-alkyne was used for the Bp conjugation via the click reaction, all other conditions remained the same as in previous experiments). The number of Bp molecules was counted (See 5.2.1.10). All types of VLPs (VLP-HA*/PEG*/Bp) were analyzed by SDS-PAGE (5.2.1.12), Western blot (5.2.1.14) and TEM (5.2.1.6) and stored in -20° C.

5.2.1.12   SDS-PAGE

<u>Materials</u>

5x Laemmli sample buffer – stored at -20° C

 5 % SDS (Sigma-Aldrich, USA)

 50 mM Tris-HCl, pH 6.8

 50 % (v/v) glycerol (Lachema, Czech Republic)

 25 % β-mercaptoethanol (Serva, Czech Republic)

 0.05 % (w/v) bromphenol blue (Lachema, Czech Republic)

Stacking gel (5 %)

 0.5 ml 30 % acrylamide

 0.375 ml Tris-HCl, pH 6.8

 30 µl 10 % SDS

 2.11 ml ddH$_2$O

 20 µl 10 % ammonium persulphate

 5 µl tetramethylenediamine

Resolving gel (10 %)

 2 ml 30 % acrylamide

 2.25 ml Tris-HCl, pH 8.8

 60 µl 10 % SDS

 1.625 ml ddH2O

 40 µl 10 % ammonium persulphate

 4.25 µl tetramethylenediamine

Running buffer, pH 8.3

      25 mM Tris

      192 mM glycine

      1 % SDS

The samples were first appropriately diluted and mixed with 5x Laemmli sample buffer in 4:1 volume ratio (Sample : Laemmli sample buffer). Samples were mixed by vortexing, incubated at 100° C (5 min) and stored at -20° C. The reagents (as summarized above) for the resolving gel were mixed, loaded into a clean assembled gel casting apparatus and ddH$_2$O was carefully layered on top of the gel. Gel was left to polymerize for 30 minutes (RT). Next, water was discarded, apparatus was dried with filtration paper, the stacking gel reagents were mixed, applied on top of the resolving gel and the electrophoresis comb was inserted in the apparatus. After polymerization (20 min, RT), the comb was removed, and the polymerized gels were transferred into an electrophoresis apparatus. The apparatus was filled with running buffer and the samples were loaded into the wells. The electrophoresis was set at 80 V (30 min) and at 140 V (~1 h). Afterwards, the gels were carefully removed from the apparatus and used further for fluorescent signal acquisition (See 5.2.1.13) and western blotting (See 5.2.1.14) or for protein staining (See 5.2.1.15).

5.2.1.13   Fluorescence Acquisition from SDS-PAGE Gel

The apparatus was cleaned, and the gel was inserted into Molecular imager Fx. The fluorescent signal was acquired at Af488 channel both at low and at high intensity with the resolution at 100 μm and at 200 μm and analyzed by fluorescence analysis software Quantity One 4.6.9.

5.2.1.14   Western Blot

<u>Material</u>

Blotting buffer – pH 8.3, 4° C

      25 mM Tris

      195 mM glycine

      20 % ethanol

SDS-PAGE gel used for fluorescence acquisition was incubated in blotting buffer (10 min, RT), the blotting sandwich was assembled as follows: One by one, four filter papers were soaked in blotting buffer and layered onto a blotting sponge onto each other. On top, a soaked Whatman paper was also applied.

The gel was placed onto the Whatman paper, and a nitrocellulose membrane was layered onto the gel. Next, one Whatman paper, four filter papers and a blotting sponge were placed on top (all soaked in blotting buffer). Air bubbles were carefully removed, the sandwich was placed in a blotting apparatus and proteins were blotted from the gel onto the membrane for 3 hours at 250 mA. After disassembling the apparatus, the membrane was washed by dH_2O and blocked by 5 % low-fat dry milk in PBS (30 min, RT). The membrane was immunostained and the chemiluminescent signal was acquired (as in Immunodot blot, see 5.2.1.3).

5.2.1.15 SDS-PAGE Gel Staining

<u>Material</u>

Imperial™ Protein Stain (Thermo Fisher Scientific, USA)

The second gel from SDS-PAGE was stained by Imperial™ Protein Stain as follows: The SDS-PAGE gel was washed three times with 100 ml ddH_2O (three times 5 min, RT). Water was discarded, the staining reagent was mixed by shaking and the SDS-PAGE gel was covered by the stain and placed on a shaker (2 h, RT). The gel was washed overnight by 200 ml of ddH_2O placed on a shaker (RT) and a scan of the stained gel was acquired.

5.2.2 NP-Cell Interaction Studies

5.2.2.1 NP - MDA-MB-231 Cell Interaction Experiments - Flow Cytometry

MDA-MB231 cells were cultivated in IMDM medium with 10 % FBS at 37° C in a humidified atmosphere containing 5 % CO_2. Before the experiment, cells were seeded in the appropriate dish as follows: the cultivation medium was aspirated, the cells were rinsed with versen, and trypsin (0,25 % v/v in PBS) was added to the cells (1 ml) and incubated in a thermobox until cells detached from the dish. Subsequently, the cells were carefully resuspended in IMDM medium containing serum (3 ml). The cells were counted in the Bürker chamber, $2*10^5$ cells were plated per well on a 12-well plate.

The cells were cultivated in a thermobox (37° C) for 24 hours. Before the addition of NPs, cells were rinsed once with serum-free IMDM medium, and fresh serum-free IMDM medium was added (300 µl) to each well.

Three experiments were performed using flow cytometry (FC1, FC2, FC3). First an optimization of the FC experiment was necessary. Thus, the procedures slightly varied in experiments FC1, FC2 and FC3 (as indicated in the Results section 6.2 – summarized schema of NP-cell interaction experiments in figure 21). In FC1 and FC2 the FC experiment was optimized, the FC3 was the final FC experiment.

Two types of samples were present in the studies; samples with pre- (FC1) or co-incubation (FC2, FC 3) of non-labeled HA free HA with NPs and cells (samples indicated as +HA) and without any incubation with free HA.

In FC1, NP samples (VLP-HA*/PEG*/Bp, ND-HA*/Bp and negative control) were tested with (+HA – monoplicates) and without (duplicates) preincubation with free HA. Free HA was added (0.2 mg/ml or 1 mg/ml) to the cells (in the samples that were to be preincubated with free HA) and the cells were incubated in a thermobox (37° C) for 1 h. Then, the medium was discarded, and fresh serum-free IMDM medium was added (300 µl). The NPs (VLPs or NDs) (7 µg of VLPs, 30 µg of NDs) or control compounds (free HA*/PEG*/Bp; final molar concentration 1,4 µM) were added to the cells. In negative controls (NC), only serum-free IMDM medium was left on the cells. The cells were incubated with the NPs in a thermobox (37° C) for 2 hours with occasional shaking.

The medium was discarded, the cells were rinsed with versen (1 ml), detached from the dish by treatment with trypsin (0.25 ml, 0.25 %) that was subsequently inactivated by the addition of the soybean trypsin inhibitor (1 mg/ml in PBS, 0.25 ml). The samples were transferred to FACS centrifugation tubes and 2 ml of cooled PBS were added. The samples were centrifuged (500x g, 4° C). Supernatant was discarded, PBS with 0.5 % BSA (300 µl) was added, samples were resuspended when placed on ice and measured by flow cytometry. NC was measured first. NC with DAPI (1 µM final concentration) was measured and the rest of the samples was measured with DAPI too.

In FC2, 2 mg/ml and in FC3, 5 mg/ml free HA was added simultaneously with the NPs and different amounts of VLPs (7 µg of VLPs, 30 µg of NDs in FC2, monoplicates; 12 µg of VLPs, 30 µg of NDs in FC3 and also 20 µg of VLP-HA* in FC3, triplicates). In FC3 also free controls (HA* 16 µM; PEG*, Bp 1.4 µM) were tested.

Data from the flow cytometer were processed in the Kaluza software 2.1 (Beckman). The gating strategy was briefly as follows: first the cell population was gated in the NC sample (negative control), furthermore singlets were selected. In the NC with DAPI, live cells were gated and in the next step, Bp positive and Bp negative cells were gated (summarized in Appendix II – Fig. S.ii). This protocol was further used for all samples that were not pre- or co-incubated with free HA.

For the samples that were pre- or co-incubated with free HA a separate NC was prepared in a similar manner (in FC1 and FC3) and this protocol was then applied to them. The median fluorescence intensity (MFI) in the total live singlet gated cell population and the % of Bp positive cells from the total live singlet gated cell population were acquired. Overlaying histograms were generated, and data were plotted (Microsoft Excel). The statistical analysis of the differences of the triplicates incubated with free HA and not incubated with free HA in FC3 was performed in GraphPad Prism 8 by the Mann Whitney test.

5.2.2.2 NP - MDA-MB-231 Cell Interaction Experiments - Fluorescence Experiments

MDA-MB231 cells were cultivated as specified above. Before the experiment, the cells were counted in the Bürker chamber, $1*10^5$ cells were plated per well on a 24-well plate (with sterilized glass coverslip) and placed in a thermobox (37° C, 24 h). Medium was discarded and cells were washed with serum-free IMDM medium, medium was discarded, and fresh serum-free IMDM medium was added (200 µl). Two fluorescence experiments were performed (FL1, FL2).

From this point on, procedures slightly varied in experiments FL1 and FL2 (as indicated in the Results section 6.2 – summarized schema of NP-cell interaction experiments in figure 21). Two types of samples were present in the experiments: (1) samples with free HA present with NPs during incubation with cells (samples indicated as +HA), and (2) samples with NPs without free HA.

In FL1, NP samples (VLP-HA*, ND-HA*) were tested on interactions with MDA cells with and without co-incubation with free HA (VLP-HA*+HA; ND-HA*+HA), all other controls were tested only without incubation with free HA (VLP-PEG*, VLP-Bp, ND-Bp, HA*, PEG*, Bp*, NC). Free HA (1.5 mg/ml) and NPs (VLP-HA* or ND-HA*, 9 µg and 30 µg respectively) were added to the MDA cells (in the samples that were to be co-incubated with free HA) and only NPs (VLP-PEG*/Bp, ND-Bp; 3.5 µg or 30 µg respectively) or controls (HA*, PEG*, Bp*; 1.4 µM) were added to samples that were not incubated with free HA. Cells were placed in a thermobox (2 h, 37° C) (alternatively 30 min, 2 h or 4 h in FL2). Medium was discarded and samples were fixed with paraformaldehyde (3.7 %, 0.5 ml, 15 min). Paraformaldehyde was aspirated, samples were washed with PBS (1 ml) and then incubated with triton X-100 (0.5 %, 0.5 ml, 5 min). The cells were washed by PBS (3 times, 1 ml). Then, 300 µl of PBS with DAPI (1 µg/ml) was added and the samples were incubated for 10 minutes in the dark. The samples were washed with PBS (3 times, 1 ml) and ddH$_2$O (0.5 ml), and then ddH$_2$O (200 µl) was added. The slides were removed from the wells, dried and mounted in glycerol (50 %, 3 µl). The slides were stored (-20° C) and later observed under the BX60F-3 fluorescence microscope.

From all samples, micrographs were acquired in NIS-Elements AR 2.30 imaging software on automatic and on manual exposition. Only representative pictures are shown in Results.

6. Results

6.1 MPyV VLP-HA* and Control Production

6.1.1 MPyV VP1 VLP Production

In the first part of the study, it was necessary to produce a sufficient amount of MPyV VLPs, four subsequent isolations of VLPs took place. A baculovirus expression system was used for VLPs production. The insect cells Sf9 were infected with recombinant baculovirus encoding the MPyV VP1 gene. VLPs are formed in the cell nucleus of infected cells and can be isolated by a standard protocol (see Methods – 5.2.1.1). VLPs were purified by isopycnic ultracentrifugation in cesium chloride gradient. Each gradient was divided into individual subfractions, which were merged into fractions (Tables 3-6 and Fig. 9-12) based on the buoyant density determined from the refractive indices of the subfractions and the presence of VP1 (determined by the signal on the Immunodot blot). The VLPs in each fraction were subsequently visualized by the transmission electron microscopy (Appendix I – S.i).

Table 3 VLP isolation 1: refractive indices of the subfractions from six (I-VI) gradients. Subfractions of the same color were merged to compose fractions 1-5. Orange – fraction 1; green – fraction 2; light blue – fraction 3; dark blue – fraction 4, pink – fraction 5.

| Subfraction	I	II	III	IV	V	VI
1	1.373	1.365	1.368	1.370	1.369	1.373
2	1.371	1.374	1.374	1.371	1.370	1.370
3	1.368	1.371	1.370	1.369	1.368	1.366
4	1.367	1.370	1.367	1.368	1.367	1.366
5	1.367	1.366	1.367	1.365	1.365	1.365
6	1.366	1.366	1.365	1.363	1.364	1.365
7	1.366	1.365	1.364	1.362	1.364	1.365
8	1.365	1.364	1.364	1.362	1.363	1.364
9	1.364	1.364	1.364	1.361	1.362	1.363
10	1.362	1.364	1.362	1.361	1.362	1.361
11	1.362	1.364	1.361	1.360	1.361	1.360
12	1.361	1.363	1.361	1.359	1.360	1.360
13	1.360	1.362	1.360	1.358	1.359	1.359
14	1.358	1.358	1.355	1.357	1.357	1.358
15		1.358	1.355	1.357	1.356	
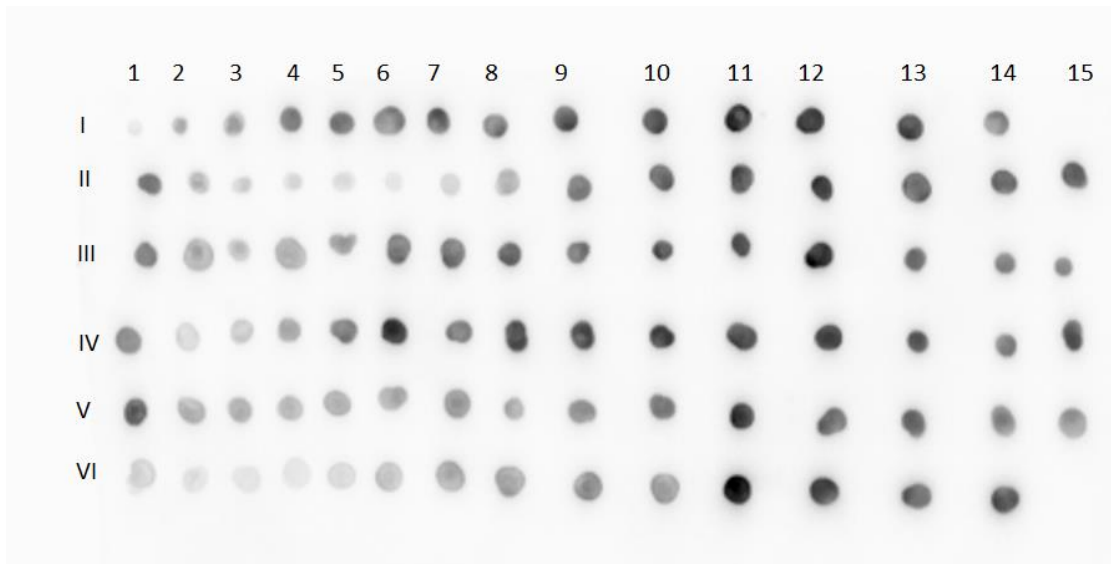
Figure 9 Immunodot blot of VLP isolation 1 was performed to detect the presence of MPyV VP1 by an αMPyV VP1 antibody in subfractions 1-15, 20 s exposition. Signal detected by Fusion-FX6.EDGE V.070.

Table 4 VLP isolation 2: refractive indices of the subfractions from six (I-VI) gradients. Subfractions of the same color were merged to compose fractions 1-5. Orange – fraction 1; green – fraction 2; light blue – fraction 3; dark blue – fraction 4, pink – fraction 5.

| Subfraction	I	II	III	IV	V	VI
1	1.366	1.370	1.370	1.369	1.365	1.364
2	1.371	1.371	1.370	1.371	1.372	1.372
3	1.368	1.366	1.368	1.369	1.370	1.367
4	1.368	1.366	1.364	1.367	1.367	1.367
5	1.365	1.365	1.363	1.365	1.366	1.364
6	1.363	1.363	1.362	1.362	1.365	1.364
7	1.363	1.362	1.362	1.361	1.364	1.363
8	1.362	1.362	1.362	1.361	1.363	1.362
9	1.361	1.362	1.362	1.361	1.363	1.362
10	1.361	1.361	1.360	1.361	1.361	1.361
11	1.361	1.361	1.360	1.360	1.361	1.360
12	1.360	1.361	1.360	1.359	1.361	1.358
13	1.358	1.359	1.359	1.359	1.359	1.358
14	1.357	1.357	1.357	1.357	1.358	1.356
15	1.352	1.355	1.352	1.353	1.357	1.356
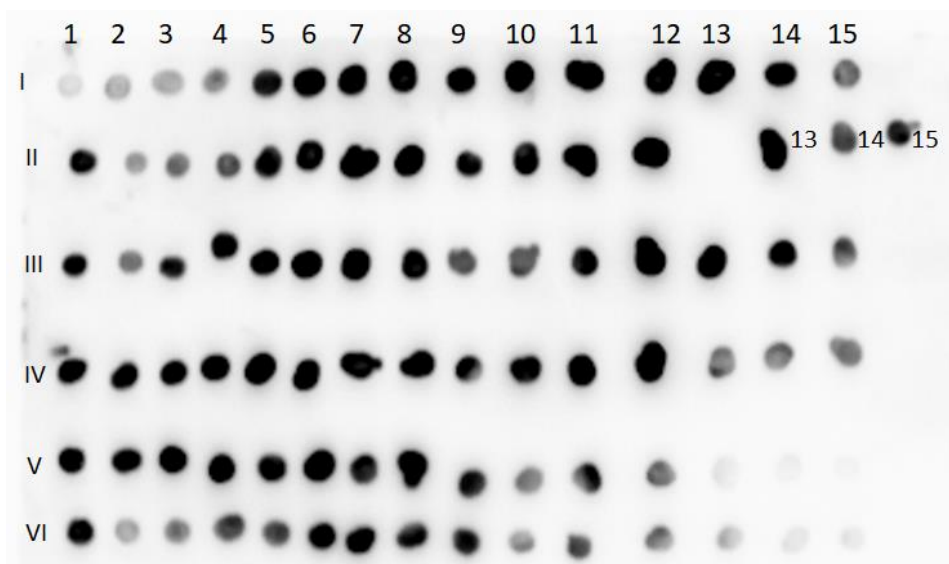
Figure 10 Immunodot blot of VLP isolation 2 was performed to detect the presence of MPyV VP1 by an αMPyV VP1 antibody in subfractions 1-15, 30 s exposition. Signal detected by Fusion-FX6.EDGE V.070.

Table 5 VLP isolation 3: refractive indices of the subfractions from six (I-VI) gradients. Subfractions of the same color were merged to compose fractions 1-4. Orange – fraction 1; green – fraction 2; light blue – fraction 3; dark blue – fraction 4.

Subfraction	I	II	III	IV	V	VI
1	1.374	1.373	1.369	1.372	1.374	1.373
2	1.371	1.372	1.372	1.371	1.37	1.371
3	1.369	1.369	1.37	1.369	1.369	1.369
4	1.367	1.368	1.368	1.367	1.367	1.367
5	1.367	1.366	1.367	1.366	1.366	1.366
6	1.365	1.366	1.366	1.364	1.365	1.365
7	1.365	1.365	1.365	1.363	1.365	1.364
8	1.364	1.364	1.364	1.363	1.364	1.363
9	1.363	1.364	1.364	1.362	1.364	1.363
10	1.363	1.363	1.363	1.362	1.362	1.362
11	1.362	1.362	1.362	1.361	1.362	1.362
12	1.362	1.362	1.362	1.36	1.362	1.361
13	1.36	1.36	1.36	1.359	1.36	1.359
14	1.359	1.36	1.36	1.357	1.359	1.359
15					1.358	
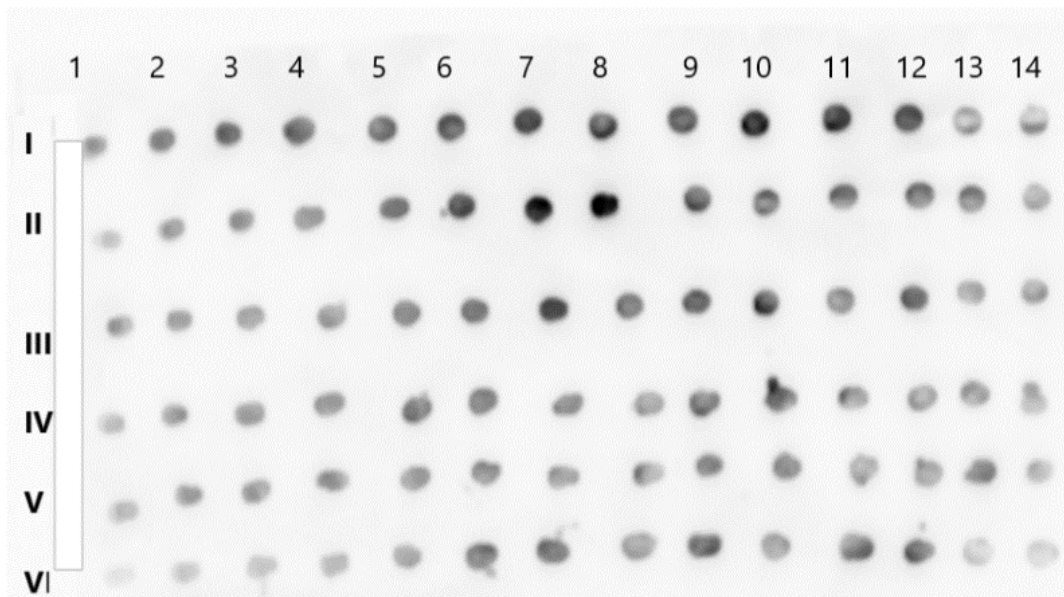
Figure 11 Immunodot blot of VLP isolation 3 was performed to detect the presence of MPyV VP1 by an αMPyV VP1 antibody in subfractions 1- 14, 30 s exposition. Signal detected by Fusion-FX6.EDGE V.070.

Table 6 VLP isolation 4: refractive indices of the subfractions from six (I-VI) gradients. Subfractions of the same color were merged to form fractions 1-4. Orange – fraction 1; green – fraction 2; light blue – fraction 3; dark blue – fraction 4.

Subfraction	I	II	III	IV	V	VI
1	1.373	1.373	1.373	1.373	1.361	1.373
2	1.371	1.370	1.370	1.371	1.373	1.372
3	1.368	1.368	1.367	1.368	1.370	1.369
4	1.366	1.366	1.365	1.366	1.367	1.367
5	1.365	1.365	1.364	1.365	1.365	1.365
6	1.364	1.364	1.363	1.363	1.364	1.364
7	1.363	1.363	1.362	1.362	1.363	1.363
8	1.362	1.362	1.362	1.362	1.362	1.362
9	1.3615	1.3615	1.361	1.361	1.3615	1.3615
10	1.361	1.361	1.360	1.360	1.361	1.361
11	1.360	1.360	1.359	1.359	1.360	1.360
12	1.358	1.358	1.358	1.358	1.359	1.359
13	1.357	1.357	1.356	1.357	1.357	1.357
14	1.356	1.356	1.355	1.356	1.356	1.356
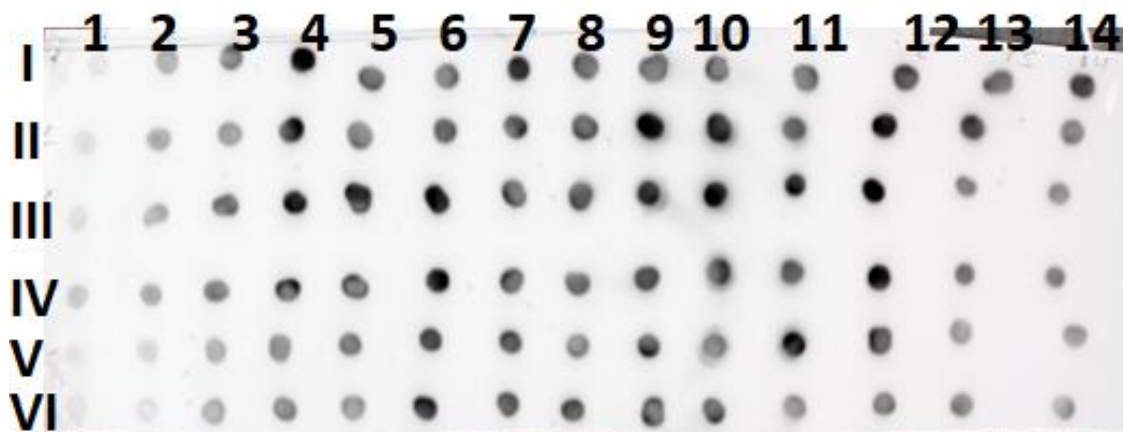
Figure 12 Immunodot blot of VLP isolation 4 was performed to detect the presence of MPyV VP1 by an αMPyV VP1 antibody in subfractions 1-14, 10 s exposition. Signal detected by Fusion-FX6.EDGE V.070.

Based on the micrographs acquired by TEM (for TEM micrographs see Appendix I - S.i), fractions from the VLP isolations 1-4 with best retained integrity (summarized in 6.1.2.1. – Table 7) were selected for the following experiments.

6.1.2 Modification of VLPs

The strategy for conjugation of HA to VLPs has been designed in the Laboratory of Synthetic Nanochemistry (IOCB). The strategy is based on a newly synthetized heterobifunctional and biorthogonal fluorescent (Bodipy) probe (Fig. 13) (synthesis was performed by Jan Bartoň, IOCB (for details see Bartoň, 2015). The probe contains two reactive groups (aminooxy and azide). The aminooxy group has been used for conjugation of aldehyde on oxidized sugar subunit of hyaluronic acid or for conjugation of a control PEG molecule (Neburkova et al., 2018). The resulting compounds were designated as HA* or PEG*, respectively. These reactions were done by Jitka Nebůrková (IOCB).

Aminooxy group for conjugation to hyaluronic acid or PEG

Azide group for conjugation to VLPs (or NDs)

Heterobifunctional probe
(Aminooxy-Bodipy-Azide)
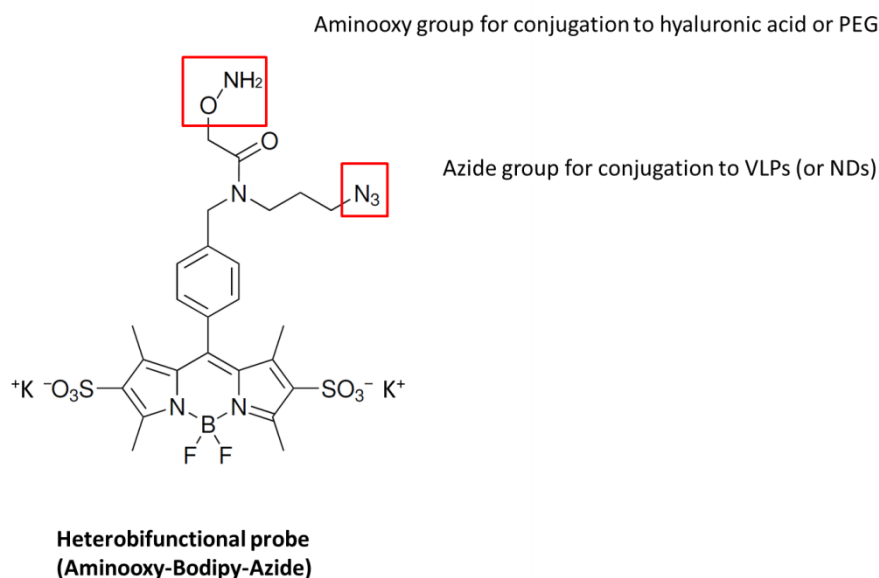
Figure 13 The chemical structure of the bifunctional florescent dye Bodipy created by Jan Bartoň (IOCB). The figure was adapted from Bartoň, 2015.

The azide group on Bp probe (present also in HA* and PEG*) was subsequently used for conjugation to VLPs (or NDs) via "click chemistry". NDs are crafted with polymers that carry alkyne moiety required for bioconjugation, whereas VLPs must be modified by a heterobifunctional linker containing propargyl and N-hydroxysuccinimidyl ester moieties to introduce the alkyne functionality for subsequent reaction. Modification of VLPs was done as part of this thesis and is described in detail in the following chapters. NDs were modified by Jitka Nebůrková (IOCB) and resulting NDs (ND-HA*, ND-Bp) were used in this thesis only as control NPs for experiments that investigated the mode of interaction of VLPs with target cells (Fig. 14 – ND TEM micrographs).
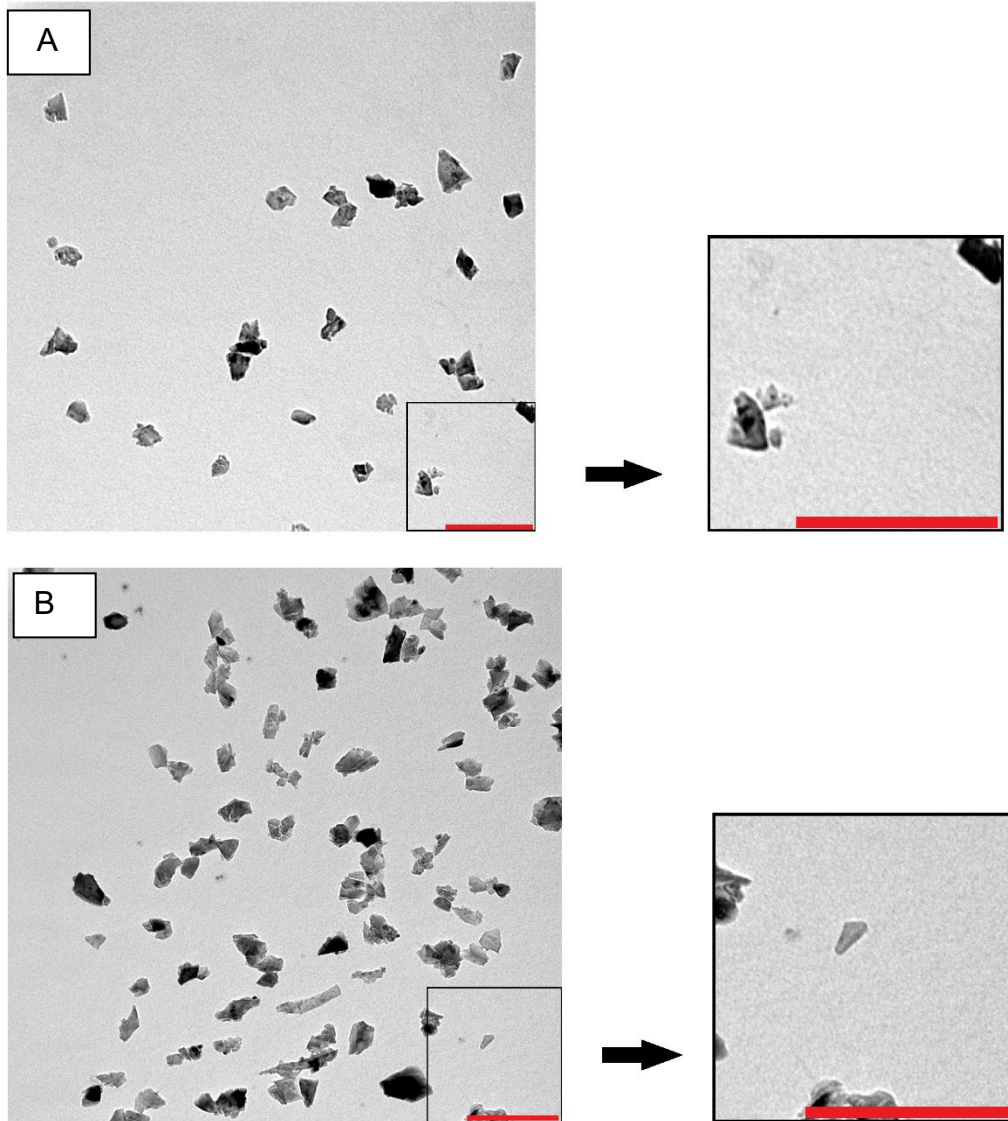
Figure 14 TEM micrographs with negative staining A) ND-HA* and B) ND-Bp. NDs were produced by Jitka Nebůrková (IOCB). Red scalebar represents 200 nm. Transmission electron microscope JEOL JEM 1200EX.

6.1.2.1 VLP-alkyne Construction and Sample Characterization

Based on the acquired TEM micrographs, the fractions from MPyV VLP isolations with intact VLPs were selected for subsequent chemical modification (conjugation of an alkyne functionality containing linker), resulting in VLP-alkyne (Table 7). VLPs were modified with the heterobifunctional propargyl-N-hydroxysuccinimidyl (NHS) ester linker. NHS ester reacts with surface lysines on VLPs. The expected number of surface lysines on VLPs is 720 and the reaction was performed in 35-fold molar excess of linker as described previously (Zackova Suchanova et al., 2017).

And the sample was further dialyzed, washed and concentrated (see details in Methods –5.2.1.7).

However, large losses occurred during repeated washing in the process. Therefore, the alkyne linker-attachment step had to be performed three times in total (see fractions used in individual batches are summarized in Table 7).

Table 7 Fractions (and the VLPs isolation number) used for alkyne linker attachment and the protein amount in three working batches (assigned as A, B, C). For TEM micrographs see Appendix I.

VLP batch	VLP isolation	Fractions used (see Appendix I)	Protein amount (mg)
A	Isolation 1	1,2,4,5	6.41
	Isolation 2	4	
B	Isolation 4	2-4	2.40
C	Isolation 2	1	4.25
	Isolation 3	3,4	

After attaching the alkyne linker, the VLPs were characterized for their capacity to bind a model fluorescent probe Af488 via Cu[I]-catalysed alkyne-azide cycloaddition. Characterization was essential primarily to estimate the number of linkers attached to the VLPs and to evaluate, whether the particles retained integrity during the click reaction. The amount of Af488 molecules bound per particle was calculated based on the absorption spectra (Fig. 15) of the samples, using a standard curve (Table 8) (see details of the click reaction and of the calculations in Methods – 5.2.1.8, 5.2.1.10). TEM micrographs were acquired before and after the click reaction to confirm, that the integrity of the VLPs was retained (data not shown).
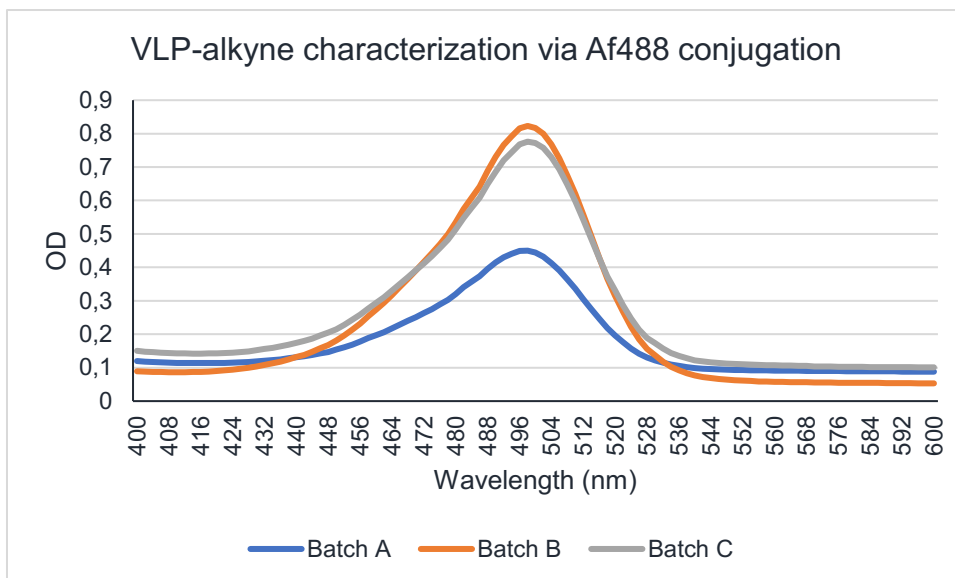
Figure 15 Absorption spectra of three VLP-alkyne working batches measured after Af488 conjugation via click chemistry. Measured by Epoch™ Microplate Spectrophotometer.

Table 8 Summary of the characterization of the VLP-alkyne batches. The number of Af488 molecules bound per VLP in each batch is shown. The number of Af488 bound per VLP indicates the number of alkyne linkers attached per VLP.

Batch	A	B	C
Af488/VLP	476	1196	880

Eventually, the individual batches of VLP-alkyne were pooled. Recurrently, electron micrographs were acquired via TEM to evaluate whether the integrity of the VLPs was preserved during the process of alkyne linker attachment (Fig. 16). Most of the VLPs retained integrity during the alkyne linker attachment step. In order to determine the final amount of VLP-alkyne, the protein concentration was measured. The total amount of VLP-alkyne was 6 mg, which is less than a half of the amount of the protein used for linker conjugation (13.06 mg).
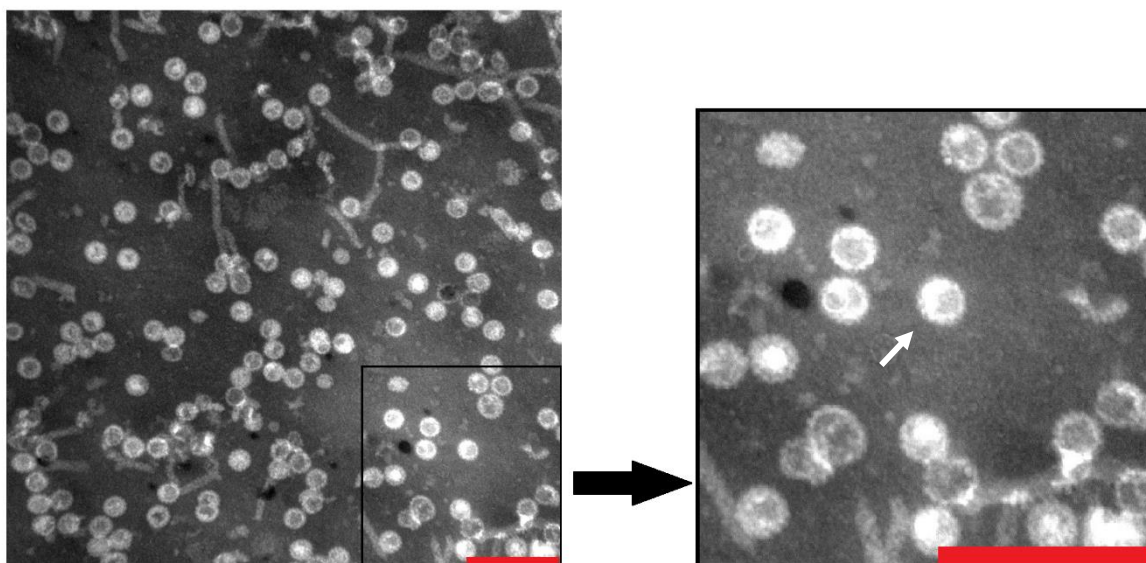
Figure 16 MPyV VP1 VLPs with alkyne linker attached after dialysis to HEPES (0.1 M, pH 7.4). Transmission electron microscopy, negative staining. Indicated red scalebar represents 200 nm. White arrow shows 1 of the VLPs-alkyne, integrity was preserved. Transmission electron microscope JEOL JEM 1200EX.

6.1.2.2 Click Reaction – VLP-HA*, VLP-PEG*, VLP-Bp Construction

After pooling the VLPs with alkyne linker attached, three types of modified VLPs were produced using click reaction: VLP-HA*, VLP-PEG*, VLP-Bp. The first type of VLPs, VLP-HA* was expected to increase the VLP binding specificity to the CD44 receptors overexpressed on cancer cells in further experiments.

Shielding of the VLPs surface with the HA molecules (8-15 kDa) was also expected to limit the broad VP1-mediated interactions of the VLPs. The other two types of particles were used as controls. VLP-PEG* was prepared by the attachment of PEG* (20 kDa), similar in size to HA*. High molecular PEG is used in nanotechnology as a shielding molecule that can decrease non-specific interactions. It served as an appropriate control for VLP modification: although lacking the targeting ligand, it should exhibit similar shielding capacity as HA. In the second type of control, Bp alone was attached to VLP-alkyne, thus the difference in cell binding of VLPs without a large shielding ligand and VLP-HA* could also be determined. Bodipy is small in size (Mw 668 Da), therefore VLP-Bp control is expected not to limit the VP1-mediated cell binding in VLPs.

Bodipy provides the possibility of quantification of HA* or PEG* molecules bound per VLP. In all VLP variants (VLP-HA*/PEG*/Bp), Bp lends VLPs fluorescence, hence the possibility of VLP detection in NP-cell interaction studies.

VLP-HA* and VLP-PEG* samples were prepared by click reaction. Non-attached molecules were removed by dialysis, VLPs were further purified (unconjugated HA* and PEG* were removed) and concentrated through a 20 % (w/w) sucrose cushion. The number of HA* or PEG* molecules on VLPs surface were estimated from the absorption UV-vis spectra of VLP-HA* and VLP-PEG* (Table 9, Figure 18) (for details see Methods – 5.2.1.11) by using two different spectrophotometers that led to slightly different results (Table 9, Figure 18).

Three molar ratios of VLP-alkyne to Bp (1: 1, 1: 0.5, 1: 0.125) were also tested in the production of VLP-Bp particles (Fig. 17), in order to determine a ratio that achieves a final coverage of VLPs with Bp molecules similar to VLP-HA* (Table 9). The concentration of the samples and the absorption spectra were measured. The number of Bp molecules bound per VLP was then calculated using a standard curve (for details see Methods – 5.2.1.10).
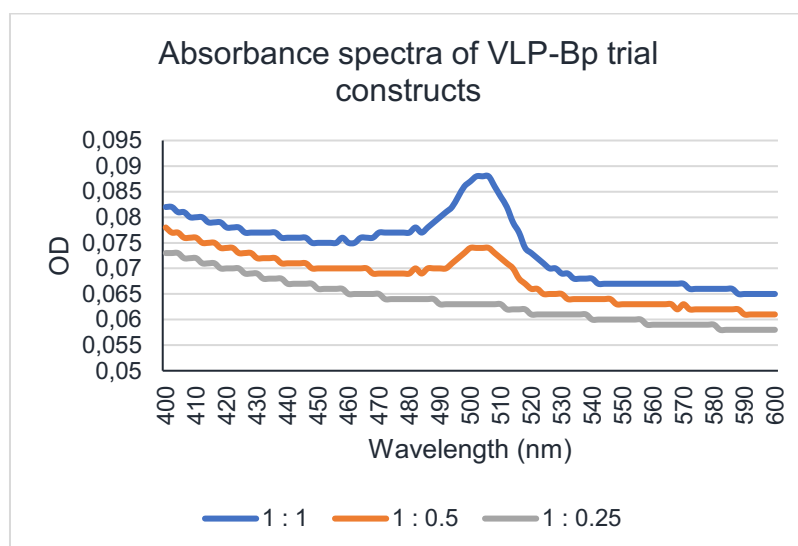
Figure 17 Absorption spectra of three molar VLP-alkyne to Bp ratios tested in click reaction: 1:1, 1:0.5 and 1:0.25. Measured by Epoch™ Microplate Spectrophotometer.

The VLP-Bp sample achieved coverage, most similar to that of VLP-HA*, when using a VLP-alkyne to Bp molar ratio of 1:0.5 during the click reaction. Therefore, this ratio was used in the final preparation of the VLP-Bp sample in large scale.

Unfortunately, after subsequent analysis (Figure 18, Table 9) the resulting number of BP molecules bound per VLP was higher than expected. The final number of Bp molecules bound per VLP-alkyne for all VLP types is summarized in Table 9.

The ND particles used in subsequent studies were prepared with the use of the same "click" chemistry in IOCB and the number of HA* and Bp on NDs was also determined by the same method (see Table 9 for summary). As seen from Figure 18 sensitivity of the spectrometer is essential for correct measurement of absorption spectra and calculation of the number of Bp molecules per VLP (Table 9). The results based on spectra shown in Figure 18B are considered valid in this thesis as they were obtained by a spectrophotometer with higher sensitivity.
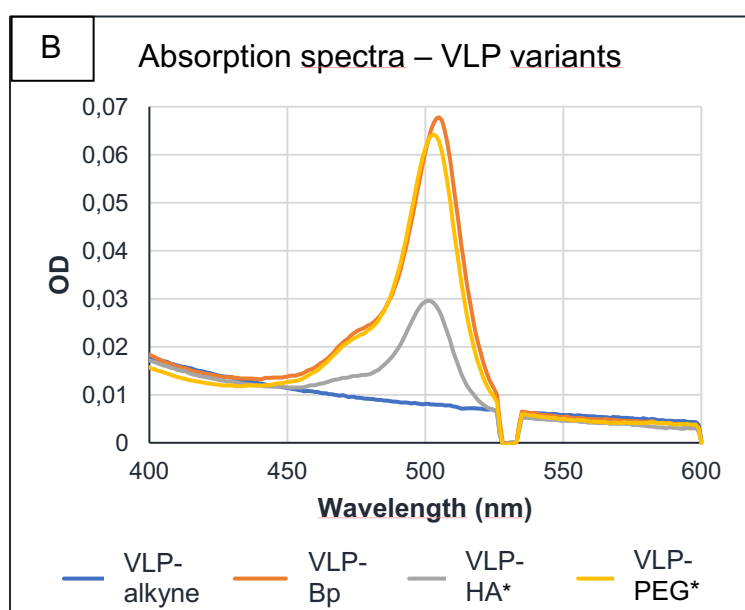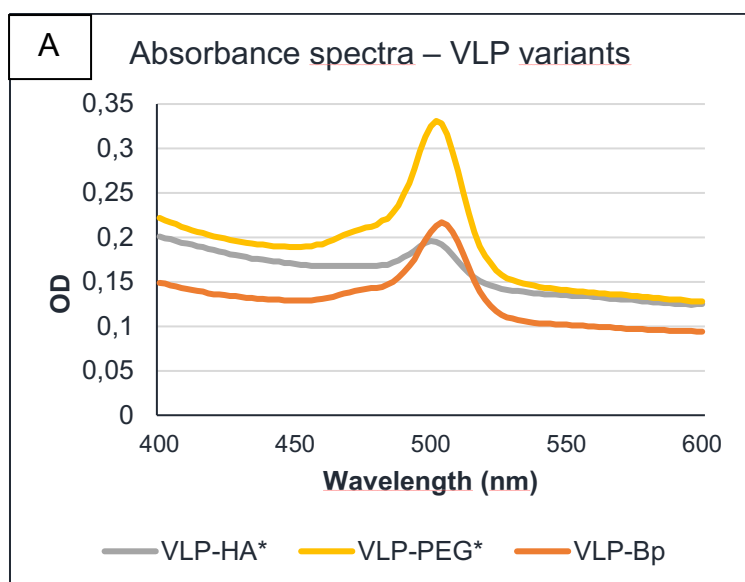
Figure 18 The UV-vis absorption spectra of VLP-HA*, VLP-PEG* and VLP-Bp samples A) acquired in our laboratory by Epoch™ Microplate absorbance spectrophotometer with lower sensitivity compared to B) measured by Jitka Nebůrková (IOCB) using Specord 250 absorbance spectrophotometer with higher sensitivity. In both graphs, VLP-Bp sample shows highest peak at Bp maximum (498 nm), nonetheless lower protein concentration than other VLP samples. VLP-HA* shows nearly half the value and VLP-alkyne as negative control shows no peak at Bp maximum.

Table 9 Summarized number of Bp molecules bound per NP in all VLP (including trial versions of VLP-Bp) and ND variants A) calculated from the absorption spectra measurement by the Epoch™ Microplate absorbance spectrophotometer of low sensitivity in our laboratory B) calculated from the absorption spectra measurement by the Specord 250 absorbance spectrophotometer with higher sensitivity by Jitka Nebůrková (IOCB). Ratio in trial Bp samples shows molar ratio of VLP-alkyne to Bp during the click reaction. The ratio with grey background was chosen for large scale production of VLP-Bp. The number of Bp molecules bound per VLP was calculated as specified in Materials and methods (5.2.1.10).

		VLP:Bp 1:1	VLP:Bp 1:0.5	VLP:Bp 1:0.125	VLP-HA*	VLP-PEG*	VLP-Bp	ND-HA*	ND-Bp
A)	Number of Bp molecules/NP	29	12	nd	6	26	36	-	-
B)	Number of Bp molecules/Np	-	-	-	56	144	153	80	153

All types of VLP constructs, modified in the above-described manner, were visualized by TEM. The results showed the preservation of the integrity of most VLPs in all types of VLP samples after the click reaction (Figure 19). However, in VLP-HA* and VLP-Bp some VLPs disassembled into pentamers could be observed too.
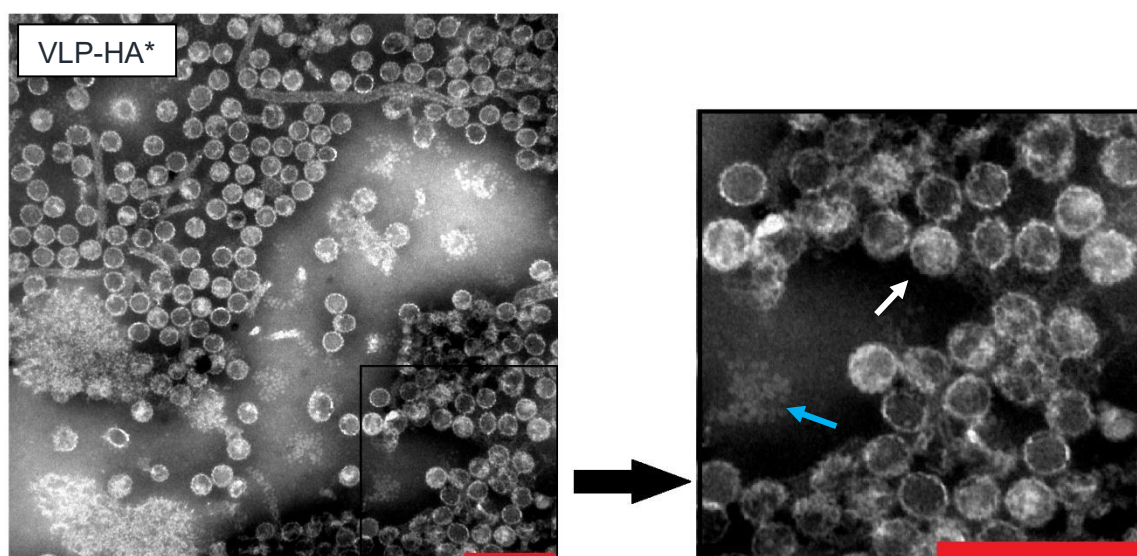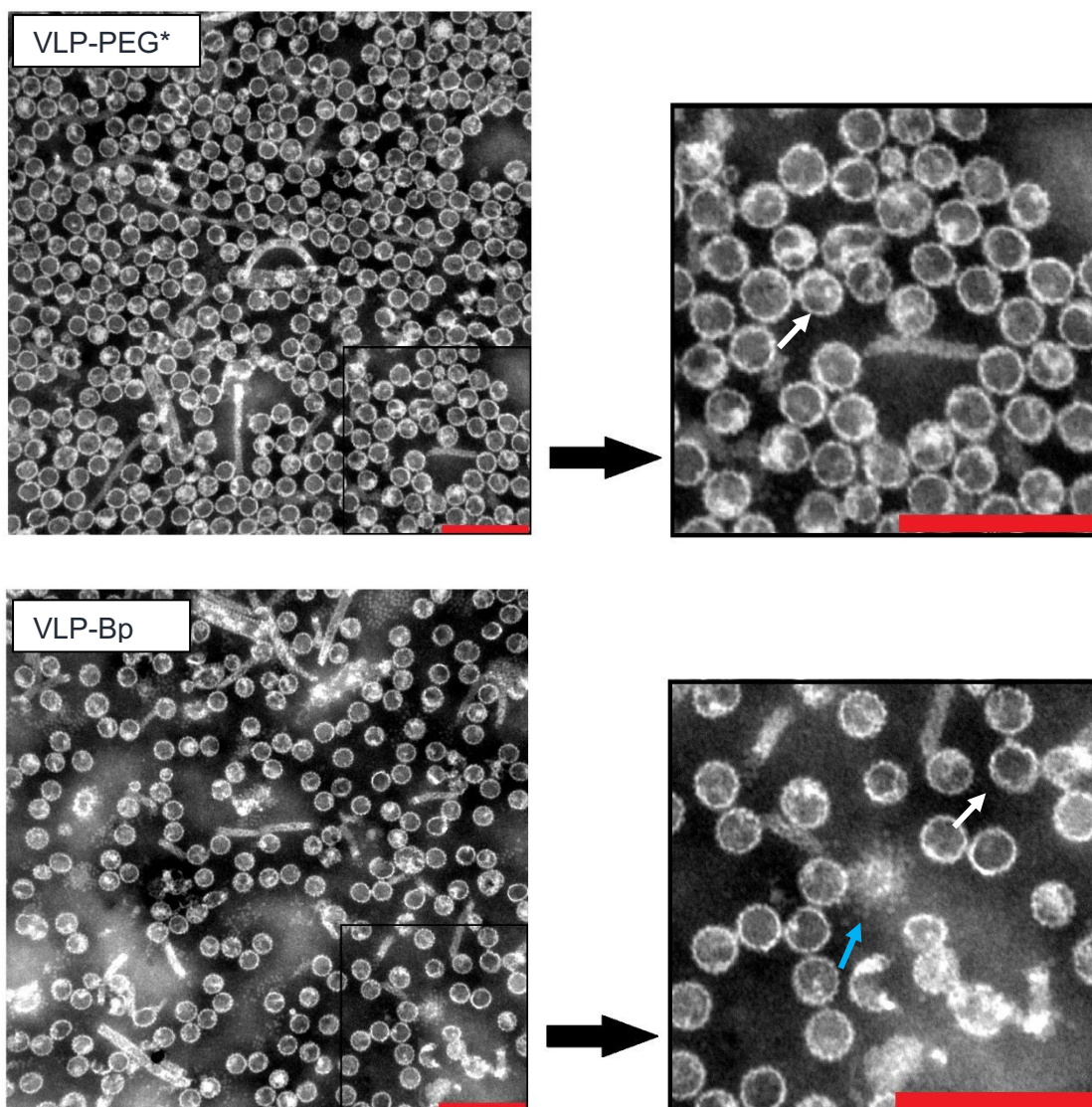
Figure 19 VLPs after click reaction VLP-HA*, VLP-PEG* and VLP-Bp, negative staining, transmission electron microscopy. The red scalebar represents 200 nm, white arrows show a representative VLP with preserved integrity. Blue arrows in VLP-HA* and VLP-Bp sample show VLPs disassembled into pentamers. Transmission electron microscope JEOL JEM 1200EX.

The samples were further characterized by SDS PAGE, by detection of fluorescence from the SDS PAGE gel, by staining of the gel and by using a western blot (Figure 20). By fluorescent signal detection from the SDS PAGE gel, it was possible to acquire a signal in all three types of VLP constructs (VLP-HA*/PEG*/Bp), as opposed to no signal in VLPs with only the alkyne linker attached (Figure 20A). No signal showing unbound HA* was detected in VLP-HA*, therefore it is expected that excess HA* that did not bind to VLPs in click reaction was successfully removed by centrifugation though a sucrose cushion.

The SDS PAGE gel, stained by Imperial protein stain, showed the presence of a protein of about 45 kDa, corresponding to the size of MPyV VP1 protein, in all VLP samples (Figure 20B). In the western blot, where the αMPyV VP1 antibody was used for MPyV VP1 detection, it was possible to confirm the presence of VP1 protein in all VLP samples (Figure 20C). In agreement with the calculation of the numbers of Bp molecules bound per VLP-alkyne (Table 9), the fluorescence of VLP-HA* (Figure 20A) was distinctly lower compared to VLP-PEG* and VLP-Bp even though the VP1 amount vas similar in all samples loaded on the gel (Figure 20B).

Figure 20 Characterization of VLPs after modification with Bp-reagents*. Samples on 10 % SDS-PAGE acrylamide gel were loaded as follows (from left to right): VLP-HA*, VLP-PEG*, VLP-Bp, VLP with alkyne linker (4 µg/well each), molecular marker, HA* and PEG* (0.4 µg/well each). (A) **Fluorescence signal detection** on gel; BioRad Molecular Imager FX. (B) **Protein detection** on gel by Imperial™ protein stain. Black rectangular with label ´45 kDa´, shows the presence of a ~45 kDa protein in VLP samples, same size as MPyV VP1. (C) **Immunodetection of MPyV VP1** by Western Blot using αMPyV VP1 antibody. Chemiluminescent signal was acquired by Fusion Fx6.*

In summary, MPyV VLPs were produced and an alkyne functionality containing linker was successfully attached to the VLPs. The relative number of the alkyne linker molecules attached per VLP was estimated by conjugating Af488 onto the VLP-alkyne via click chemistry and subsequently the number of Af488 molecules bound per VLP was counted using a standard curve. Next, HA*, PEG* or Bp were conjugated onto VLP-alkyne.

The samples were characterized via SDS-PAGE and it was confirmed that the MPyV VP1 protein (45 kDa) was present in all VLP samples. In addition, a fluorescent signal was detected in all VLP constructs (VLP-HA*/PEG*/Bp) except for the negative control (VLP-alkyne). TEM showed preserved integrity of VLP variants after click reaction. Furthermore, the VLP constructs were tested for interactions with CD44 overexpressing cancer.

6.2 NP-Cell Interaction Studies - Flow Cytometry and Fluorescence Microscopy

After modifying the VLPs, it was possible to use them for evaluation of their interaction with cancer cells overexpressing the CD44 receptor. Human breast adenocarcinoma cells, MDA-MB-231 were selected for the experiments, as they have already been used in the past for CD44 targeting experiments (Surace et al., 2009).

A total of three experiments were performed to detect the interactions of NPs with the MDA cells using flow cytometry (FC1, FC2, FC3) and two fluorescence experiments (FL1, FL2) were performed to visualize the interaction with cells. In all experiments three types of VLP constructs (VLP-HA*, VLP-PEG* and VLP-Bp) and two types of ND constructs (ND-HA* and ND-Bp) were used. The sequence of the experiments was as follows: FC1,2; FL1,2; FC3 (simplistic schema of the experiments summarized in figure 21).
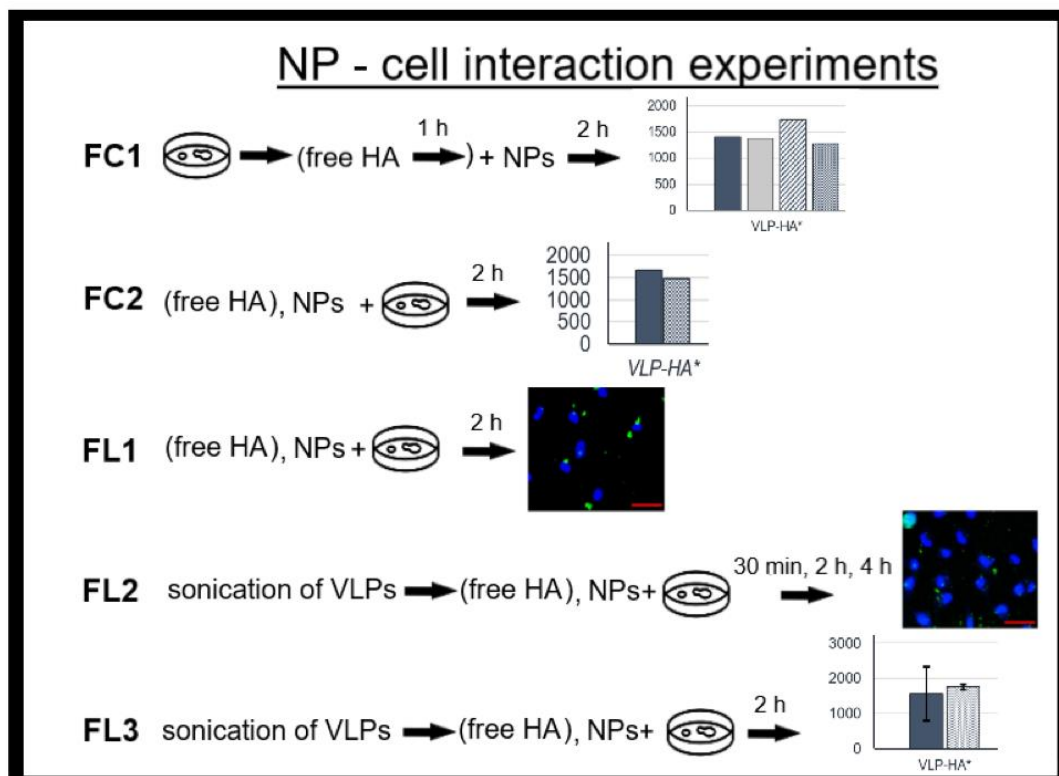
Figure 21 Schema showing the basic procedure of the NP-MDA cell interaction experiments: Flow cytometry 1,2, and 3 and fluorescence microscopy 1,2. Free HA in brackets represents selected samples being incubated with free HA during incubation of NPs with cells (in the competitive cell-binding assay). Petri dish represents MDA-MB-231 cells. NPs represents the VLP and ND variants. Different amounts of NPs and free HA were used in the experiments as indicated in Methods – 5.2.2. In FC1 free HA was aspirated after incubation.

6.2.1 Optimization of the FC Experiment

In the FC experiments, NPs were incubated with the cells for 2 hours and the NP-cell interactions were detected by flow cytometry. To evaluate, whether the NPs interact with the CD44 receptor, a competitive cell-binding study was performed like it was previously done in other studies (Xiao et al., 2015). Hereby, free HA (non-fluorescent) competes for the HA binding site at CD44 receptors with the NPs. Thus, a reduction of NP-cell interactions should be observed in samples incubated with free HA compared to samples not incubated with free HA, if the NPs enter mainly via the CD44.

Therefore, in the current study it was expected that a reduction of NP-cell interactions would only be detectable in VLP-HA* and ND-HA* samples, as specifically these samples are expected to enter the cells via the CD44 receptor, due to the HA-CD44 binding.

The FC experiments were briefly as follows: The MDA cells were plated on a 12-well plate ($2*10^5$ cells per well) and incubated overnight. The cells were washed and fresh serum-free IMDM medium was added (300 µl). Then, procedures were slightly different in experiments FC1, FC2 and FC3. However, two types of samples were always present in the studies, samples with pre- (FC1) or co-incubation (FC2, FC 3) of free HA and NPs with cells (samples indicated as +HA) and samples without incubation with free HA (Fig. 23-29). Thus, it would be possible to determine the normal NP-cell interactions and the NP-cell interactions in conditions, where NPs and free HA compete for the binding site at CD44 receptors. NPs were incubated with MDA cells for 2h in FC1, FC2 and FC3.

In FC1, the NP samples were tested with and without preincubation with free HA. Free HA was added to the cells 1-hour prior to the incubation with NPs and medium containing free HA was discarded prior to adding NPs (VLPs 7 µg, NDs 30 µg). Two concentrations of free HA were tested (0.2 mg/ml or 1 mg/ml). In literature excess of free HA is usually used (5 or 10 mg/ml) (Li et al., 2016; Wang et al., 2018). Therefore, it was expected that a higher concentration of free HA in the competitive cell-binding assay would cause a more distinct reduction of NP-cell interactions in NP-HA* samples (VLP-HA* and ND-HA*).

Alternatively, free HA in FC2 (2 mg/ml) and in FC3 (5 mg/ml) was added simultaneously with the NPs. In FC2 standard amount of NPs was used (VLPs 7 µg,

NDs 30 µg per well), whereas a higher amount of VLP-HA* was used in FC3 (VLPs 12 µg, NDs 30 µg, VLP-HA* also 20 µg per well). After co-incubation with NPs, the cells were washed and prepared for flow cytometry detection of NP-cell interactions. Data obtained from the flow cytometry were processed using Kaluza software 2.1 (see gating strategy in Appendix II - S.ii).

In FC1 the effect of incubation of cells with free HA prior to incubation with NPs was observable in the ND-HA* sample, the higher the amount of free HA delivered for preincubation (1 mg/ml), the larger the reduction of the median fluorescence intensity (MFI) value, and the larger the reduction of the NP-cell interactions (Figure 23B). Nonetheless, the differences within the ND-HA* replicates were large. In the VLP-HA* sample, lower concentration of free HA (0.2 mg/ml) in preincubation was not having any effect on reduction of the NP-cell interactions, surprisingly a slight increase could be observed instead.

Another result of the FC1 experiment were the surprisingly high NP-cell interactions of ND-Bp and VLP-Bp. In the VLP-Bp sample this was expected as this result can be explained by the rather high VP1-mediated interactions of NPs with the cells, which is characteristic for VLPs. As Bp is small in size it does not hinder the VP1-specific interactions as effectively as large ligands. However, nonspecific interactions with cells have not been reported for ND samples that were obtained for this study, they were not expected to interact with cells when not modified, therefore the increased MFI value was surprising and might potentially be an effect of the dye. Moreover, both VLP-Bp and ND-Bp had a higher number of Bp molecules attached to NPs than their VLP-HA*/PEG* or ND-HA* counterparts (Fig. 22), which affects the final MFI value. Compared to VLP-PEG*, VLP-HA* exhibited slightly increased cell binding, but it was probably not mediated by CD44, since no reduction of NP-cell interactions could be observed in the VLP-HA* sample after preincubation with non-labeled HA. Free controls (HA*, PEG*, Bp; 1.4 µM) were tested too and showed low or almost no interaction with the MDA cells.
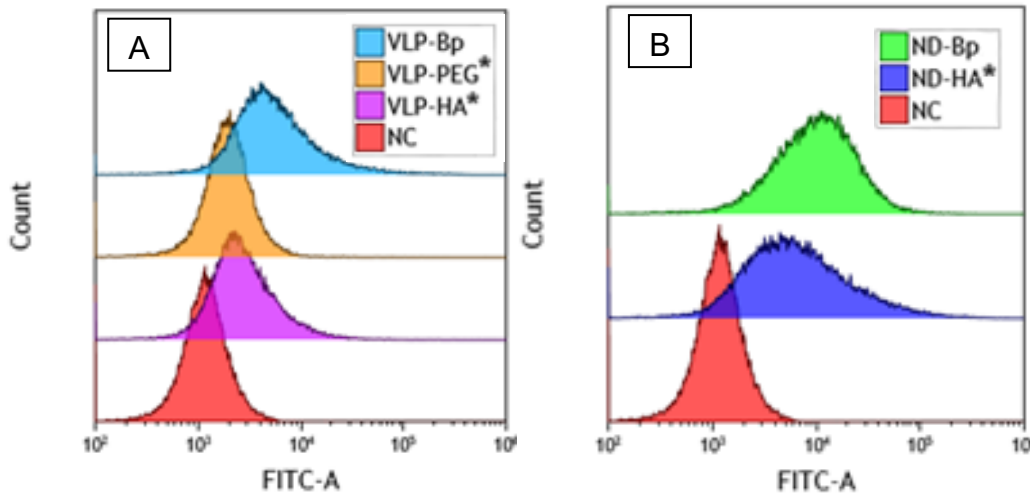
Figure 22 Overlaying histograms of gated live singlets of all A) VLP and B) ND variants (samples not incubated with free HA) compared to NC from FC1 experiment, mean data of duplicates are shown. Kaluza 2.1

As no reduction of NP-cell interactions was observed in the VLP-HA* sample (22A, C) after preincubation with free HA in FC1, it was determined that a different strategy in competitive cell-binding assay will be used in further experiments.

Free HA could be rapidly internalized and previously published studies also used higher concentration of free HA in similar experiments. Hence in FC2, FC3 free HA was added to the MDA cells simultaneously with NPs and was not discarded before the incubation with NPs (co-incubation of free HA and NPs with cells). Moreover, a larger amount of free HA was used in the competitive cell-binding experiments.
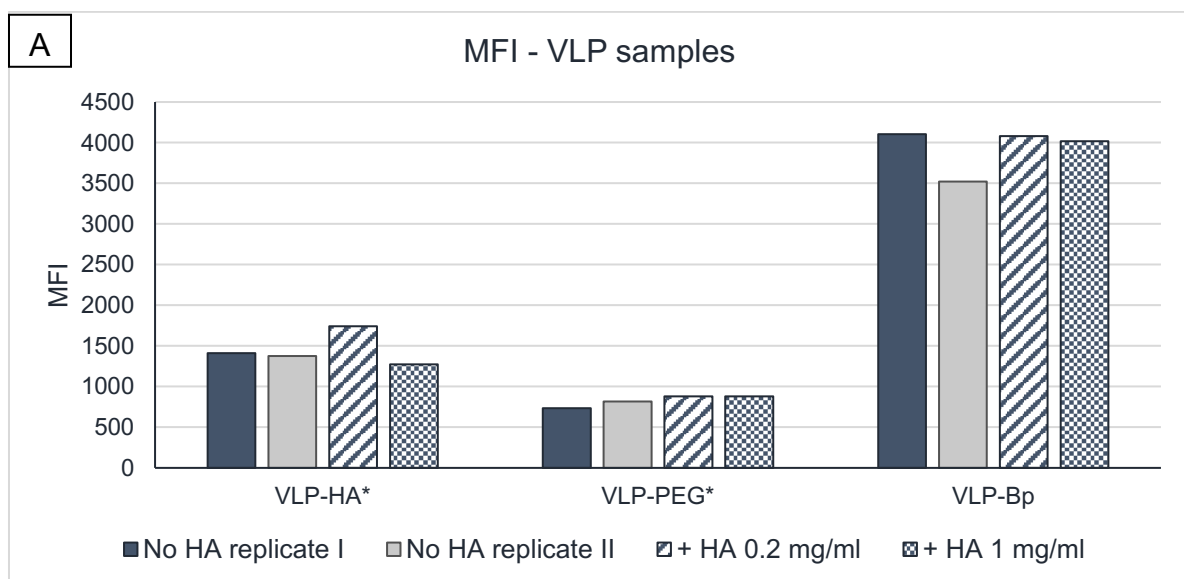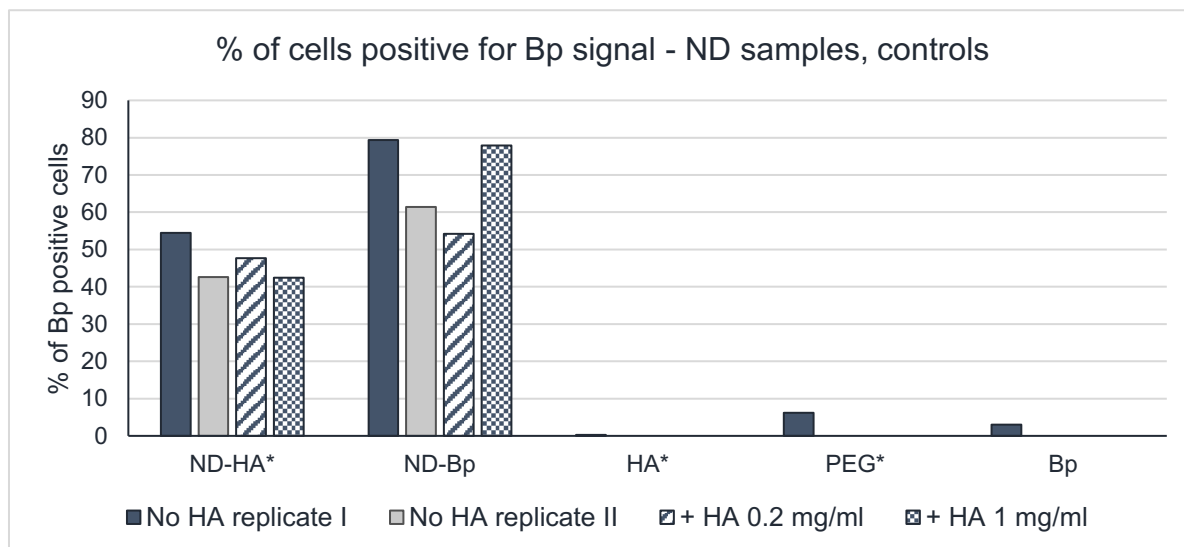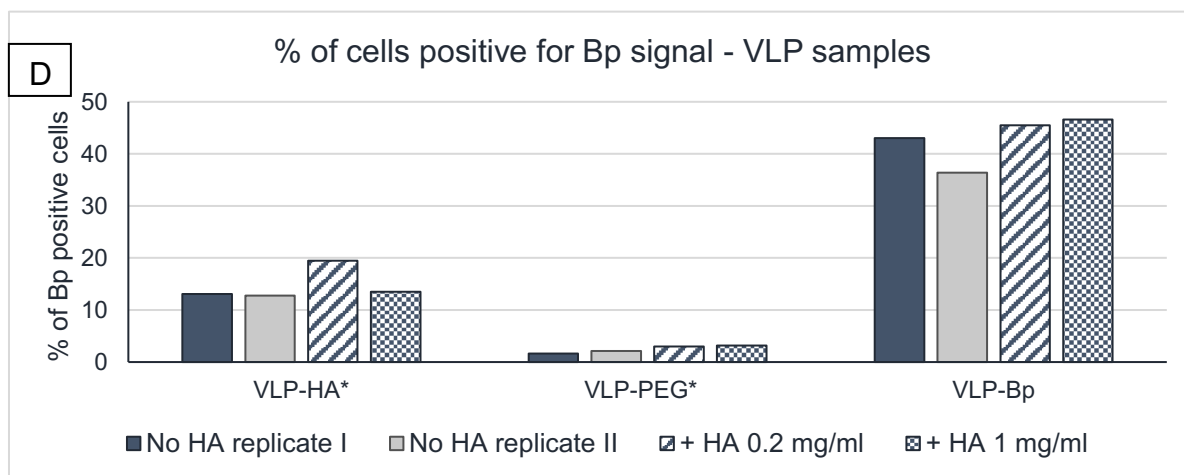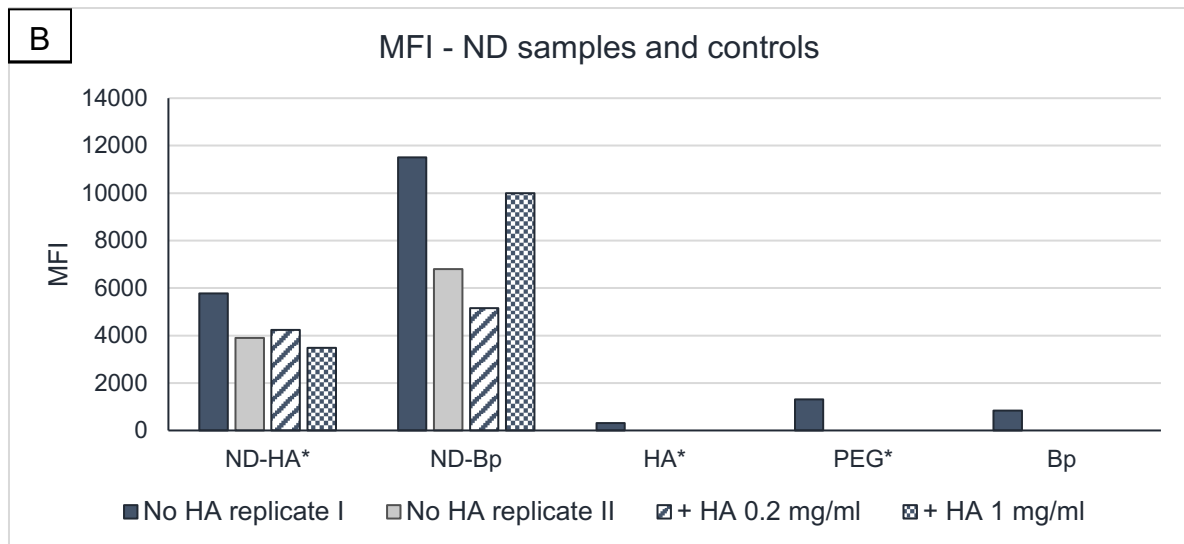
Figure 23 Graphs of the MFI values and the % of cells positive for the Bp signal from the FC1 experiment. Fully colored columns indicate two replicates – I and II of samples not incubated with free HA, dashed columns indicate preincubation of samples with free HA 0.2 mg/ml, checkered columns indicate preincubation with 1 mg/ml free HA. The first two graphs show the median fluorescent intensity (MFI) in live cell population in A) VLP samples and in B) ND samples and free controls. The other two graphs show the % of cells positive for the Bp signal in C) VLP samples and D) in ND samples and free controls. A slight effect of HA preincubation is shown as NP-cell interaction reduction in NP-HA*.

Based on the results from the first NP-cell interaction experiment, it was decided to repeat the experiment ("FC2 experiment"), this time with co-incubation of HA and NPs with the MDA cells and using a higher concentration of free HA for the co-incubation (2 mg/ml), which was expected to increase the effect of the incubation with free HA in ND-HA* and VLP-HA* samples, hence show a greater reduction of the NP-cell-interactions.

As a result, it was possible to observe a strong effect of co-incubation with free HA on NP-cell interactions in ND-HA*, the MFI was reduced by almost a half in the ND-HA* sample co-incubated with free HA compared to the sample without co-incubation with free HA. A slight reduction in NP-cell interactions could also be observed in the VLP-HA* sample co-incubated with free HA compared to the VLP-HA* sample not incubated with free HA.
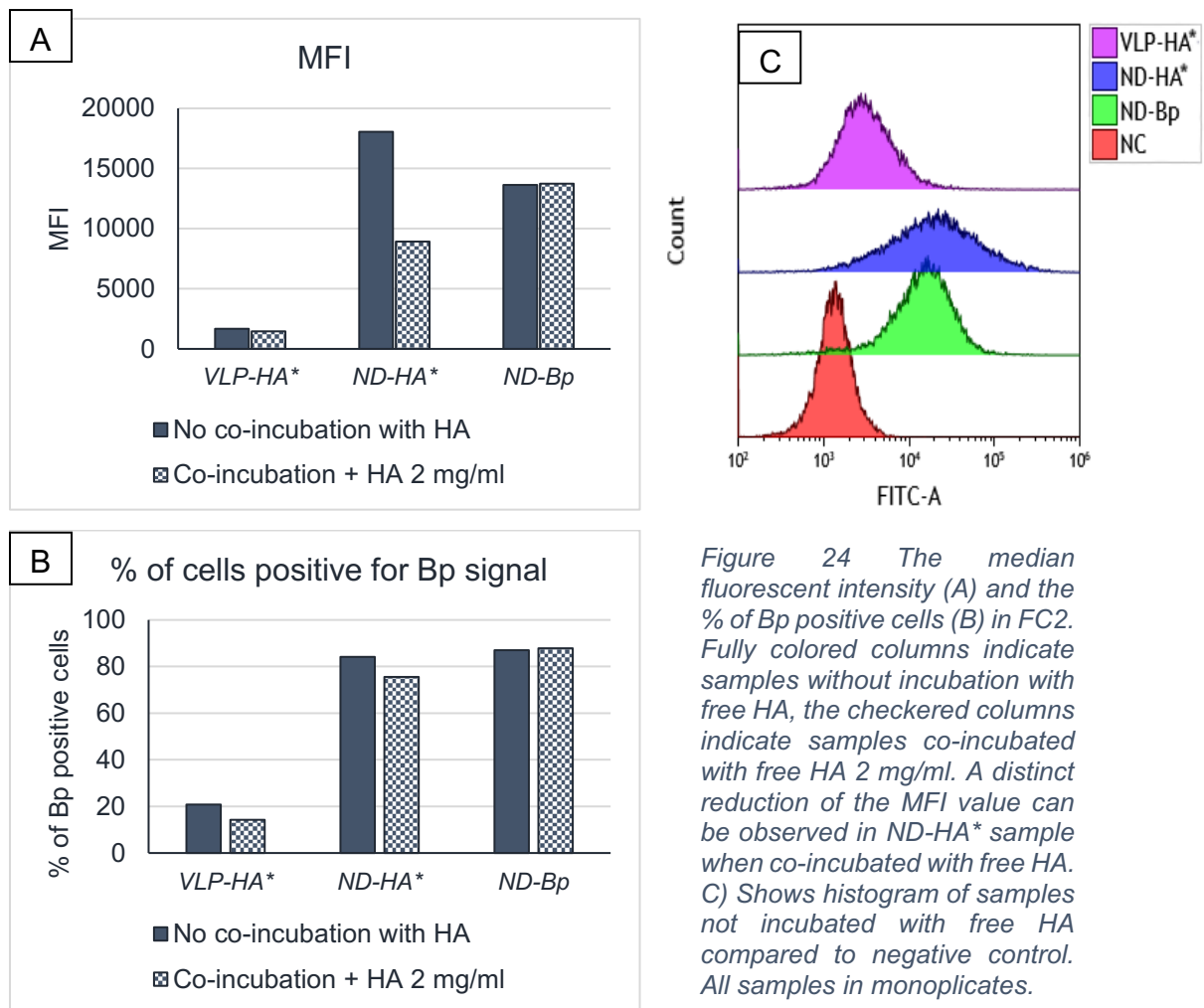
Figure 24 The median fluorescent intensity (A) and the % of Bp positive cells (B) in FC2. Fully colored columns indicate samples without incubation with free HA, the checkered columns indicate samples co-incubated with free HA 2 mg/ml. A distinct reduction of the MFI value can be observed in ND-HA sample when co-incubated with free HA. C) Shows histogram of samples not incubated with free HA compared to negative control. All samples in monoplicates.*

VLP-HA* interacted with the MDA cells distinctly less than ND-HA* (Figure 24). The reason for the low signal in VLP-HA* could be, the difference in surface coverage of NPs by HA*, as the surface coverage is lower in VLPs than in NDs. Based on the calculations about 56 (in VLP-HA*) compared to ~80 (in ND-HA*) molecules of HA* were estimated to be bound per NP (see Table 9). Therefore, a larger amount of VLP-HA* was used in subsequent experiments (FL1,2, FC3).

6.2.2 Fluorescent Microscopy Experiments

Subsequently, the interaction of the NPs with the cells was observed in two fluorescence experiments – FL1 and FL2. The fluorescence experiments were performed to obtain qualitative information about the NPs-cell interactions. As a large difference between VLP and ND samples in the NP-cell interactions was detected in FC1 and FC2, showing higher NP-cell interactions in ND samples, it was necessary to visualize the NP-cell interactions. It was expected that a large difference might be caused e.g. by excessive aggregation of VLP samples, which could be confirmed by fluorescence microscopy.

Like in the FC experiments, adherent cells were incubated with NPs for 2 h (FL1), alternatively for 30 min, 2 h and 4 h (FL2). In a competitive cell-binding assay some NP samples were also co-incubated with free HA and the cells(1.5 mg/ml) to evaluate, whether a reduction in NP-cell interactions would be observable in samples co-incubated with free HA compared to the samples that were not incubated with free HA. The amount of VLP-HA* in the experiment was increased to correspond to the fluorescent units of all other NPs.

The procedure was briefly as follows: The MDA cells ($1*10^5$ cells per well) were plated on a 24-well plate and left to grow overnight. The cells were washed, and serum-free IMDM medium was added (200 µl). Then, the procedure was slightly different in experiments FL1 and FL2. Two types of samples were present in the experiments: Samples with free HA and NPs co-incubated with cells (samples indicated as +HA) and samples without incubation with free HA. In the FL1, free HA (1.5 mg/ml) and NPs (only in VLP-HA* and ND-HA* sample, 9 µg and 30 µg respectively) or only NPs (of free controls) were added to the cells.

The samples were incubated for 2 hours (alternatively for 30 min, 2 h or 4 h in FL2) and further prepared for fluorescence microscopy (for details see Methods – 5.2.2.2). Micrographs were acquired using manual and automatic exposition.

As assumed, frequent aggregation could be observed in all VLP samples (VLP-HA*, VLP-PEG*, VLP-Bp) (Fig. 25). The aggregation was most distinct in the VLP-Bp sample. Due to the aggregation in all VLP variants, it was subsequently possible to observe high local fluorescence, however, often outside the cells. Therefore, VLPs were sonicated before incubation with cells in further experiments (FL2 and FC3).

	VLP-Bp	
	ND-HA*	
	ND-HA* +HA	
	ND-Bp	
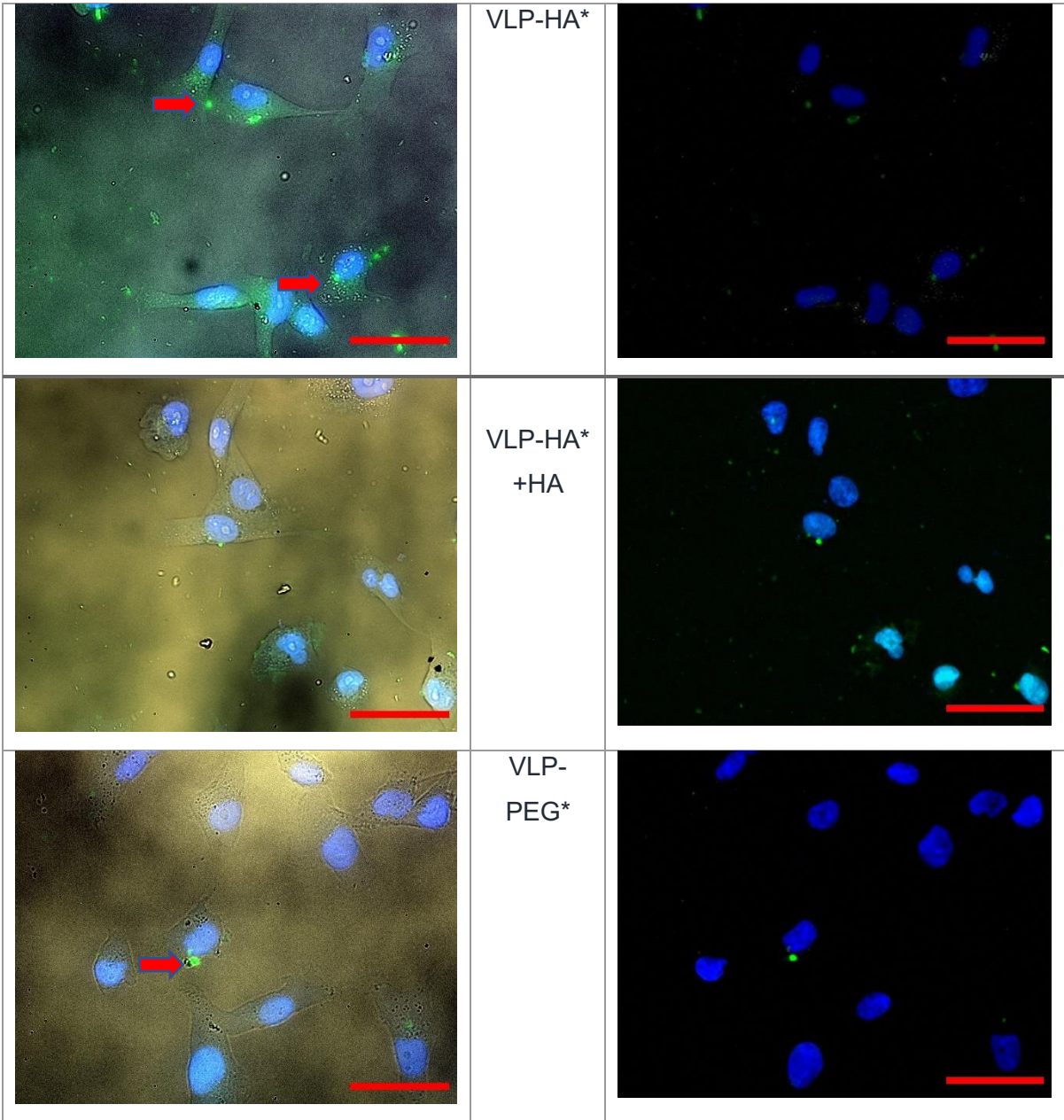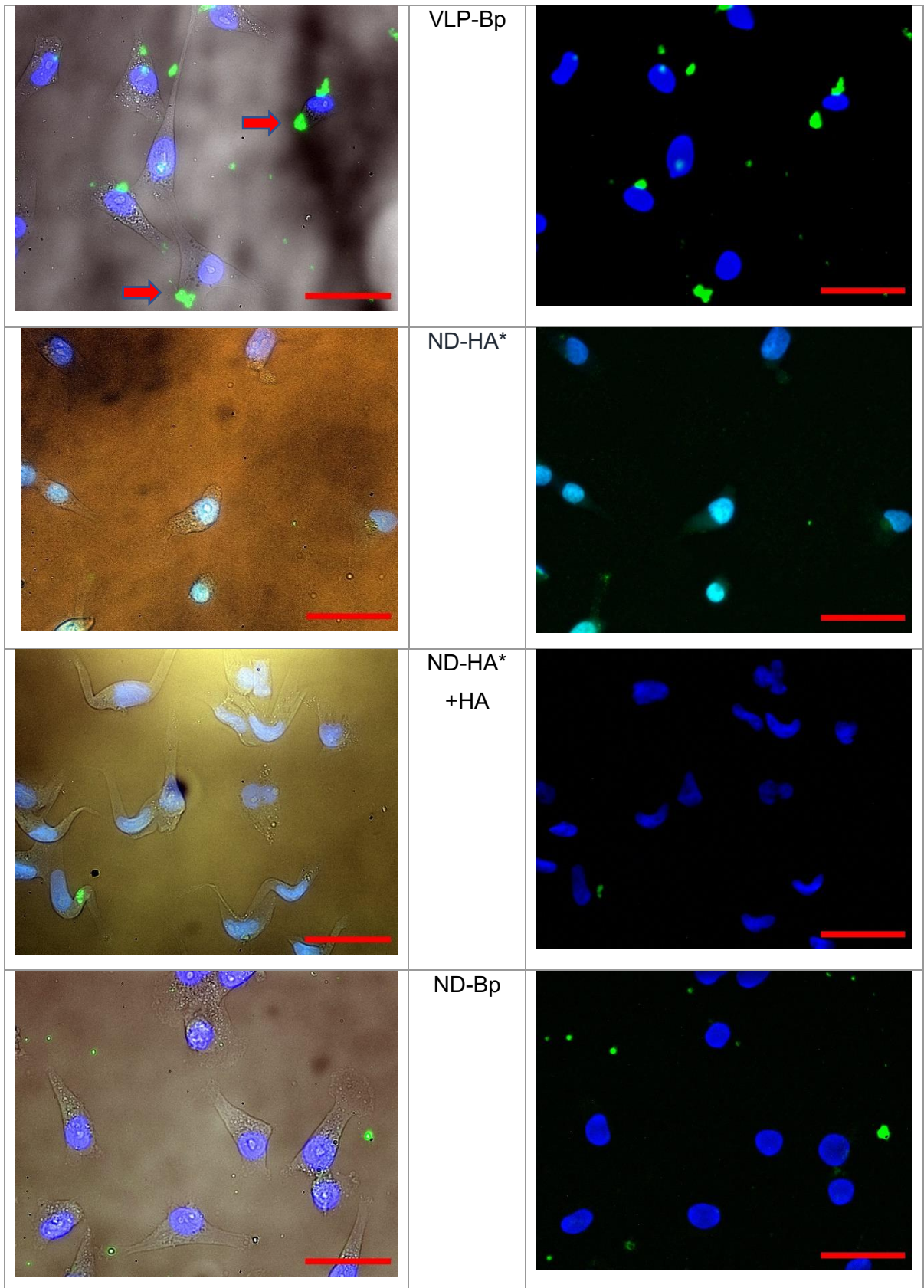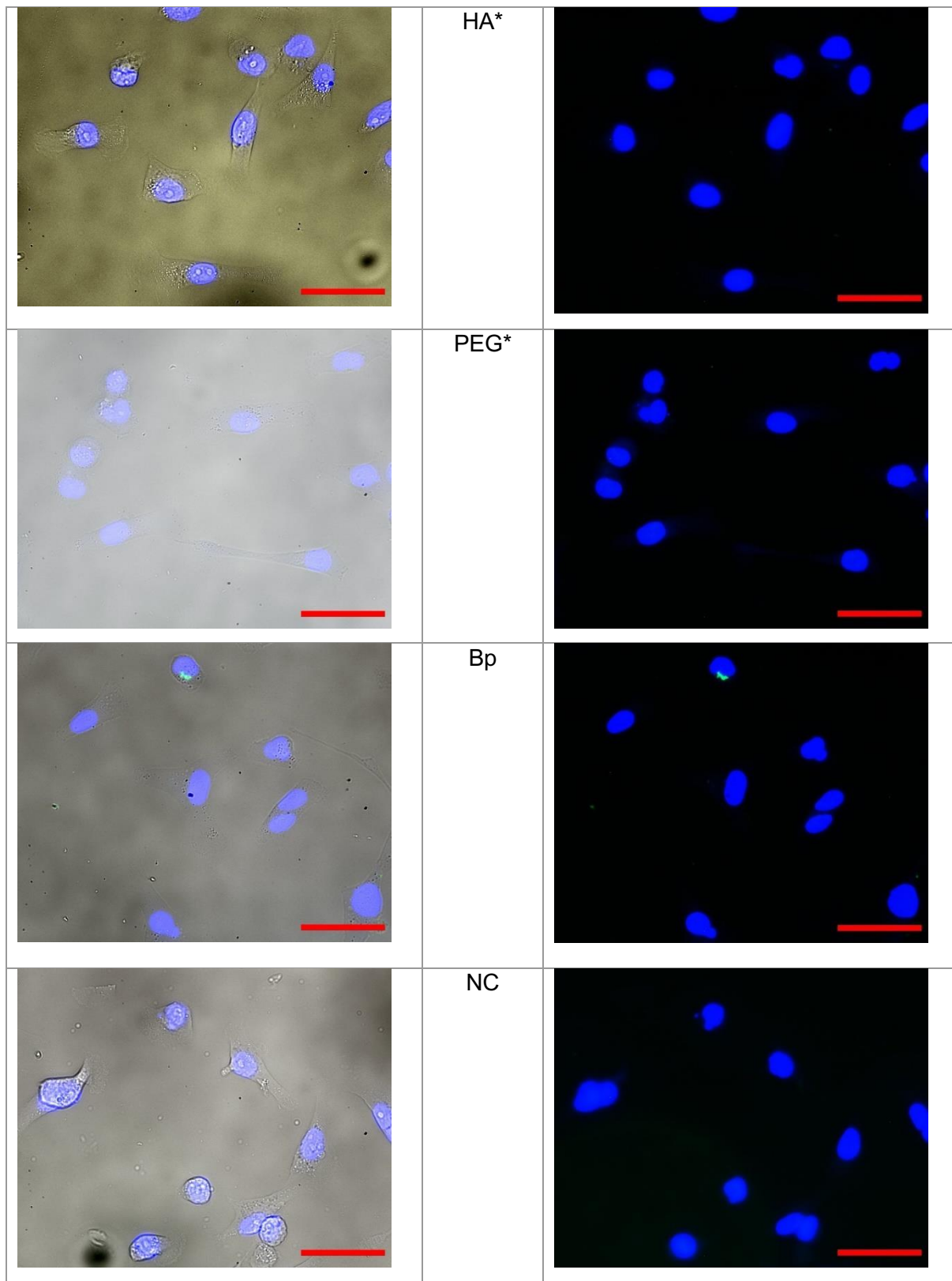
Figure 25 FL1 – incubation of NPs (NDs 15 µg, VLP-HA* 9 µg, VLP-PEG*/Bp 3.5 µg in 200 µl of serum-free IMDM medium), of free controls (HA*, PEG*, Bp; 1.4 µM), or only of serum-free IMDM medium (NC) with MDA-MB231 cells, 2 h. Micrographs of merged images from brightfield projection, DAPI staining (blue) and Bp signal (green) are shown in the left panels and merged images from DAPI and Bp signals only are shown in the right panels. Samples indicated as +HA (VLP-HA*+HA, ND-HA*+HA) were co-incubated with free HA (1.5 mg/ml). Red arrows indicate aggregates in VLP samples. Indicated red scalebars show 50 µm. The samples were observed under fluorescent microscope BX60F-3.

NDs did not exhibit aggregation and were analyzed in detail during longer exposure times (Fig. 26).
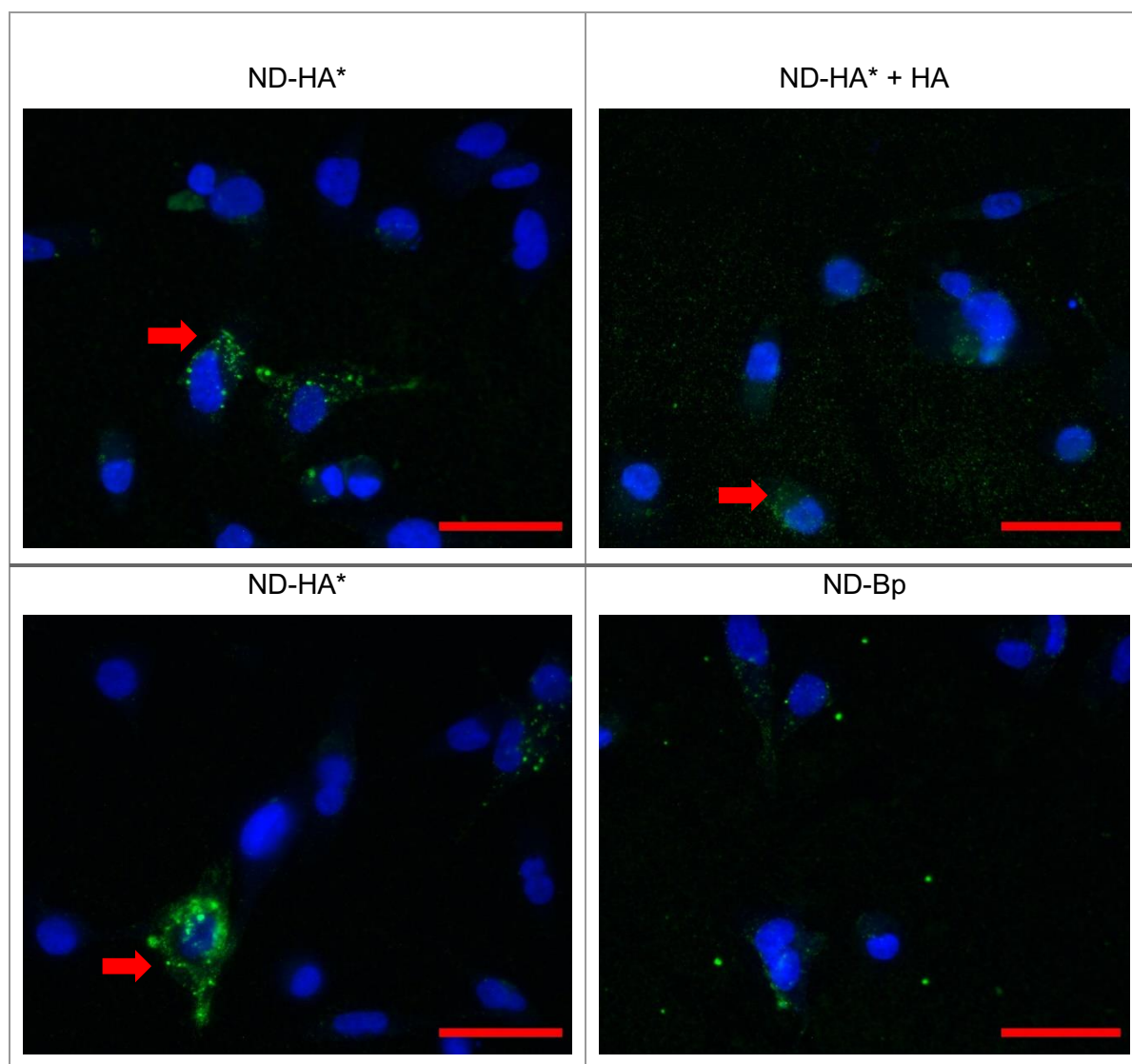
Figure 26 ND samples, fluorescent images captured with automatic exposure, DAPI (blue) and Bp (green) signals acquired; + HA samples indicate co-incubation of NDs with free HA (1.5 mg/ml) and MDA-MB231 cells. Red arrows show NDs accumulated at the cell surface or inside the cells. Less Bp fluorescent signal can be observed in cells in the ND-HA* +HA sample compared to the sample not incubated with free HA – the ND-HA* sample. NPs mostly scattered outside the cells can be observed in the ND-Bp sample. Indicated red scalebars show 50 µm. The samples were observed under the fluorescent microscope BX60F-3.

The FL1 experiment for visualizing the interaction of NPs with cells using fluorescence microscopy was repeated in FL2. Due to aggregates found in VLP samples in FL1, the VLPs in FL2 were sonicated prior to incubation with cells.

Also, since the incubation time could affect the number of internalized particles, different lengths of incubation time of NPs with cells (30 min, 2 h, 4 h) were tested. In previous experiments, the incubation time was set at 2 hours. Nevertheless, other studies used longer incubations (3 or 4 h) (Xiao et al., 2015; Yu et al., 2013).

Only VLP-HA*, VLP-Bp and ND-HA* with the longest NP-cell incubation time (4 h) were also tested on co-incubation with free HA (1.5 mg/ml) as it was done in FL1. The VLP samples appeared less aggregated due to sonication. Nonetheless, it would probably be appropriate to sonicate the samples longer. After 30 minutes, most of the particles were present outside of the cells and after two hours, NPs could be detected partly in the cells. At 4 hours of incubation, the situation was similar to two hours, nevertheless slightly better, as more Bp signal could be detected in the cells in the ND-HA* sample.

The co-incubation of NPs and free HA with the cells reduced the NP-cell interactions of ND-HA* (Fig. 27), while in VLP-HA* samples, this effect was almost unobservable. A similar result as in VLP-HA* was observed in the control (VLP-Bp), where it was expected that co-incubation with free HA should not have any effect on the NP-cell interactions (only representative micrographs of 4 h incubation shown in Figure 27).
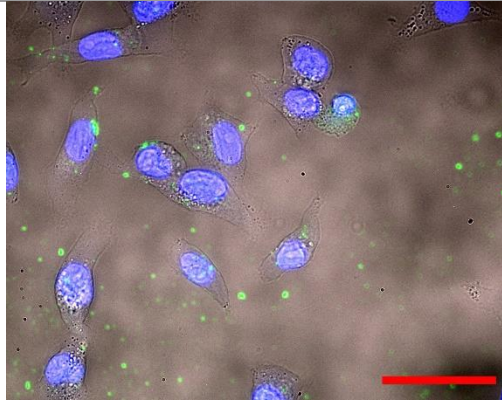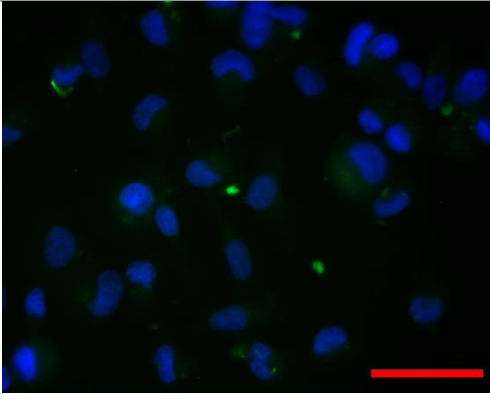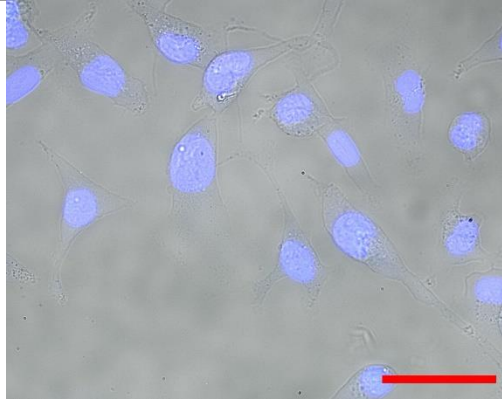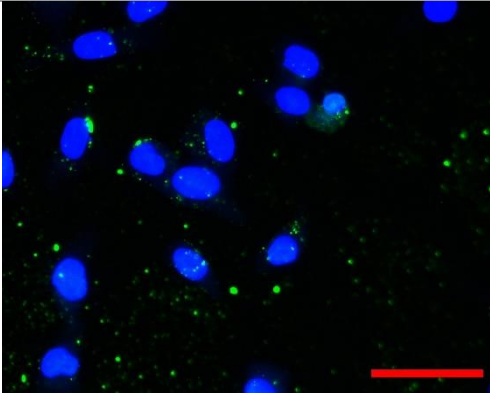
4 hours incubation

ND-HA*

VLP-HA*

VLP-Bp

NC

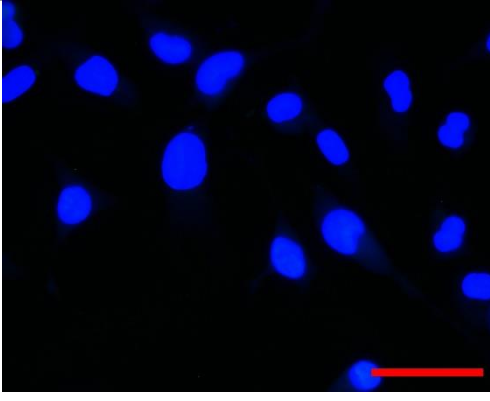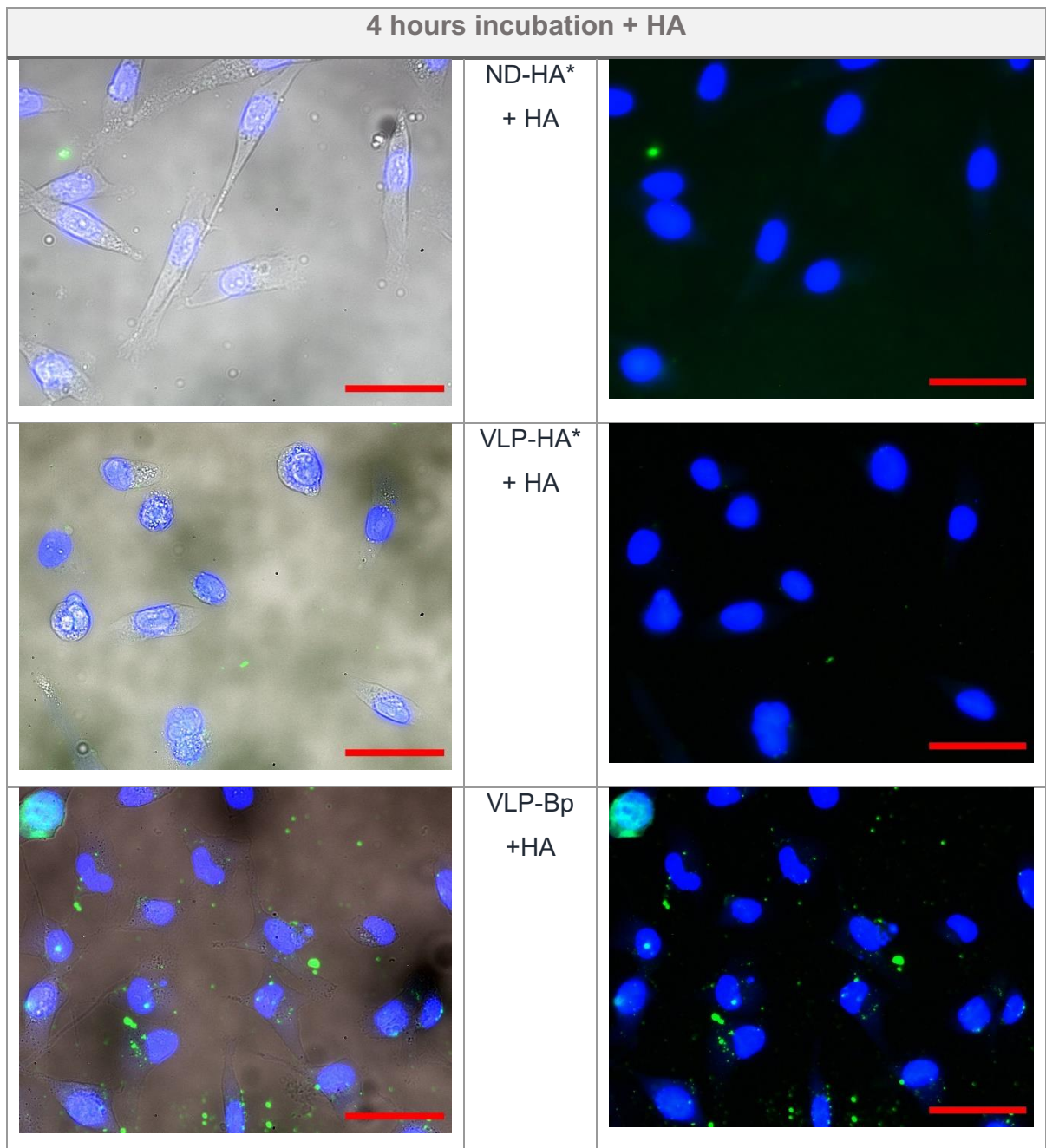| 4 hours incubation + HA		
	ND-HA* + HA	
	VLP-HA* + HA	
	VLP-Bp +HA	
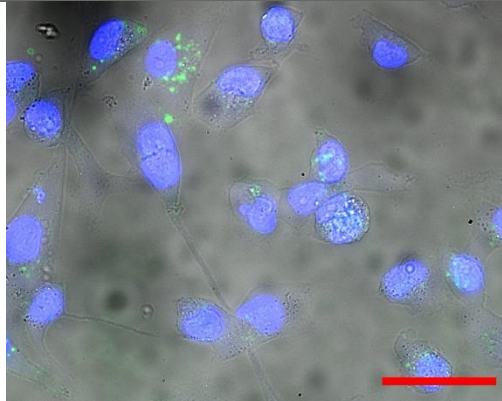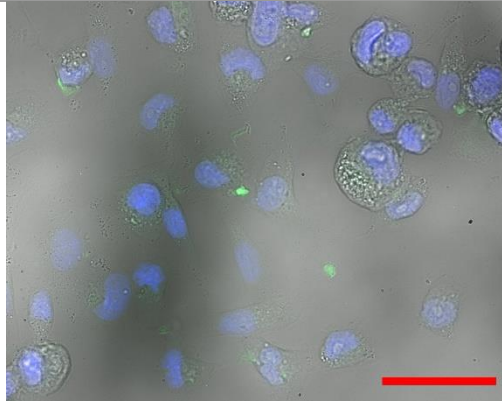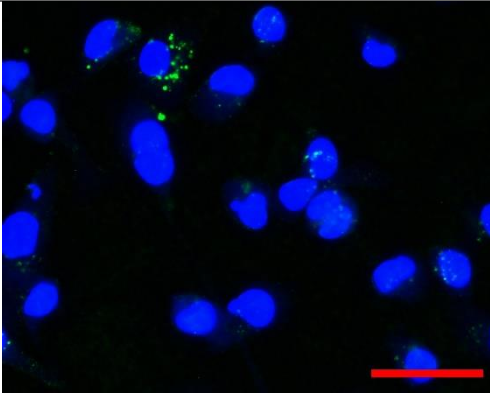
Figure 27 FL2 – 4-hour long incubation of NPs (ND-HA* 15ug, VLP-HA* 9 µg, VLP-Bp 3.5 µg in 200 µl of serum-free IMDM medium) or only serum-free IMDM medium (NC) with MDA-MB231 cells. Summarized micrographs of merged images from brightfield projection, DAPI staining (blue) and Bp signal (green) are shown in the left panels and merged images from merged DAPI and Bp signals only are shown in the right panels. Samples indicated as +HA (VLP-HA*+HA, ND-HA*+HA, VLP-Bp+HA) were co-incubated with free HA (1.5 mg/ml). Micrographs were acquired with manual exposition per each projection. Indicated red scalebars show 50 µm. The samples were observed under the fluorescent microscope BX60F-3.

In summary, the findings from the previous experiments were as follows: In the competitive cell-binding assay, co-incubation of free HA and NPs with cells, and a higher concentration of free HA in the co-incubation caused a larger reduction of NP-cell interactions in the ND-HA* sample in FC2. Aggregates were found in VLP samples in FL1; therefore, VLP samples were sonicated prior to incubation with the cells (FL2). Furthermore, a larger amount of VLP-HA* compared to other NPs was used for incubation with the MDA cells in FL1,2 due to a lower surface coverage by Bp in the sample compared to all other NP samples. Eventually, these findings from the previous experiments were applied to the final experiment, FC3.

6.2.3 The Final Flow Cytometry Experiment – FC3

In FC3, standard (12 µg as other VLP samples) and larger (20 µg) amounts of VLP-HA* were incubated with the MDA cells. The NPs were incubated with the cells for standard 2 hours. All types of NPs were used in triplicates and were co-incubated with, due to limited availability of materials, the highest concentration of free HA of 5 mg/ml. Finally the concentration of free HA used in the competitive cell-binding assay was comparable to other studies. Thus, it was expected that a distinct reduction of NP-cell interactions would be observable in NP-HA* samples after co-incubation with free HA. Because VLP internalization could also be negatively affected by excessive aggregation, VLP samples were sonicated before incubation with cells.

The FC3 experiment was similar to FC1 and FC2 and was arranged as follows: the MDA cells were plated on a 12-well plate ($2*10^5$) and incubated overnight. The cells were washed, and fresh serum-free IMDM medium was added (300 µl). Two types of samples were present in the FC3 experiment, samples with co-incubation of free HA (5 mg/ml) and NPs with the cells and samples without incubation with free HA. Hereby, normal NP-cell interactions and the NP-cell interactions when NPs compete for the binding site at CD44 with free HA could be compared. If a reduction in NP-cell interactions would be observed in the samples incubated with free HA, it would be expected that the NPs enter via the CD44 receptor.

Furthermore, free HA (5 mg/ml) was added simultaneously with the NPs (VLPs 12 µg, NDs 30 µg, also 20 µg tested for VLP-HA*). The samples were washed and prepared for flow cytometry detection of the NP-cell interactions. Data obtained from the FC3 were processed using Kaluza software 2.1 (see gating strategy in Appendix II – Fig. S.ii).

No reduction of the MFI value was observed in VLP-HA* (12 µg) co-incubated with free HA, compared to the counterpart that was not incubated with free HA. However, a slight reduction of the MFI value was detected in VLP-HA* (20 µg) samples after co-incubation with free HA. This reduction was nonetheless not observable in the percentage of cells positive for Bp signal (Fig. 28 and 29).

This could recurrently be explained by the presence of aggregates in VLP samples as aggregated VLPs might provide high fluorescent signals to single cells when internalized. In the correspondent control, VLP-PEG*, almost no effect of the co-incubation with free HA was detected as expected. Surprisingly, an increase in the percentage of cells positive for Bp signal was detected. In the VLP-Bp control an increase could also be observed in both, the MFI value and in the percentage of cells positive for Bp signal.
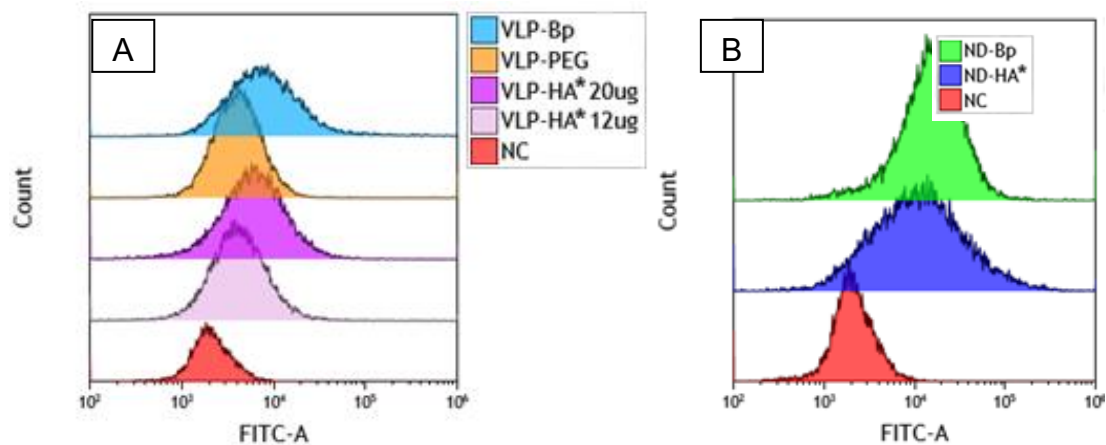

Figure 28 Overlaying histograms of gated live singlets of all A) VLP and B) ND variants (samples not incubated with free HA) compared to NC from the FC3 experiment, merged data of triplicate samples are shown. Kaluza 2.1

The co-incubation of the ND-HA* sample and free HA with the MDA cells showed a reduction in the NP-cell interactions compared to the sample that was not incubated with free HA. A reduction could be observed in both, the MFI value (a reduction by 60 %) and the percentage of cells positive for the Bp signal (Fig. 29), which confirms the expectation, that ND-HA* probably enter the cells via the CD44 receptor.

NPs with conjugated Bp, i.e. VLP-Bp and ND-Bp showed high values, both the MFI and the percentage of cells positive for the Bp signal that was not influenced by the addition of free HA, thus showing a CD44 non-specific interaction or uptake of these NPs.

To confirm that the MDA cells are able to interact with HA *per se*, the HA* compound was used in the control assay. According to the expectation, high MFI value of cells was observed after the addition of HA* (16 μM), which shows that HA* is taken up by the cells, plausibly via the overexpressed CD44 receptors. Controls PEG* and Bp show almost no interactions with MDA cells as expected.
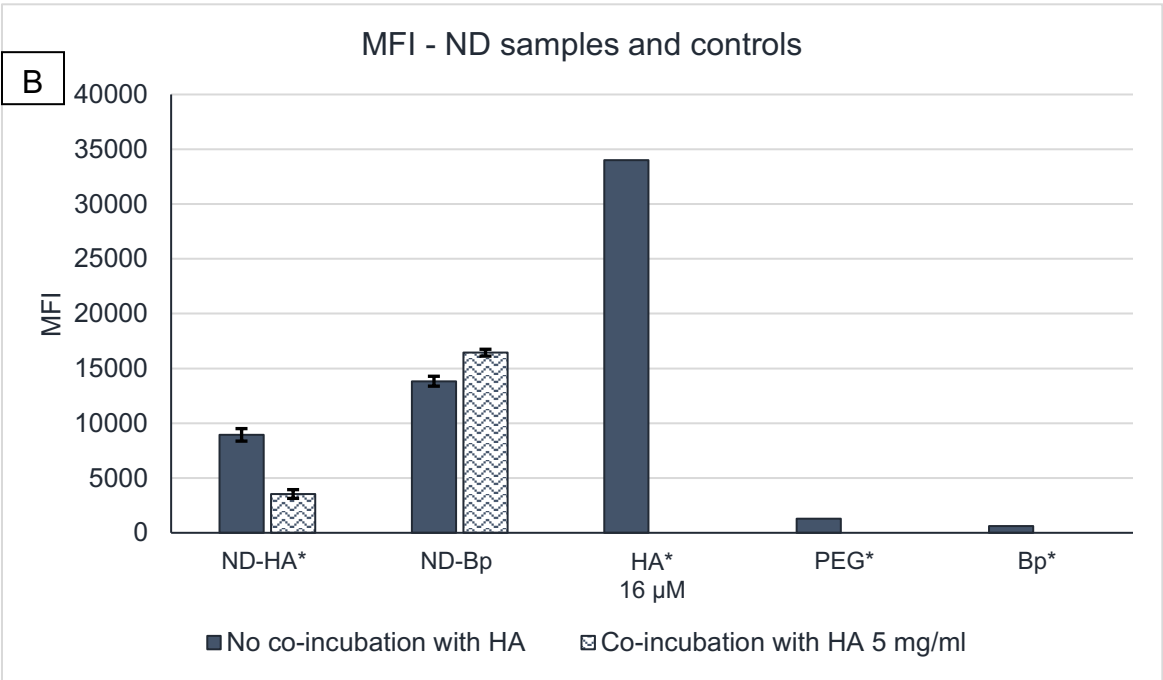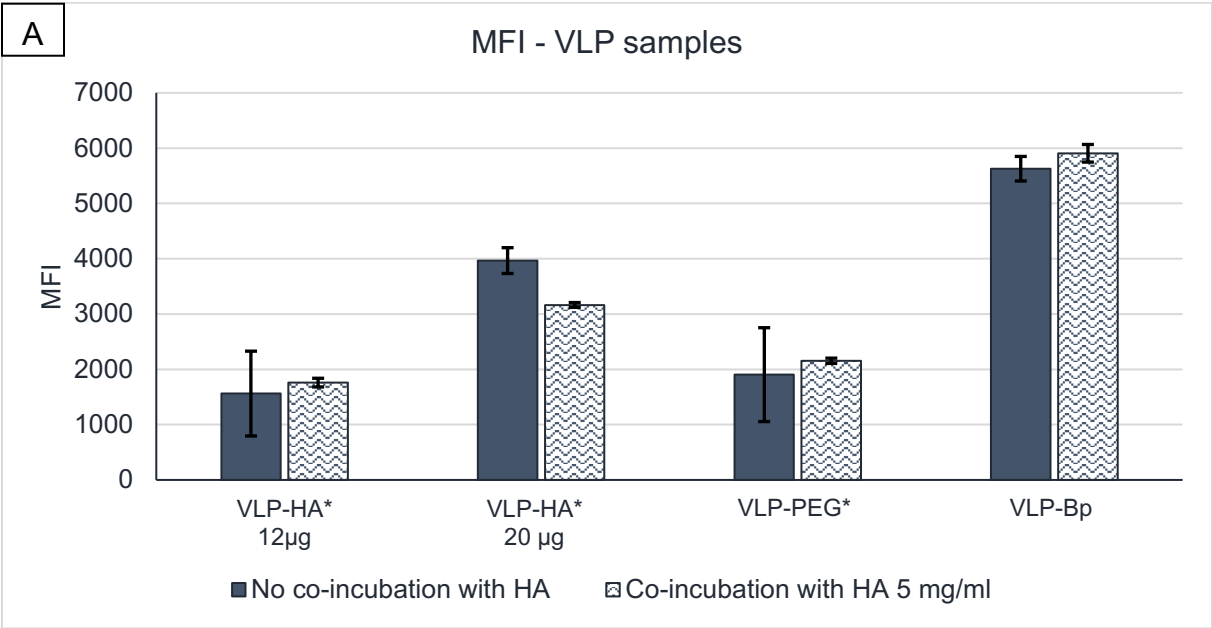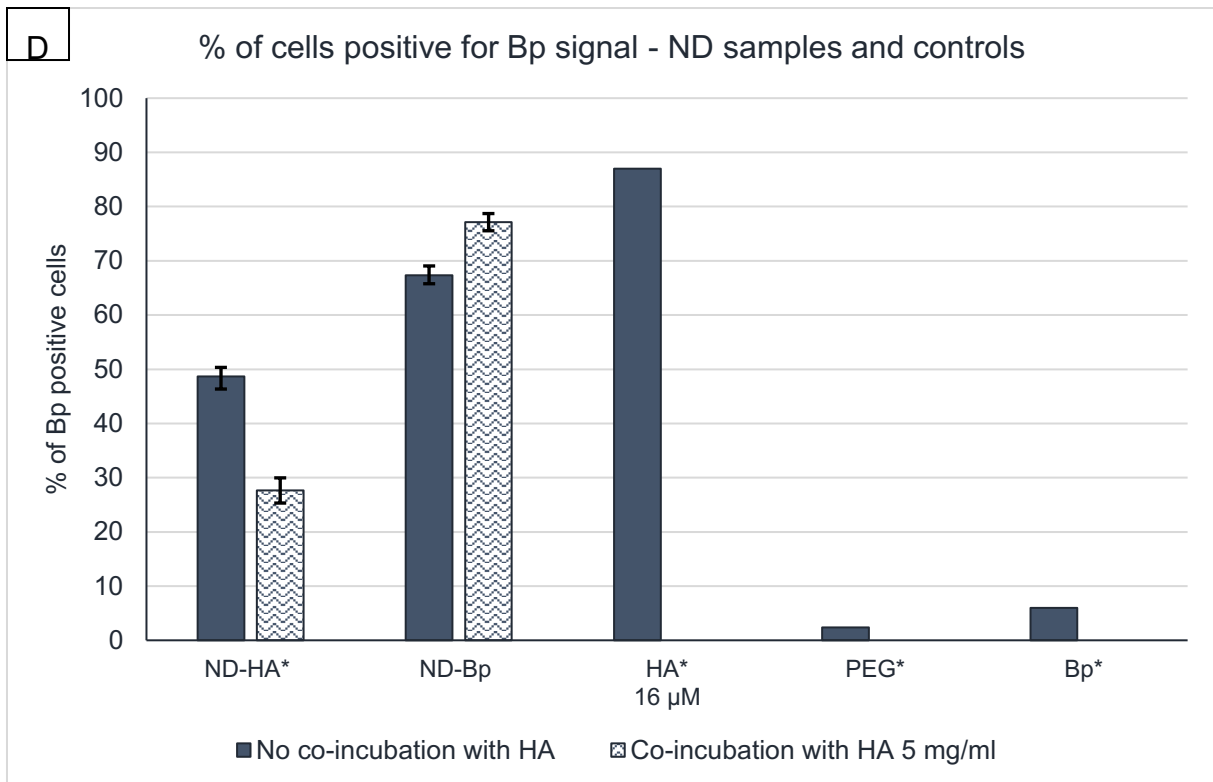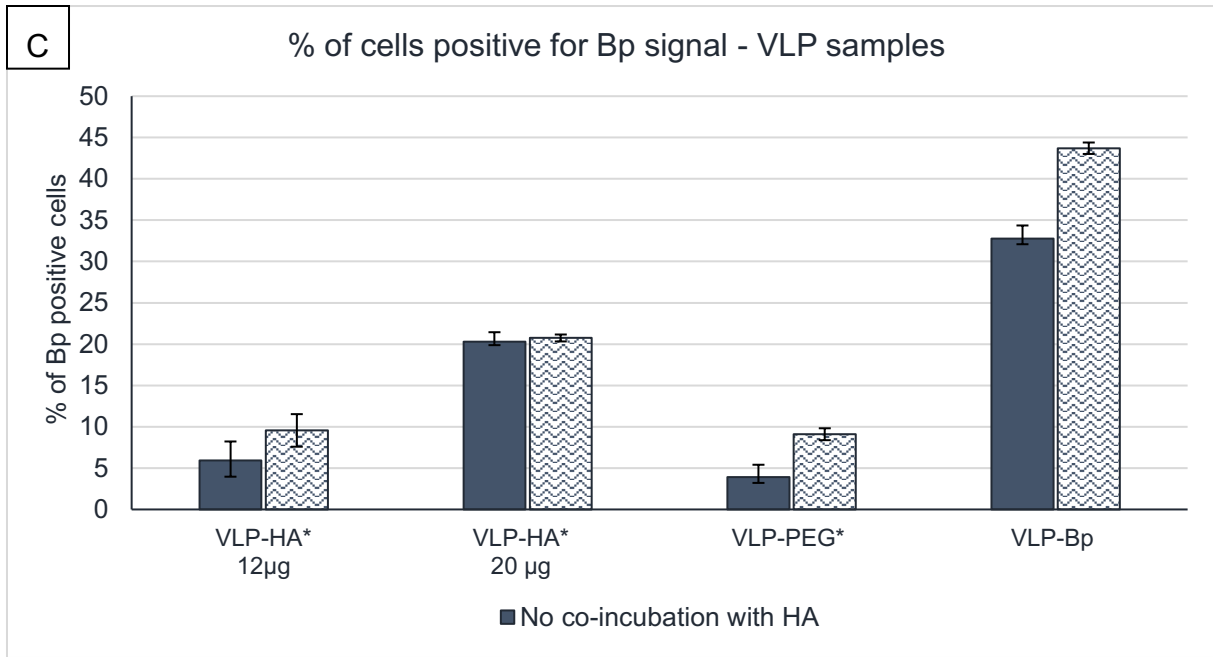
Figure 29 Graphs of the MFI values and of the % of Bp positive cells of live gated singlets in FC3. Fully colored columns indicate samples without incubation with free HA, patterned columns indicate co-incubation with HA (2 mg/ml). VLP-HA* 12 µg indicates 12 µg of VLP-HA* in incubation with cells, VLP-HA* 20 µg indicates 20 µg of VLP-HA* (in 300 µl of IMDM medium). In all other VLP samples 12 µg and in ND-samples 30 µg were incubated with cells for 2 hours (in 300 µl of IMDM medium).

The first two graphs show the median fluorescent intensity in live cell population in A) VLP samples and in B) ND samples and controls (HA*, PEG*, Bp). The other two graphs show the % of Bp positive cells in C) VLP samples and D) in ND samples and free controls. Data shows mean of measurement in triplicates, error bars indicate the standard deviation of the triplicates. Differences between samples incubated with free HA and samples not incubated with free HA were analyzed in GraphPad Prism 8 by the Mann Whitney statistical test and were insignificant, nevertheless a strong trend was observed.

Resulting values (MFI, % of BP positive cells) of the samples that were not incubated with free HA and the samples incubated with free HA were compared. The data were analyzed by the Mann Whitney statistical test and showed statistically insignificant differences; however, a strong trend was observed, hence more measurements could be performed to obtain a higher statistical power.

In conclusion, our data showed that modification of VLP with HA*, in contrast to ND-HA*, did not result in the efficient CD44-mediated interactions with CD44 positive cells. The lower interaction of VLP-PEG* control with MDA cells compared to VLP-Bp* suggested that PEG* (20 kDa) provided efficient shielding capacity from the VP1-mediated interactions to the VLPs. VLP-Bp and ND-Bp showed high (unexpected in case of ND-Bp) interacting potential with the MDA cells, these results require further analysis.

7. Discussion

Nanoparticles are widely studied in the field of cancer research as advantageous drug delivery and diagnostic platforms; they can protect the payload and be specifically targeted to cancer biomarkers. Various targeting moieties were conjugated onto NPs in previous studies (e.g. folate, , transferrin, hyaluronic acid) and numerous nanoparticle types were tested (e.g. polymeric, lipidic, protein-based) (Zackova Suchanova et al., 2017; Byeon et al., 2018; Neburkova et al., 2018).

The MPyV VLPs could potentially serve as theragnostic agents. Nonetheless, the main problem of a plausible VLP use in active targeting, is their interaction with a wide range of cells based on the VP1 interaction with its ubiquitous receptors. This project aimed to achieve two goals simultaneously: hinder the broad VP1-specific interactions with cells and at the same time re-target the VLPs to a "cancer associated" target. In the current study specifically to the CD44 receptor overexpressed on many types of cancer cells. In the past, transferrin has already been tested as cancer cells targeting moiety in VLPs (Zackova Suchanova 2012; Zackova Suchanova et al., 2017).

Fluorescently labeled HA (Mw 8-15 kDa) was used in this study; to modify the surface of the MPyV VLPs by conjugation via an alkyne linker (resulting in VLP-HA*) and to re-target the VLPs to the CD44 receptor. Other VLP variants were prepared too to serve as controls: Fluorescently labeled PEG (~Mw 20 kDa) was conjugated onto VLPs, resulting in VLP-PEG*. Due to a similar size to the HA*, PEG* should provide a similar shielding capacity from the VP1-specific interactions to the VLPs as HA* in VLP-HA*. Bodipy alone was also conjugated onto VLPs, resulting in VLP-Bp. The small-sized fluorescent probe partially allows the VLPs the VP1-mediated cell interactions. Moreover, free controls (HA*, PEG*, Bp) were also tested. Another type of NPs, nanodiamonds with either fluorescent HA* (ND-HA*) of Bp (ND-Bp) were provided by Jitka Neburková (IOCB) to serve as controls.

.

7.1 MPyV VLP Constructs Production and NP Characterization

MPyV VLPs were produced, the alkyne linker was attached and subsequently HA*/PEG*/Bp were conjugated onto VLP-alkyne using click chemistry. Different numbers of HA* (VLP-HA* ~ 56 HA*), PEG* (VLP-PEG* ~ 144 PEG*) and Bp molecules (VLP-Bp ~ 153 Bp) per VLP-alkyne were conjugated. The difference in the number of the fluorescent probes attached in the VLP constructs could also be observed from the fluorescence signal detection from the SDS-PAGE gel. Even though the protein amount loaded onto the gel was the same in all VLP variants, the fluorescent signal of the VLP-PEG* and VLP-Bp samples was distinctly more intensive than that of the VLP-HA* sample.

The reason for a different number of HA* and PEG* molecules conjugated to VLP-alkyne could be as follows: In the HA* material received from Jitka Nebůrková (IOCB), used for the click reaction, a large amount of unlabeled HA was probably present. This was due to a less efficient conjugation of HA with Bp (than that of PEG with Bp). Hence, unconjugated unlabeled HA probably remained present in the HA* material during the click conjugation of HA* onto VLP-alkyne, which might explain why the resulting surface coverage of VLP-alkyne by HA* (in VLP-HA*) was lower than that by PEG* (in VLP-PEG*).

The reason for a high number of Bp molecules conjugated per VLP during the click reaction (~153 Bp/VLP-alkyne) in the VLP-Bp sample compared to the VLP-HA* is probably different. In the click reaction, the VLP-alkyne to Bp ratio was adjusted so that the resulting number of the Bp molecules bound per VLP-alkyne would correspond approximately to the number of HA* molecules bound per VLP surface in the VLP-HA* sample. As already mentioned, the fluorescent dye, Bp, is relatively small in size, it can achieve better access to alkyne functionalities on alkyne linkers due to lower steric hindrance. Steric hindrance might affect the efficiency of click reaction (Bock et al., 2006). Thus, the efficiency of the click reaction could be higher when conjugating VLP-alkyne with Bp than with larger ligands, such as HA* or PEG*.

NDs (ND-HA*, ND-Bp) used as control NPs in this thesis were prepared by Jitka Nebůrková (IOCB). NDs were modified by direct conjugation of HA* or Bp onto NDs by click reaction and resulted also in a different ligand per VLP number, ~80 (ND-HA*) and ~153 (ND-Bp) respectively.

7.2 NP-Cell Interaction Studies

The NP-cell interactions of VLP-HA* (and all other NP constructs and controls) with the human breast adenocarcinoma MDA-MB-231 cells, which overexpress the CD44 receptor were studied. The MDA cells have repeatedly been used in similar studies, nonetheless with alternative CD44-targeted NP types; and the conjugation of HA provided increased NP-cell interactions (Surace et al., 2009; Lee et al., 2013; Wang et al., 2018).

Briefly, all NP types (VLP-HA*, VLP-PEG*, VLP-Bp, ND-HA*, ND-Bp) and free controls (HA*, PEG*, Bp) were, usually for 2 hours, incubated with the MDA cells. Thereafter, the fluorescent signal was measured by flow cytometry or visualized by fluorescence microscopy. It was monitored whether the NPs would specifically interact with the CD44 receptor, which was evaluated by the competitive cell-binding assay. The principle of this assay was blocking the CD44 receptors before or during the incubation with NPs. This was performed in previously published studies in two ways, either by using an αCD44 monoclonal antibody (specific for the HA binding site, e.g. Hermes-1) or by using excess of unlabeled free HA, competing for the HA-binding site at CD44 receptors with the NPs (Surace et al., 2009; Ganesh et al., 2013b;). In both ways, the HA binding site at the CD44 receptor should be occupied, and consequently it should be possible to detect a reduction in NP-cell interactions (hence the MFI value). In this study, free HA was used for the competitive cell-binding assay.

In NP-MDA cell interaction studies, it was expected that HA* modified NPs, the VLP-HA* and ND-HA* nanoparticles would interact most with the MDA cells as HA provides the NPs CD44-specific targeting ability.

In the VLP constructs, it was expected that VLP-PEG* would show lower cell interactions than VLP-HA*, because PEG* should provide the same shielding capacity from broad VP1-specific cell-interactions as HA*. At the same time PEG*, however, lacks the targeting capability. VLP-Bp were expected to permit, at least partially, the VP1-specific interactions with the cells. NDs, unless modified, should not interact with the cells. Thus, it was expected that ND-HA* would interact more with the cells than ND-Bp. In free controls (HA*, PEG*, Bp) it was expected that HA* would interact the most with the cells due to binding to the CD44 receptors.

Nevertheless, as shown by previous studies, many factors may affect the efficiency of the cancer cell-NP interactions such as: the NP surface coverage by HA, HA molecular weight, the length of incubation time of NPs with cells, NP concentration used for incubation with cells, free HA concentration used for receptor competitive cell-binding assay and pre/co-incubation of NPs and free HA with cells (Eliaz and Szoka, 2001; Xiao et al., 2015; Zhao et al., 2015; Xiong et al., 2016; Sanfilippo et al., 2020).

The differences between ND samples and VLP samples in the interactions with the MDA cells in the first flow cytometry experiments (FC1, FC2) were markable, with NDs interacting with the MDA cells distinctly more. Already during the VLPs production, aggregation was frequently observed in the samples. Moreover, large differences between mean and median fluorescence were detected in the VLP samples, indicating non-homogenous behavior of the NPs in cell binding. So, it was hypothesized that the NP-cell interactions could be affected by a plausible excessive aggregation of the VLP samples, which was then also observed in the fluorescence experiments. Aggregates were observed in all VLP variants, compared to ND variants. Therefore, the VLP samples were sonicated in further experiments, before incubation with cells, which improved the problem with VLP aggregation (in FL2). Nonetheless, in the FC3 the NDs still interacted more intensely with the MDA cells than the VLPs.

Higher interaction with the MDA cells would be expected for the ND-HA* sample, however, not for the ND-Bp sample. As already mentioned, unmodified NDs were not expected to interact with cells and as Bp is small in size, it cannot cover the ND-surface.

It was surprising that ND-Bp appeared to interact most intensely with the cells in all NP-cell interaction experiments. This could be partially explained by obtaining the highest fluorescent signals in ND-Bp compared to other NPs due to the highest number of Bp molecules attached per NP (~153). Nevertheless, VLP-Bp were estimated to have the same number of Bp molecules attached (~153) and showed lower NP-cell interactions.

Therefore, it could be discussed that it could either be the NP type (VLPs or NDs) or the alkyne linker presence (present in VLPs, not present in NDs) that might affect the NP-cell interactions.

On VLPs the number of alkyne linkers attached per VLP was estimated from the Af488 fluorescent probe conjugation by click chemistry. As the expected number of surface lysines present per VLP is 720 and also higher numbers of alkyne linker molecules per VLP were calculated (476; 1196; 880 in VLP-alkyne working batches A, B and C respectively), it is expected that some disassembled particles were present in the samples, providing extra lysines for alkyne linker conjugation. Nevertheless, the estimated number of alkyne linkers attached per VLP was distinctly higher than the number of HA*/PEG*/Bp conjugated per VLP. Thus, multiple extra alkyne linkers are present at VLP surface.

O´Connor et al studied ordered lipid domains (typical for cancer and multidrug resistance cells) detection by lipophilic probes – Bodipy was conjugated to cholesterol either directly or a hexyl linker was introduced. The length of the linker affected the final localization of the probe, the probe with the linker introduced showed strong plasma membrane associations (O' Connor et al., 2019). It should be taken into consideration, that the NP-cell interactions could also be affected by the presence of the alkyne linkers on VLP surface.

Moreover, Bp-bound controls (VLP-Bp, ND-Bp) showed higher NP-cell interactions than their NP counterparts (VLP-Bp than VLP-PEG *, VLP-HA *; ND-Bp than ND-HA*): however, also the surface coverage by Bp in both types of NPs is highest in NP-Bp samples, and so it is believed that the highest values (both the MFI value and the % of Bp positive cells) are caused by the highest fluorescence of these samples. Therefore, the fluorescent signal in NP-cell interaction studies could be more pronounced.

An alternative explanation, unlikely, could be that Bp itself promotes the interactions of the NPs with the MDA cells. It was already presented that the fluorescent dye type may alter cellular uptake of NPs. In 2017 Snipstad et alia encapsulated six types of fluorescent dyes in commonly used NPs and it was shown that the dye type affected the cellular uptake (Snipstad et al., 2017). However, the free control - Bp did not show increased interactions with cells compared to other free controls; and when the approximate fluorescence normalization was estimated, VLP-HA* and VLP-Bp showed similar cell-interactions.

Therefore, it is expected that the reason for the high values of the fluorescent signal of the NP-Bp (mainly of VLP-Bp) in the FC experiments is as mentioned above, the high number of the BP molecules attached to the NP surface in the NP-Bp samples. Despite the same number of Bp molecules attached in VLP-Bp and ND-Bp, in all experiments, ND-Bp showed higher interactions with the MDA cells. In further studies it would be interesting to test ND conjugated with another type of fluorescent dye on NP-cell interactions in a similar manner to see whether the fluorescent dye type is affecting the NP-cell interactions.

The differences in the NP-cell interactions in the VLP samples were as follows: VLP-PEG* always showed the lowest NP-cell interactions, VLP-HA* intermediate and VLP-Bp interacted with the MDA cells similarly as VLP-HA*, nevertheless contained a different number of Bp molecules attached than VLP-HA*. As PEG* is of similar size as HA* (8-15 kDa), it should provide a similar shielding capacity from the VP1-specific interactions to the VLPs. However, the surface coverage by the shielding ligand is lower in the VLP-HA* (~56) compared to VLP-PEG* (~153). Thus, one of the explanations for the difference between VLP-HA* and VLP-PEG* NP-cell interactions would be, that VLP-PEG* possesses a higher shielding capacity, and hereby reduces more the broad VP1-specific interactions with cells than VLP-HA*. VLP-Bp then, due to the smallest size, possesses the lowest shielding capacity, hence the broad VP1-specific cell interactions are strongest in the VLP-Bp sample. Moreover, VLP-Bp possesses the highest number of Bp molecules attached (compared to other VLP variants), that enhances the fluorescent signal and hereby the NP-cell interactions appear to be highest.

The effect of the length of the incubation time of NPs with the MDA cells was also tested in the current thesis. In our study, we used an incubation length of 2 hours, as well as e.g. Cho et alia in 2011. Longer incubations (usually 3 or 4 hours) were used more often in similar studies (Li et al., 2014; Zhong et al., 2015) frequently also two different incubation times were tested (Xiao et al., 2015; Zhao et al., 2015; Li et al., 2016; Xiong et al., 2016). After longer incubation of NPs with cells, higher NP-cell interactions might be achieved. However, we observed the effect of the difference in the incubation length on NP-cell interactions only qualitatively using fluorescence microscopy.

In the ND-HA* sample a positive effect of longer incubation time of NPs with cancer cells on NP-cell interactions could be plausibly observed, which is in agreement with other studies (Xiong et al., 2016). In further experiments, it would be desirable to perform a quantitative experiment, to evaluate the effect of the NP-cell incubation time length on the NP-cell interactions quantitatively too. The concentration of the NPs in the incubation with the cells might also affect the resulting NP-cell interactions. Uptake in concentration-dependent manner was observed e.g. in Zhao et alia (2015), which is in agreement with our results as different amounts of VLP-HA* (12 µg and 20 µg) were provided to NP-cell incubation FC3 experiment, with higher amount showing higher NP-cell interactions.

Furthermore, incubation with excess non-labeled free HA was studied in the competitive cell-binding assay. First, free HA was added in two concentrations (0.2 or 1 mg/ml) to the MDA cells 1 hour prior to incubating with NPs (and discarded prior to NP addition), preincubation was also used in previously published studies (Ganesh et al., 2013b; Lee et al., 2015; Zhao et al., 2015; Zhong et al., 2015). Due to free HA competing for binding sites at CD44 receptors, it was expected that for samples that enter via CD44 a reduction in NP-cell interactions would be observed after incubation with free HA. A mild reduction of the NP-cell interactions was observed in the ND-HA* sample with the higher free HA concentration (1 mg/ml) used in the competitive cell-binding assay. Previously published studies usually use higher excess of free HA (5 or 10 mg/ml) and often co-incubate free HA and NPs with MDA cells (as summarized in 2.2.2 - Table 1).

Thus, a higher concentration (2 mg/ml) of free HA for the competitive cell-binding assay was used in the following experiment (FC2) as it was used in Zhao et alia (2015).

Moreover, the internalization of HA is very rapid, so co-incubation of NPs and free HA with the cells was used further (Choi et al., 2010; Xiao et al., 2015; Li et al., 2016). Additionally, it was proposed to use relatively high Mw of free HA (e.g. 100 kDa, 102 kDa) for the competitive cell-binding assay, to achieve CD44 saturation by multivalent interactions (Li et al., 2016; Zhong et al., 2019). Due to limited availability of materials, HA Mw 8-15 kDa was used as free HA in the competitive cell-binding studies in this thesis.

After implementing the above mentioned changes in the competitive cell-binding assay, finally, a reduction of the NP-cell interactions could be observed in ND-HA* when co-incubated with free HA (compared to sample that was not incubated with free HA) and slightly in VLP-HA* too. In 2001 Eliaz et alia tested increasing concentrations of free HA used for the incubation with CD44-targeted liposomes and cancer cells and increasing concentration of free HA in incubation caused larger reduction of NP-cell interactions (with a saturation point) in CD44 targeted liposomes compared to no reduction in non-targeted liposomes. Therefore, free HA provided to cells and NPs for the incubation in the competitive cell-binding assay was increased to the maximal concentration that could be used (due to limited availability of materials) in the FC3 experiment– 5 mg/ml, finally reaching the free HA concentration in the competitive cell-binding assay, that is usually used in similar studies (summarized in 2.2.2 – Table 1).

Blocking cellular CD44 receptors by free HA during co-incubation distinctly reduced the ND-HA* interactions with MDA cells by 60 %, which is in agreement with the results obtained in similar studies (see summarized in 2.2.2 - Table 1). Thus, ND-HA* likely enters the MDA cells via the overexpressed CD44 receptors. This could not be deduced from the VLP-HA* sample results. The cause might be e.g. a different surface coverage of ND-HA* (~80) and VLP-HA* (~56) by HA*, nonetheless the difference in the estimated HA* number bound per NP was not distinct.

In 2018 Neburkova et alia showed that due to a ubiquitous presence of VP1 receptors, MPyV VLPs provide a broad tropism and a low density of poly(HPMA) bound to MPyV VLP surface could not inhibit the VP1-specific binding, however a high surface density of short PEG chains was sufficient to enable retargeting of VLPs .

Hence a low HA* surface coverage of VLP-HA* might not be sufficient to completely re-target VLP-HA* from the natural receptor, VLP-HA* might partially retain the VP-1 mediated interactions with the cells. Therefore, it would be desirable to analyze this further, by producing VLPs with higher surface coverage by HA* and test the VLPs in a similar manner.

Moreover, when free controls were tested on interactions with the MDA cells, it was expected that HA* *per se* would show highest interactions, which was not observed in FC1. As already mentioned (in 7.1), because of the process of HA* production, non-labeled HA was also present in the sample, and the HA*- cell interaction could hereby be blocked by non-labeled HA competing for the binding site at CD44. When a higher concentration of HA* was used (16 µM) in FC3, this sample provided the overall highest (due to the highest molar concentration) NP-cell interactions, and hereby it was shown that HA* *per se* interacts with cells.

Due to the non-labeled HA present in the HA* sample, it was suspected, that some non-labeled HA could also remain in the VLP-HA* sample and hereby block the CD44 binding by competing for the binding site. Nonetheless, no band showing unbound HA* in fluorescent signal acquiring from the SDS-PAGE gel was observed after the click reaction in the VLP-HA* sample. Therefore, it was deduced, that all excessive HA* that did not bind to VLP-alkyne during the click reaction was successfully removed by the following sucrose cushion centrifugation. It is expected that if non-labeled HA was also present in the sample, it would behave similarly as labeled HA*, hence it would be removed by the sucrose cushions. Thus, it is expected that the reason for lower NP-cell interactions in VLP-HA* sample compared to ND-HA* sample and the ineffective competition of free HA in competitive cell-binding studies is not caused by the presence of non-labeled HA in VLP-HA* sample.

Even when the VLP-HA* number provided for incubation with cells was twice as high as ND-HA* in FC3, ND-HA* still showed higher NP-cell interactions. If fluorescent units should be similar to those of HA* (16 µM) that was tested in FC3, VLP-HA* added to the incubation with cells would have to be distinctly higher. VLP-HA* did not show a desirable CD44-targeting ability and so optimization is needed. Resulting values (MFI, % of BP positive cells) of NPs not incubated with free HA and NPs incubated with free HA in the FC3 experiment were compared and data were analyzed by the Mann Whitney statistical test. Results were statistically insignificant, but strong trends were observed, and more measurements should be performed to obtain a greater statistical power.

Since VLP-HA* examined in this diploma thesis did not show strong affinity for the MDA cells, several other factors should be addressed in the future. It has been shown in the literature that not only surface coverage density by HA, but also the molecular weight of HA has a fundamental effect on the binding affinity for CD44 receptors (Li et al., 2014; Zhong et al., 2019). Because HA with a higher Mw has been shown to have a higher affinity for the CD44 receptor, high molecular weight HA has often been used as a targeting moiety (Surace et al., 2009). Zhong et alia (2019) compared three different HA Mw (7,63,102 kDa) conjugated onto NPs in cancer cell targeting; and HA Mw of 63 kDa proved to be the most suitable here. It showed a sufficient CD44 binding affinity and the availability of receptors was not affected by CD44 clustering as much as in the 102 kDa Mw HA. Thus, similar Mw of HA should be tested for conjugation on NPs in further experiments (Zhong et al., 2019).

Various types of cells could be used, as is frequent in other studies, because different cell types can show different affinity of CD44 for HA. Usually the expression rate of CD44 is assessed by using a fluorescent αCD44 antibody to detect surface CD44 receptors by flow cytometry or other methods prior to the NP-cell interaction experiments (Ganesh et al., 2013) . NP-cell interactions should preferably be tested on multiple cell types overexpressing the CD44 receptor (e.g. B16F10, A549, Hela, HCT-116 or HepG2 cells). As control the NP-cell interactions should also be tested on normal healthy cells with low CD44 expression or on cells lacking the CD44 receptor (e.g.MCF-7, U87MG, NIH-3T3, HK2 cells) (Surace et al., 2009; Li et al., 2014; Zhao et al., 2015).

Moreover, longer incubation time of NPs with cells should be tested in the flow cytometry NP-cell interaction studies as it might result in an increase of the NP-cell interactions (Xiong et al., 2016; Zhong et al., 2019).

To assess the NPs internalization via the CD44 receptor by the competitive cell-binding assay, excess of free HA (e.g. 10 mg/ml), preferably of higher Mw (~100 kDa), should be used in co-incubation of free HA and NPs with cells, alternatively an αCD44 monoclonal antibody specific against the HA binding site might be used for receptor blocking during this assay (Surace et al., 2009; Lee et al., 2015; Li et al., 2016).

8. Summary

MPyV VP1 VLPs were produced with the use of the baculovirus expression system. Alkyne linker was attached onto the surface of the VLPs. Bodipy, fluorescently labeled HA (Bodipy bound HA) or fluorescently labeled PEG (Bodipy-bound PEG) were conjugated onto the VLP-alkyne by the Cu^I-catalyzed alkyne-azide cycloaddition. The numbers of the Bp, HA* and PEG* molecules bound per VLP-alkyne were calculated to be 153, 56, and 144 respectively. Control NPs – nanodiamonds with HA* or Bp prepared in a similar manner were produced by Jitka Nebůrková (IOCB).

Interactions of ND (ND-HA*, ND-Bp) and VLP (VLP-HA*/PEG*/Bp) variants with human breast adenocarcinoma MDA-MB-231 cells overexpressing the CD44 receptor were tested by flow cytometry and analyzed by fluorescence microscopy. The interaction of the NPs with the MDA cells via the CD44 receptor was assessed by the competitive cell-binding assay, where the NPs competed with non-labeled free HA for binding sites at the CD44 receptors. Hence, a reduction in NP-cell interactions should be detected, if NPs interact with the cells via the CD44 receptor. The control ND-HA* showed a reduction in the interactions with the MDA cells by 60 % after incubation with free HA (compared to ND-HA* not incubated with free HA). Therefore, it is deduced that ND-HA* plausibly interact with the MDA cells via the CD44 receptor. However, VLP-HA* did not show comparable reduction in NP-cell interactions after incubation with free HA. VLP-Bp and ND-Bp surprisingly exhibited high non-specific interaction with the MDA cells, whereas VLP-PEG* did not associate with the cells as expected.

In conclusion, our study demonstrated that MPyV VLPs can be successfully modified by conjugation with HA*. The surface coverage by HA* in VLP-HA* was plausibly not sufficient to limit virus-specific interactions with the cells and provide complete re-targeting to the CD44 receptor. The preparation of VLP-HA* with higher number of HA* molecules will be required to further analyze the specific interaction of VLP-HA* with the CD44 receptor. The results obtained with control ND-HA* suggest that NPs targeting to CD44 can be achieved, but the role of non-specific interaction of Bp with the MDA cells in the current targeting system must be determined.

9. Bibliography

Autio, K.A., Dreicer, R., Anderson, J., Garcia, J.A., Alva, A., Hart, L.L., Milowsky, M.I., Posadas, E.M., Ryan, C.J., Graf, R.P., Dittamore, R., Schreiber, N.A., Summa, J.M., Youssoufian, H., Morris, M.J., Scher, H.I., 2018. Safety and Efficacy of BIND-014, a Docetaxel Nanoparticle Targeting Prostate-Specific Membrane Antigen for Patients With Metastatic Castration-Resistant Prostate Cancer: A Phase 2 Clinical Trial. JAMA Oncol. 4, 1344. https://doi.org/10.1001/jamaoncol.2018.2168

Barenholz, Y., 2012. Doxil® — The first FDA-approved nano-drug: Lessons learned. J. Controlled Release 160, 117–134. https://doi.org/10.1016/j.jconrel.2012.03.020

Besanceney-Webler, C., Jiang, H., Zheng, T., Feng, L., Soriano del Amo, D., Wang, W., Klivansky, L.M.,Marlow, F.L., Liu, Y., Wu, P., 2011. Increasing the Efficacy of Bioorthogonal Click Reactions for Bioconjugation: A Comparative Study. Angew. Chem. Int. Ed. 50, 8051–8056. https://doi.org/10.1002/anie.201101817

Bartoň, J., 2015. Hydrosolubilization of BODIPY for optical labelling of biomolecules.

Bock, V.D., Hiemstra, H., van Maarseveen, J.H., 2006. CuI-Catalyzed Alkyne-Azide "Click" Cycloadditions from a Mechanistic and Synthetic Perspective. Eur. J. Org. Chem. 2006, 51–68. https://doi.org/10.1002/ejoc.200500483

Byeon, Y., Lee, J.-W., Choi, W.S., Won, J.E., Kim, G.H., Kim, M.G., Wi, T.I., Lee, J.M., Kang, T.H., Jung, I.D., Cho, Y.-J., Ahn, H.J., Shin, B.C., Lee, Y.J., Sood, A.K., Han, H.D., Park, Y.-M., 2018. CD44-targeted PLGA nanoparticles incorporating paclitaxel and FAK siRNA overcome chemoresistance in epithelial ovarian cancer. Cancer Res. canres.3871.2017. https://doi.org/10.1158/0008-5472.CAN-17-3871

Calzolari, A., Oliviero, I., Deaglio, S., Mariani, G., Biffoni, M., Sposi, N.M., Malavasi, F., Peschle, C., Testa, U., 2007. Transferrin receptor 2 is frequently expressed in human cancer cell lines. Blood Cells. Mol. Dis. 39, 82–91. https://doi.org/10.1016/j.bcmd.2007.02.003

Chan, K.T., Choi, M.Y., Lai, K.K.Y., Tan, W., Tung, L.N., Lam, H.Y., Tong, D.K.H., Lee, N.P., Law, S., 2014. Overexpression of transferrin receptor CD71 and its tumorigenic properties in esophageal squamous cell carcinoma. Oncol. Rep. 31, 1296–1304. https://doi.org/10.3892/or.2014.2981

Cheng, L., Ji, K., Shih, T.-Y., Haddad, A., Giatsidis, G., Mooney, D.J., Orgill, D.P., Nabzdyk, C.S., 2017. Injectable Shape-Memorizing Three-Dimensional Hyaluronic Acid Cryogels for Skin Sculpting and Soft Tissue Reconstruction. Tissue Eng. Part A 23, 243–251. https://doi.org/10.1089/ten.tea.2016.0263

Cho, H.-J., Yoon, H.Y., Koo, H., Ko, S.-H., Shim, J.-S., Lee, J.-H., Kim, K., Chan Kwon, I., Kim, D.-D., 2011. Self-assembled nanoparticles based on hyaluronic acid-ceramide (HA-CE) and Pluronic® for tumor-targeted delivery of docetaxel. Biomaterials 32, 7181–7190. https://doi.org/10.1016/j.biomaterials.2011.06.028

Choi, K.Y., Chung, H., Min, K.H., Yoon, H.Y., Kim, K., Park, J.H., Kwon, I.C., Jeong, S.Y., 2010. Self-assembled hyaluronic acid nanoparticles for active tumor targeting. Biomaterials 31, 106–114. https://doi.org/10.1016/j.biomaterials.2009.09.030

Cowman, M.K., Lee, H.-G., Schwertfeger, K.L., McCarthy, J.B., Turley, E.A., 2015. The Content and Size of Hyaluronan in Biological Fluids and Tissues. Front. Immunol. 6. https://doi.org/10.3389/fimmu.2015.00261

Csóka, A.B., Scherer, S.W., Stern, R., 1999. Expression Analysis of Six Paralogous Human Hyaluronidase Genes Clustered on Chromosomes 3p21 and 7q31. Genomics 60, 356–361. https://doi.org/10.1006/geno.1999.5876

Davis, M.E., Zuckerman, J.E., Choi, C.H.J., Seligson, D., Tolcher, A., Alabi, C.A., Yen, Y., Heidel, J.D., Ribas, A., 2010. Evidence of RNAi in humans from systemically administered siRNA via targeted nanoparticles. Nature 464, 1067–1070. https://doi.org/10.1038/nature08956

Du, L., Wang, H., He, L., Zhang, J., Ni, B., Wang, X., Jin, H., Cahuzac, N., Mehrpour, M., Lu, Y., Chen, Q., 2008. CD44 is of Functional Importance for Colorectal Cancer Stem Cells. Clin. Cancer Res. 14, 6751–6760. https://doi.org/10.1158/1078-0432.CCR-08-1034

Eliaz, R.E., Szoka, F.C., 2001. Liposome-encapsulated doxorubicin targeted to CD44: a strategy to kill CD44-overexpressing tumor cells. Cancer Res. 61, 2592–2601.

English, N.M., Lesley, J.F., Hyman, R., 1998. Site-specific de-N-glycosylation of CD44 can activate hyaluronan binding, and CD44 activation states show distinct threshold densities for hyaluronan binding. Cancer Res. 58, 3736–3742.

Fallacara, A., Baldini, E., Manfredini, S., Vertuani, S., 2018. Hyaluronic Acid in the Third Millennium. Polymers 10, 701. https://doi.org/10.3390/polym10070701

Fang, J., Islam, W., Maeda, H., 2020. Exploiting the dynamics of the EPR effect and strategies to improve the therapeutic effects of nanomedicines by using EPR effect enhancers. Adv. Drug Deliv. Rev. S0169409X2030051X. https://doi.org/10.1016/j.addr.2020.06.005

Forstová, J., Krauzewicz, N., Sandig, V., Elliott, J., Palková, Z., Strauss, M., Griffin, B.E., 1995. Polyoma Virus Pseudocapsids as Efficient Carriers of Heterologous DNA into Mammalian Cells. Hum. Gene Ther. 6, 297–306. https://doi.org/10.1089/hum.1995.6.3-297

Fraiberk, M., Hájková, M., Krulová, M., Kojzarová, M., Drda Morávková, A., Pšikal, I., Forstová, J., 2017. Exploitation of stable nanostructures based on the mouse polyomavirus for development of a recombinant vaccine against porcine circovirus 2. PLOS ONE 12, e0184870. https://doi.org/10.1371/journal.pone.0184870

Ganesh, S., Iyer, A.K., Gattacceca, F., Morrissey, D.V., Amiji, M.M., 2013a. In vivo biodistribution of siRNA and cisplatin administered using CD44-targeted hyaluronic acid nanoparticles. J. Controlled Release 172, 699–706. https://doi.org/10.1016/j.jconrel.2013.10.016

Ganesh, S., Iyer, A.K., Morrissey, D.V., Amiji, M.M., 2013b. Hyaluronic acid based self-assembling nanosystems for CD44 target mediated siRNA delivery to solid tumors. Biomaterials 34, 3489–3502. https://doi.org/10.1016/j.biomaterials.2013.01.077

Garouniatis, A., Zizi-Sermpetzoglou, A., Rizos, S., Kostakis, A., Nikiteas, N., Papavassiliou, A.G., 2013. FAK, CD44v6, c-Met and EGFR in colorectal cancer parameters: tumour progression, metastasis, patient survival and receptor crosstalk. Int. J. Colorectal Dis. 28, 9–18. https://doi.org/10.1007/s00384-012-1520-9

Georgakopoulos, P., Kyriakidis, M., Perpinia, A., Karavidas, A., Zimeras, S., Mamalis, N., Kouvela, M., Charpidou, A., 2019. The Role of Metoprolol and Enalapril in the Prevention of Doxorubicin-induced Cardiotoxicity in Lymphoma Patients. Anticancer Res. 39, 5703–5707. https://doi.org/10.21873/anticanres.13769

Gibbs, A.J., Ohshima, K., Phillips, M.J., Gibbs, M.J., 2008. The Prehistory of Potyviruses: Their Initial Radiation Was during the Dawn of Agriculture. PLoS ONE 3, e2523. https://doi.org/10.1371/journal.pone.0002523

Gupta, R.C., Lall, R., Srivastava, A., Sinha, A., 2019. Hyaluronic Acid: Molecular Mechanisms and Therapeutic Trajectory. Front. Vet. Sci. 6, 192. https://doi.org/10.3389/fvets.2019.00192

Harris, E.N., Weigel, P.H., 2008. The ligand-binding profile of HARE: hyaluronan and chondroitin sulfates A, C, and D bind to overlapping sites distinct from the sites for heparin, acetylated low-density lipoprotein, dermatan sulfate, and CS-E. Glycobiology 18, 638–648. https://doi.org/10.1093/glycob/cwn045

Holmberg, Å.S., Philipson, B.T., 1984. Sodium Hyaluronate in Cataract Surgery. Ophthalmology 91, 53–59. https://doi.org/10.1016/S0161-6420(84)34340-8

Hu, D., Mezghrani, O., Zhang, L., Chen, Y., Ke, X., Ci, T., 2016. GE11 peptide modified and reduction-responsive hyaluronic acid-based nanoparticles induced higher efficacy of doxorubicin for breast carcinoma therapy. Int. J. Nanomedicine Volume 11, 5125–5147. https://doi.org/10.2147/IJN.S113469

Höfling, B., Bolte, H.-D., 1981. Acute negative inotropic effect of adriamycin (doxorubicin). Naunyn. Schmiedebergs Arch. Pharmacol. 317, 252–256. https://doi.org/10.1007/BF00503826

Hustedová, A., 2019. Metabolic labelling of mouse polyomavirus virus-like particles using unnatural amino acids and click chemistry

Jeffers, L.J., Cortes, R.A., Bejarano, P.A., Oh, E., Regev, A., Smith, K.M., De Medina, M., Smith-Riggs, M., Colon, M., Hettinger, K., Jara, S., Mendez, T.P., Schiff, E.R., 2007. Prospective Evaluation of FIBROSpect II for Fibrosis Detection in Hepatitis C and B Patients Undergoing Laparoscopic Biopsy. Gastroenterol. Hepatol. 3, 367–376.

Karakocak, B.B., Liang, J., Biswas, P., Ravi, N., 2018. Hyaluronate coating enhances the delivery and biocompatibility of gold nanoparticles. Carbohydr. Polym. 186, 243–251. https://doi.org/10.1016/j.carbpol.2018.01.046

Ke, C., Sun, L., Qiao, D., Wang, D., Zeng, X., 2011. Antioxidant acitivity of low molecular weight hyaluronic acid. Food Chem. Toxicol. 49, 2670–2675. https://doi.org/10.1016/j.fct.2011.07.020

Kothapalli, D., Zhao, L., Hawthorne, E.A., Cheng, Y., Lee, E., Puré, E., Assoian, R.K., 2007. Hyaluronan and CD44 antagonize mitogen-dependent cyclin D1 expression in mesenchymal cells. J. Cell Biol. 176, 535–544. https://doi.org/10.1083/jcb.200611058

Lawrance, W., Banerji, S., Day, A.J., Bhattacharjee, S., Jackson, D.G., 2016. Binding of Hyaluronan to the Native Lymphatic Vessel Endothelial Receptor LYVE-1 Is Critically Dependent on Receptor Clustering and Hyaluronan Organization. J. Biol. Chem. 291, 8014–8030. https://doi.org/10.1074/jbc.M115.708305

Lee, G.Y., Kim, J.-H., Choi, K.Y., Yoon, H.Y., Kim, K., Kwon, I.C., Choi, K., Lee, B.-H., Park, J.H., Kim, I.-S., 2015. Hyaluronic acid nanoparticles for active targeting atherosclerosis. Biomaterials 53, 341–348. https://doi.org/10.1016/j.biomaterials.2015.02.089

Lee, H., Shields, A.F., Siegel, B.A., Miller, K.D., Krop, I., Ma, C.X., LoRusso, P.M., Munster, P.N., Campbell, K., Gaddy, D.F., Leonard, S.C., Geretti, E., Blocker, S.J., Kirpotin, D.B., Moyo, V., Wickham, T.J., Hendriks, B.S., 2017. [64] Cu-MM-302 Positron Emission Tomography Quantifies Variability of Enhanced Permeability and Retention of Nanoparticles in Relation to Treatment Response in Patients with Metastatic Breast Cancer. Clin. Cancer Res. 23, 4190–4202. https://doi.org/10.1158/1078-0432.CCR-16-3193

Lee, T., Lim, E.-K., Lee, J., Kang, B., Choi, J., Park, H.S., Suh, J.-S., Huh, Y.-M., Haam, S., 2013. Efficient CD44-targeted magnetic resonance imaging (MRI) of breast cancer cells using hyaluronic acid (HA)-modified MnFe2O4 nanocrystals. Nanoscale Res. Lett. 8, 149. https://doi.org/10.1186/1556-276X-8-149

Lesley, J., English, N., Perschl, A., Gregoroff, J., Hyman, R., 1995. Variant cell lines selected for alterations in the function of the hyaluronan receptor CD44 show differences in glycosylation. J. Exp. Med. 182, 431–437. https://doi.org/10.1084/jem.182.2.431

Li, J., He, Y., Sun, W., Luo, Y., Cai, H., Pan, Y., Shen, M., Xia, J., Shi, X., 2014. Hyaluronic acid-modified hydrothermally synthesized iron oxide nanoparticles for targeted tumor MR imaging. Biomaterials 35, 3666–3677. https://doi.org/10.1016/j.biomaterials.2014.01.011

Li, W., Yi, X., Liu, X., Zhang, Z., Fu, Y., Gong, T., 2016. Hyaluronic acid ion-pairing nanoparticles for targeted tumor therapy. J. Controlled Release 225, 170–182. https://doi.org/10.1016/j.jconrel.2016.01.049

Liu, L., Liu, Y., Li, J., Du, G., Chen, J., 2011. Microbial production of hyaluronic acid: current state, challenges, and perspectives. Microb. Cell Factories 10, 99. https://doi.org/10.1186/1475-2859-10-99

Mallepally, N., Abu-Sbeih, H., Ahmed, O., Chen, E., Shafi, M.A., Neelapu, S.S., Wang, Y., 2019. Clinical Features of Rituximab-associated Gastrointestinal Toxicities: Am. J. Clin. Oncol. 42, 539–545. https://doi.org/10.1097/COC.0000000000000553

Meyer, K. and Palmer, J.W.,1934. The polysaccharide of the vitreous humor. Journal of Biological Chemistry, 107, 629-634.

Misra, S., Hascall, V.C., Markwald, R.R., Ghatak, S., 2015. Interactions between Hyaluronan and Its Receptors (CD44, RHAMM) Regulate the Activities of Inflammation and Cancer. Front. Immunol. 6. https://doi.org/10.3389/fimmu.2015.00201

Montross, L., Watkins, S., Moreland, R.B., Mamon, H., Caspar, D.L., Garcea, R.L., 1991. Nuclear assembly of polyomavirus capsids in insect cells expressing the major capsid protein VP1. J. Virol. 65, 4991–4998.

Nair, H.B., Huffman, S., Veerapaneni, P., Kirma, N.B., Binkley, P., Perla, R.P., Evans, D.B., Tekmal, R.R., 2011. Hyaluronic Acid-Bound Letrozole Nanoparticles Restore Sensitivity to Letrozole-Resistant Xenograft Tumors in Mice. J. Nanosci. Nanotechnol. 11, 3789–3799. https://doi.org/10.1166/jnn.2011.3871

Neburkova, J., Sedlak, F., Zackova Suchanova, J., Kostka, L., Sacha, P., Subr, V., Etrych, T., Simon, P., Barinkova, J., Krystufek, R., Spanielova, H., Forstova, J., Konvalinka, J., Cigler, P., 2018. Inhibitor–GCPII Interaction: Selective and Robust System for Targeting Cancer Cells with Structurally Diverse Nanoparticles. Mol. Pharm. 15, 2932–2945. https://doi.org/10.1021/acs.molpharmaceut.7b00889

Neburkova, J., 2018. Targeted biocompatible nanoparticles for therapy and cancer diagnostics

Nobile, V., Buonocore, D., Michelotti, A., Marzatico, F., 2014. Anti-aging and filling efficacy of six types hyaluronic acid based dermo-cosmetic treatment: double blind, randomized clinical trial of efficacy and safety. J. Cosmet. Dermatol. 13, 277–287. https://doi.org/10.1111/jocd.12120

O' Connor, D., Byrne, A., Keyes, T.E., 2019. Linker length in fluorophore–cholesterol conjugates directs phase selectivity and cellular localisation in GUVs and live cells. RSC Adv. 9, 22805–22816. https://doi.org/10.1039/C9RA03905H

Orasan, O.H., Ciulei, G., Cozma, A., Sava, M., Dumitrascu, D.L., 2016. Hyaluronic acid as a biomarker of fibrosis in chronic liver diseases of different etiologies. Med. Pharm. Rep. 89, 24–31. https://doi.org/10.15386/cjmed-554

Pattenden, L.K., Middelberg, A.P.J., Niebert, M., Lipin, D.I., 2005. Towards the preparative and large-scale precision manufacture of virus-like particles. Trends Biotechnol. 23, 523–529. https://doi.org/10.1016/j.tibtech.2005.07.011

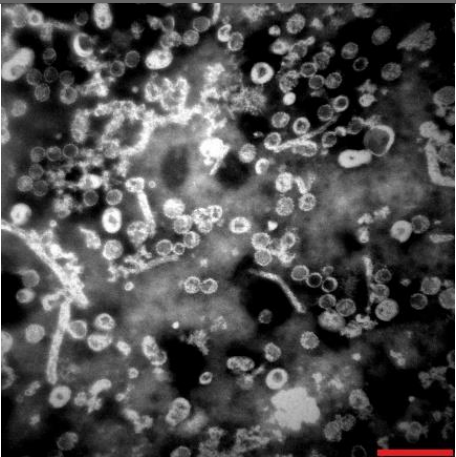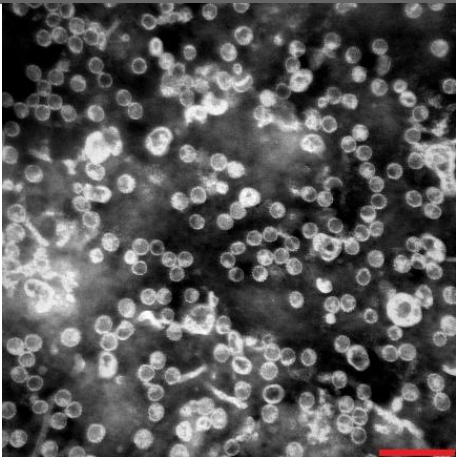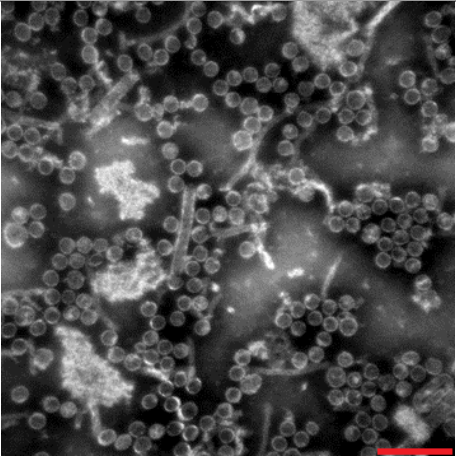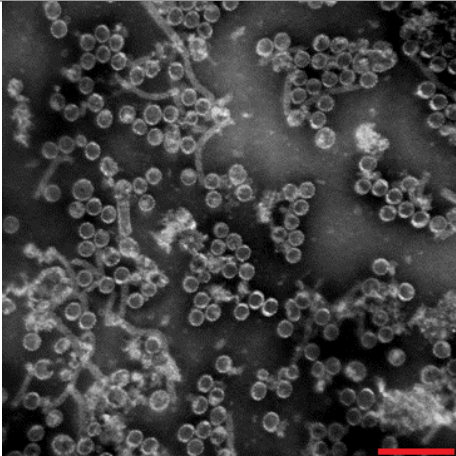Polidarova, M., 2016. Utilization of mouse polyomavirus derived virus-like particles for cargo delivery into cells

Prince, M.E., Sivanandan, R., Kaczorowski, A., Wolf, G.T., Kaplan, M.J., Dalerba, P., Weissman, I.L., Clarke, M.F., Ailles, L.E., 2007. Identification of a subpopulation of cells with cancer stem cell properties in head and neck squamous cell carcinoma. Proc. Natl. Acad. Sci. 104, 973–978. https://doi.org/10.1073/pnas.0610117104

Qhattal, H.S.S., Hye, T., Alali, A., Liu, X., 2014. Hyaluronan Polymer Length, Grafting Density, and Surface Poly(ethylene glycol) Coating Influence *in Vivo* Circulation and Tumor Targeting of Hyaluronan-Grafted Liposomes. ACS Nano 8, 5423–5440. https://doi.org/10.1021/nn405839n

Qiu, L., Zhu, M., Huang, Y., Gong, K., Chen, J., 2016. Mechanisms of cellular uptake with hyaluronic acid—octadecylamine micelles as drug delivery nanocarriers. RSC Adv. 6, 39896–39902. https://doi.org/10.1039/C5RA27532F

Rayahin, J.E., Buhrman, J.S., Zhang, Y., Koh, T.J., Gemeinhart, R.A., 2015. High and Low Molecular Weight Hyaluronic Acid Differentially Influence Macrophage Activation. ACS Biomater. Sci. Eng. 1, 481–493. https://doi.org/10.1021/acsbiomaterials.5b00181

Rezaei, S., Kashanian, S., Bahrami, Y., Cruz, L.J., Motiei, M., 2020. Redox-Sensitive and Hyaluronic Acid-Functionalized Nanoparticles for Improving Breast Cancer Treatment by Cytoplasmic 17α-Methyltestosterone Delivery. Molecules 25, 1181. https://doi.org/10.3390/molecules25051181

Rivas, F., Zahid, O.K., Reesink, H.L., Peal, B.T., Nixon, A.J., DeAngelis, P.L., Skardal, A., Rahbar, E., Hall, A.R., 2018. Label-free analysis of physiological hyaluronan size distribution with a solid-state nanopore sensor. Nat. Commun. 9, 1037. https://doi.org/10.1038/s41467-018-03439-x

Safra, T., Muggia, F., Jeffers, S., Tsao-Wei, D.D., Groshen, S., Lyass, O., Henderson, R., Berry, G., Gabizon, A., 2000. Pegylated liposomal doxorubicin (doxil): Reduced clinical cardiotoxicity in patients reaching or exceeding cumulative doses of 500 mg/m2. Ann. Oncol. 11, 1029–1034. https://doi.org/10.1023/A:1008365716693

Sanfilippo, V., Caruso, V.C.L., Cucci, L.M., Inturri, R., Vaccaro, S., Satriano, C., 2020. Hyaluronan-Metal Gold Nanoparticle Hybrids for Targeted Tumor Cell Therapy. Int. J. Mol. Sci. 21, 3085. https://doi.org/10.3390/ijms21093085

Sarafraz, Z., Ahmadi, A., Daneshi, A., 2018. Transtympanic Injections of N-acetylcysteine and Dexamethasone for Prevention of Cisplatin-Induced Ototoxicity: Double Blind Randomized Clinical Trial. Int. Tinnitus J. 22. https://doi.org/10.5935/0946-5448.20180007

Skelton, T.P., Zeng, C., Nocks, A., Stamenkovic, I., 1998. Glycosylation Provides Both Stimulatory and Inhibitory Effects on Cell Surface and Soluble CD44 Binding to Hyaluronan. J. Cell Biol. 140, 431–446. https://doi.org/10.1083/jcb.140.2.431

Sleeman, J., Rudy, W., Hofmann, M., Moll, J., Herrlich, P., Ponta, H., 1996. Regulated clustering of variant CD44 proteins increases their hyaluronate binding capacity. J. Cell Biol. 135, 1139–1150. https://doi.org/10.1083/jcb.135.4.1139

Smith, A.E., Lilie, H., Helenius, A., 2003. Ganglioside-dependent cell attachment and endocytosis of murine polyomavirus-like particles. FEBS Lett. 555, 199–203. https://doi.org/10.1016/S0014-5793(03)01220-1

Snipstad, S., Hak, S., Baghirov, H., Sulheim, E., Mørch, Ý., Lélu, S., von Haartman, E., Bäck, M., Nilsson, K.P.R., Klymchenko, A.S., de Lange Davies, C., Åslund, A.K.O., 2017. Labeling nanoparticles: Dye leakage and altered cellular uptake: Labeling Nanoparticles with Dyes. Cytometry A 91, 760–766. https://doi.org/10.1002/cyto.a.22853

Stehle, T., Harrison, S.C., 1996. Crystal structures of murine polyomavirus in complex with straight-chain and branched-chain sialyloligosaccharide receptor fragments. Structure 4, 183–194. https://doi.org/10.1016/S0969-2126(96)00021-4

Streckmann, F., Balke, M., Lehmann, H.C., Rustler, V., Koliamitra, C., Elter, T., Hallek, M., Leitzmann, M., Steinmetz, T., Heinen, P., Baumann, F.T., Bloch, W., 2018. The preventive effect of sensorimotor- and vibration exercises on the onset of Oxaliplatin- or vinca-alkaloid induced peripheral neuropathies - STOP. BMC Cancer 18, 62. https://doi.org/10.1186/s12885-017-3866-4

Su, Z., Liu, D., Chen, L., Zhang, J., Ru, L., Chen, Z., Gao, Z., Wang, X., 2019. CD44-Targeted Magnetic Nanoparticles Kill Head And Neck Squamous Cell Carcinoma Stem Cells In An Alternating Magnetic Field. Int. J. Nanomedicine Volume 14, 7549–7560. https://doi.org/10.2147/IJN.S215087

Suchanova, J., 2012. Targeting prostate tumor cells by polyomavirus virus-like particles

Sun, S.-F., Chou, Y.-J., Hsu, C.-W., Hwang, C.-W., Hsu, P.-T., Wang, J.-L., Hsu, Y.-W., Chou, M.-C., 2006. Efficacy of intra-articular hyaluronic acid in patients with osteoarthritis of the ankle: a prospective study. Osteoarthritis Cartilage 14, 867–874. https://doi.org/10.1016/j.joca.2006.03.003
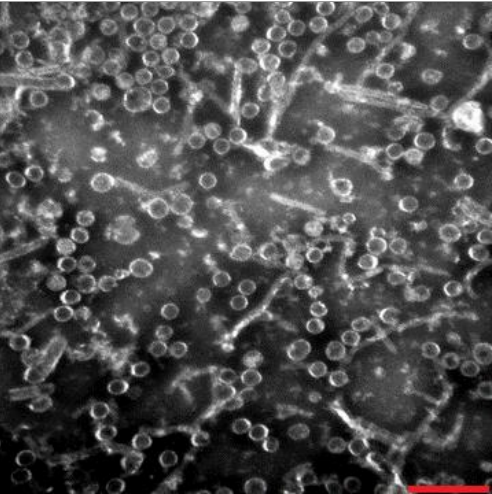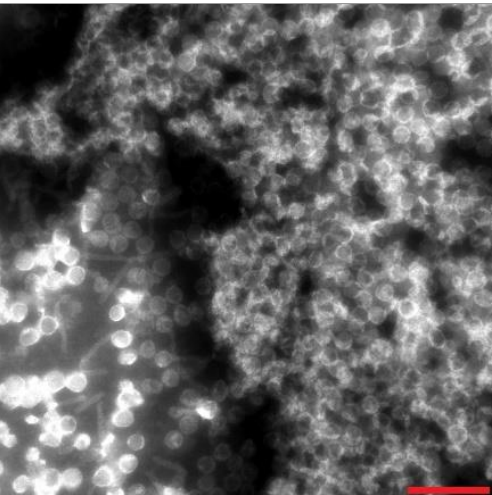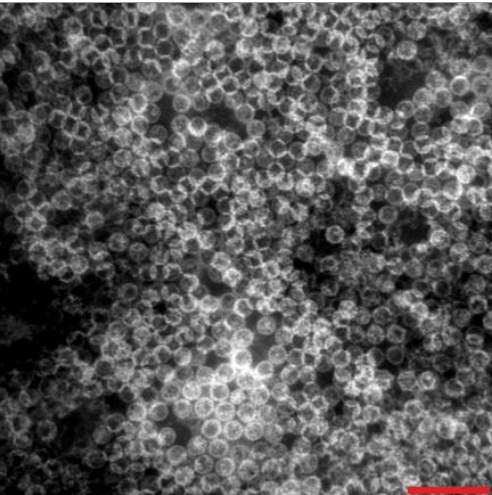
Surace, C., Arpicco, S., Dufaÿ-Wojcicki, A., Marsaud, V., Bouclier, C., Clay, D., Cattel, L., Renoir, J.-M., Fattal, E., 2009. Lipoplexes Targeting the CD44 Hyaluronic Acid Receptor for Efficient Transfection of Breast Cancer Cells. Mol. Pharm. 6, 1062–1073. https://doi.org/10.1021/mp800215d

Takaishi, S., Okumura, T., Tu, S., Wang, S.S.W., Shibata, W., Vigneshwaran, R., Gordon, S.A.K., Shimada, Y., Wang, T.C., 2009. Identification of Gastric Cancer Stem Cells Using the Cell Surface Marker CD44. Stem Cells 27, 1006–1020. https://doi.org/10.1002/stem.30

Todaro, M., Gaggianesi, M., Catalano, V., Benfante, A., Iovino, F., Biffoni, M., Apuzzo, T., Sperduti, I., Volpe, S., Cocorullo, G., Gulotta, G., Dieli, F., De Maria, R., Stassi, G., 2014. CD44v6 Is a Marker of Constitutive and Reprogrammed Cancer Stem Cells Driving Colon Cancer Metastasis. Cell Stem Cell 14, 342–356. https://doi.org/10.1016/j.stem.2014.01.009

Usui, T., 2003. Hyaluronan synthase in trabecular meshwork cells. Br. J. Ophthalmol. 87, 357–360. https://doi.org/10.1136/bjo.87.3.357

van Zandwijk, N., Pavlakis, N., Kao, S.C., Linton, A., Boyer, M.J., Clarke, S., Huynh, Y., Chrzanowska, A., Fulham, M.J., Bailey, D.L., Cooper, W.A., Kritharides, L., Ridley, L., Pattison, S.T., MacDiarmid, J., Brahmbhatt, H., Reid, G., 2017. Safety and activity of microRNA-loaded minicells in patients with recurrent malignant pleural mesothelioma: a first-in-man, phase 1, open-label, dose-escalation study. Lancet Oncol. 18, 1386–1396. https://doi.org/10.1016/S1470-2045(17)30621-6

Vuorio, J., Vattulainen, I., Martinez-Seara, H., 2017. Atomistic fingerprint of hyaluronan–CD44 binding. PLOS Comput. Biol. 13, e1005663. https://doi.org/10.1371/journal.pcbi.1005663

Wang, Z., Sau, S., Alsaab, H.O., Iyer, A.K., 2018. CD44 directed nanomicellar payload delivery platform for selective anticancer effect and tumor specific imaging of triple negative breast cancer. Nanomedicine Nanotechnol. Biol. Med. 14, 1441–1454. https://doi.org/10.1016/j.nano.2018.04.004

Wolny, P.M., Banerji, S., Gounou, C., Brisson, A.R., Day, A.J., Jackson, D.G., Richter, R.P., 2010. Analysis of CD44-hyaluronan interactions in an artificial membrane system: insights into the distinct binding properties of high and low molecular weight hyaluronan. J. Biol. Chem. 285, 30170–30180. https://doi.org/10.1074/jbc.M110.137562

Xiao, B., Han, M.K., Viennois, E., Wang, L., Zhang, M., Si, X., Merlin, D., 2015. Hyaluronic acid-functionalized polymeric nanoparticles for colon cancer-targeted combination chemotherapy. Nanoscale 7, 17745–17755. https://doi.org/10.1039/C5NR04831A

Xiong, H., Du, S., Ni, J., Zhou, J., Yao, J., 2016. Mitochondria and nuclei dual-targeted heterogeneous hydroxyapatite nanoparticles for enhancing therapeutic efficacy of doxorubicin. Biomaterials 94, 70–83. https://doi.org/10.1016/j.biomaterials.2016.04.004

Yang, C., Cao, M., Liu, H., He, Y., Xu, J., Du, Y., Liu, Y., Wang, W., Cui, L., Hu, J., Gao, F., 2012. The High and Low Molecular Weight Forms of Hyaluronan Have Distinct Effects on CD44 Clustering. J. Biol. Chem. 287, 43094–43107. https://doi.org/10.1074/jbc.M112.349209

Yang, X., Iyer, A.K., Singh, A., Choy, E., Hornicek, F.J., Amiji, M.M., Duan, Z., 2015. MDR1 siRNA loaded hyaluronic acid-based CD44 targeted nanoparticle systems circumvent paclitaxel resistance in ovarian cancer. Sci. Rep. 5, 8509. https://doi.org/10.1038/srep08509

You, J., O'Hara, S.D., Velupillai, P., Castle, S., Levery, S., Garcea, R.L., Benjamin, T., 2015. Ganglioside and Non-ganglioside Mediated Host Responses to the Mouse Polyomavirus. PLOS Pathog. 11, e1005175. https://doi.org/10.1371/journal.ppat.1005175

Yu, M., Jambhrunkar, S., Thorn, P., Chen, J., Gu, W., Yu, C., 2013. Hyaluronic acid modified mesoporous silica nanoparticles for targeted drug delivery to CD44-overexpressing cancer cells. Nanoscale 5, 178–183. https://doi.org/10.1039/C2NR32145A

Zackova Suchanova, J., Hejtmankova, A., Neburkova, J., Cigler, P., Forstova, J., Spanielova, H., 2020. The Protein Corona Does Not Influence Receptor-Mediated Targeting of Virus-like Particles. Bioconjug. Chem. 31, 1575–1585. https://doi.org/10.1021/acs.bioconjchem.0c00240

Zackova Suchanova, J., Neburkova, J., Spanielova, H., Forstova, J., Cigler, P., 2017. Retargeting Polyomavirus-Like Particles to Cancer Cells by Chemical Modification of Capsid Surface. Bioconjug. Chem. 28, 307–313. https://doi.org/10.1021/acs.bioconjchem.6b00622

Zhang, Xiaoqing, Ren, X., Tang, J., Wang, J., Zhang, Xiang, He, P., Yao, C., Bian, W., Sun, L., 2020. Hyaluronic acid reduction-sensitive polymeric micelles achieving co-delivery of tumor-targeting paclitaxel/apatinib effectively reverse cancer multidrug resistance. Drug Deliv. 27, 825–835. https://doi.org/10.1080/10717544.2020.1770373

Zhao, Q., Liu, J., Zhu, W., Sun, C., Di, D., Zhang, Y., Wang, P., Wang, Z., Wang, S., 2015. Dual-stimuli responsive hyaluronic acid-conjugated mesoporous silica for targeted delivery to CD44-overexpressing cancer cells. Acta Biomater. 23, 147–156. https://doi.org/10.1016/j.actbio.2015.05.010

Zhong, L., Liu, Y., Xu, L., Li, Q., Zhao, D., Li, Z., Zhang, Huicong, Zhang, Haotian, Kan, Q., Sun, J., He, Z., 2019. Exploring the relationship of hyaluronic acid molecular weight and active targeting efficiency for designing hyaluronic acid-modified nanoparticles. Asian J. Pharm. Sci. 14, 521–530. https://doi.org/10.1016/j.ajps.2018.11.002

Zhong, Y., Zhang, J., Cheng, R., Deng, C., Meng, F., Xie, F., Zhong, Z., 2015. Reversibly crosslinked hyaluronic acid nanoparticles for active targeting and intelligent delivery of doxorubicin to drug resistant CD44+ human breast tumor xenografts. J. Controlled Release 205, 144–154. https://doi.org/10.1016/j.jconrel.2015.01.012

10. Appendix I

Before MPyV VLPs were used for chemical modification by the alkyne functionality containing linker, TEM micrographs using negative staining were acquired. According to the micrographs, the fractions were evaluated. If the integrity of the VLPs was preserved, the fractions were selected for the chemical modification. The micrographs acquired by TEM are summarized in figure S.i.

VLP-alkyne batch	VLP Isolation		
A	Isolation 1	Fraction 1	Fraction 2
		Fraction 4	Fraction 5

| | Isolation 2 |
Fraction 4 |
|---|---|---|
| **B** | Isolation 4 |
Fraction 2 |
| | |
Fraction 3 |

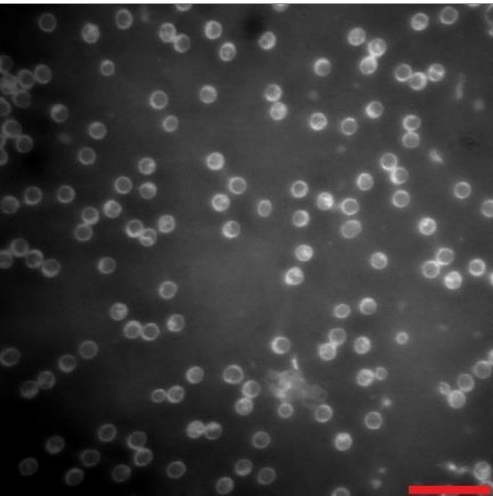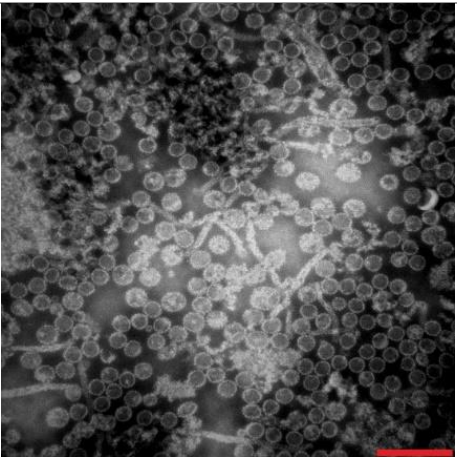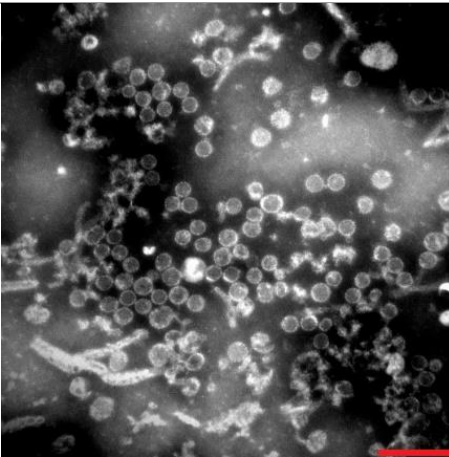|		
		Fraction 4
C	Isolation 2	
		Fraction 1
	Isolation 3	
		Fraction 3 Fraction 4
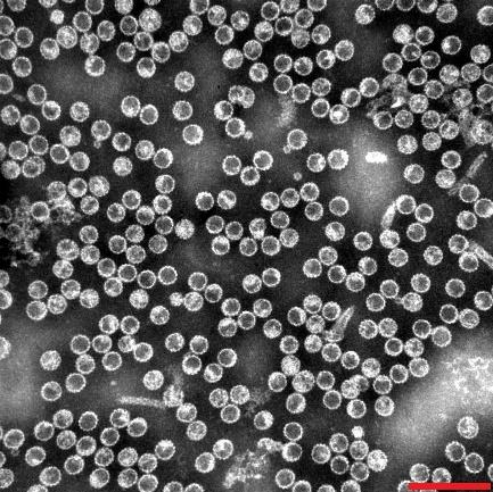
Figure S.i TEM micrographs using negative staining acquired after VLP isolations. In this figure micrographs of fractions from multiple VLP isolation experiments (four VLP isolations – indicated as Isolation 1,2,3,4) selected for further experiments (alkyne linker attachment, click reaction and subsequent NP-cell interaction experiments) are summarized. Red scalebar indicates 200 nm.

11. Appendix II

After obtaining the data from the NP-cell interaction studies by flow cytometry, the data were gated according to the summary shown in figure S.ii.
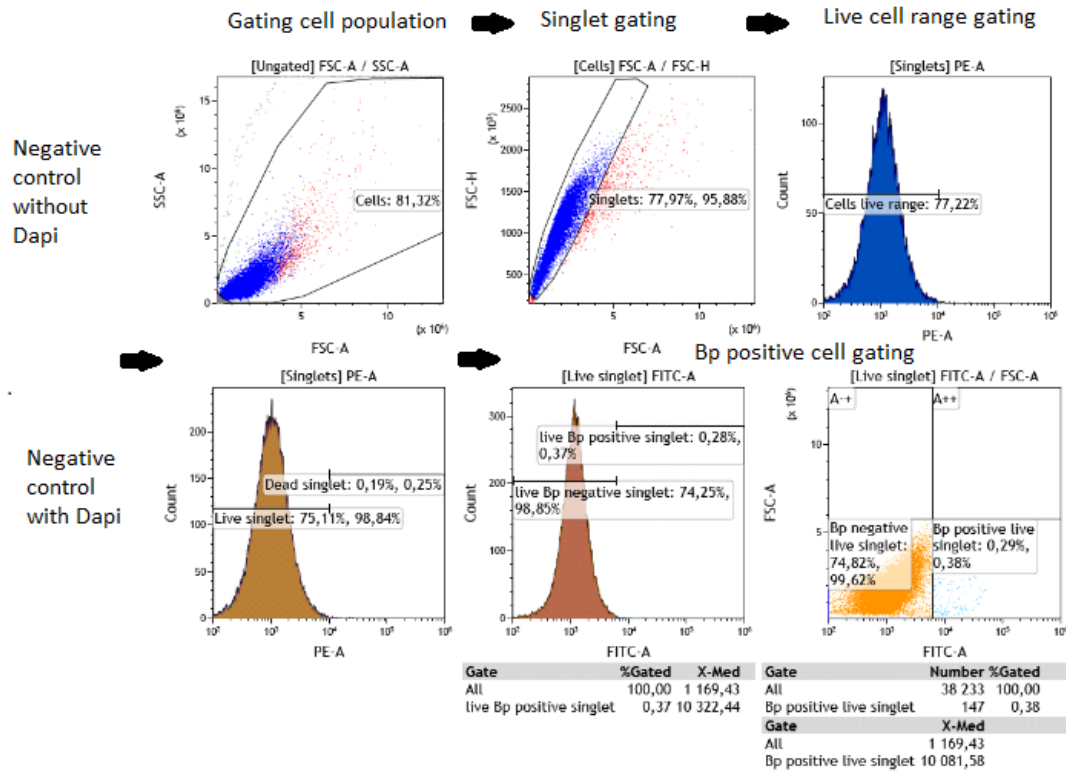

Figure S.ii The gating strategy used to process data from all FC experiments is shown. Population and singlet gating were set in the negative control samples without DAPI, also live cell range was set. Live and dead cells were gated in the negative control with DAPI. The cells with positive fluorescent signal were gated using negative control with DAPI too. Data were processed in the Kaluza software 2.1.